Energy-Smart Calculation of Thermal Loads in Mobile and Stationary Heating, Ventilation, Air Conditioning, and Refrigeration Systems

by

Mohammad Ali Fayazbakhsh

M.Sc., Sharif University of Technology, 2009
B.Sc., Sharif University of Technology, 2006

Thesis Submitted in Partial Fulfillment of the
Requirements for the Degree of
Doctor of Philosophy

In the
School of Mechatronic Systems Engineering
Faculty of Applied Sciences

SIMON FRASER UNIVERSITY

Fall 2015

Approval

Name: **Mohammad Ali Fayazbakhsh**

Degree: **Doctor of Philosophy**

Title: ***Energy-Smart Calculation of Thermal Loads in Mobile and Stationary Heating, Ventilation, Air Conditioning, and Refrigeration Systems***

Examining Committee: **Chair:** Dr. Jiacheng (Jason) Wang
Assistant Professor

Dr. Majid Bahrami, P. Eng.
Senior Supervisor
Professor

Dr. John Jones
Supervisor
Associate Professor

Dr. Erik Kjeang
Supervisor
Assistant Professor

Dr. Carlo Menon
Internal Examiner
Associate Professor
School of Engineering Science

Dr. Phalguni Mukhopadhyaya
External Examiner
Associate Professor
Department of Mechanical Engineering
University of Victoria

Date Defended/Approved: 10 November 2015

Abstract

The energy consumption by heating, ventilation, air conditioning, and refrigeration systems forms a large portion of the total energy usage in buildings. Vehicle fuel consumption and emissions are also significantly affected by air conditioning. Air conditioning is also a critical system for hybrid electric vehicles and electric vehicles as the second most energy consuming system after the electric motor. Proper design and efficient operation of air conditioning systems require accurate calculation of thermal loads as well as appropriate design and selection of the refrigeration cycle. The control logic applied to the system further defines the operational costs associated with the performance of the air conditioning or refrigeration system.

The common practice in air conditioning engineering includes a primary calculation of thermal loads. Consecutively, the refrigeration system is selected to provide the required cooling or heating load. An alternate design approach in which the thermal loads are not only calculated as the initial design step but are also calculated in real-time is proposed in this thesis. Modern air conditioning systems are equipped with feedback controllers to allow the system to sustain thermal comfort. The real-time calculation and prediction of the room thermal loads improved by measurements is beneficial for energy-efficient control of air conditioning systems especially in vehicle applications that experience highly dynamic load variations. The calculation procedure can be implemented in a load-based controller to provide advanced intelligence for the system operation. This approach can optimize the system performance for the current as well as future conditions and can also be used as a tool for retrofitting existing systems.

The objective of the present research is to establish intelligent real-time thermal load calculation methods that can be used to develop energy-efficient control systems in both stationary and mobile air conditioning and refrigeration applications. The proposed methodology consists of developing a variety of models for law-driven and data-driven calculation of thermal loads in mobile and stationary applications. The proposed models are applicable to heating, air conditioning, and refrigeration applications. The contributions of this study include design recommendations that can result in up to 50% increase in energy efficiency for mobile and stationary air conditioning systems.

Keywords: HVAC-R; Thermal Loads; Mobile Air Conditioning; Intelligent Methods; Data-Driven Methods; Air Conditioning Control

To my beloved father, mother, sister, and brother

Acknowledgements

I would like to thank my senior supervisor, Dr. Majid Bahrami, for his kind support and guidance throughout this research. It was a privilege for me to work with and learn from him.

I am also indebted to Dr. John Jones and Dr. Erik Kjeang for the useful discussions and comments, which helped me define the project and pursue its goals. I would also like to thank Dr. Carlo Menon and Dr. Phalguni Mukhopadhyaya for their time reading and refining this thesis.

I would like to thank my colleagues and lab mates at Laboratory for Alternative Energy Conversion at Simon Fraser University. Their helps, comments, and assistance played an important role in the development of this thesis. In particular, I want to thank Marius Haiducu, Dr. Wendell Huttema, Dr. Claire McCague, and Dr. Mehran Ahmadi.

I have received financial support from Natural Sciences and Engineering Research Council (NSERC) of Canada, Automotive Partnership Canada (APC), Future Vehicle Technologies (FVT), Cool-It, Saputo Inc., and Simon Fraser University, for which I am grateful. I would also like to appreciate our industrial collaborator, Mr. Saeed (Steve) Zaeri for his time, help, and kind cooperation.

I have to thank my family who have endlessly encouraged and supported me through all stages of my life. Without their heart-warming support, no achievement would be possible in my life.

Table of Contents

List of Tables

List of Figures

List of Acronyms

HVAC-R	Heating, Ventilation, Air Conditioning, and Refrigeration
AC	Air Conditioning
HEV	Hybrid Electric Vehicle
EV	Electric Vehicle
MAC	Mobile Air Conditioning
RC	Resistance-Capacitance
PEV	Plug-in Electric Vehicle
ASHRAE	American Society of Heating, Refrigeration, and Air Conditioning Engineers
HBM	Heat Balance Method
ES	Energy Simulation
CFD	Computational Fluid Dynamics
TES	Thermal Energy Storage
PCM	Phase Change Material
MPC	Model Predictive Control
NN	Neural Network
GA	Genetic Algorithm
PID	Proportional-Integral-Derivative
VRF	Variable Refrigerant Flow
VAV	Variable Air Volume
ISO	International Organization for Standardization
FVT	Future Vehicle Technologies
SFTP	Supplemental Federal Test Procedure
RPM	Revolutions Per Minute
GPS	Global Positioning System
DC	Direct Current
DAQ	Data Acquisition System

Symbols

a		Sigmoid Function Parameter
A	$\left[m^2\right]$	Surface Area
A_{Du}	$\left[m^2\right]$	DuBois Body Surface Area
b	$\left[m\right]$	Wall Thickness
c	$\left[J/kg°C\right]$	Specific Heat
C	$\left[F\right]$	Electric Capacitance
c_1	$\left[°C\right]$	Temperature Correlation Parameter
c_2	$\left[°C\right]$	Temperature Correlation Parameter
c_3	$\left[s\right]$	Temperature Correlation Parameter
D		Desired Calculation Output
DTM	$\left[J/°C\right]$	Deep Thermal Mass
e	$\left[J/kg\right]$	Enthalpy
E	$\left[W\right]$	Power
f		Sigmoid Function
g	$\left[m/s^2\right]$	Gravitational Constant
h	$\left[W/m^2°C\right]$	Convection Coefficient
H	$\left[m\right]$	Wall Height
H_p	$\left[m\right]$	Passenger Height
I	$\left[A\right]$	Current
$\dot{I}$	$\left[W/m^2\right]$	Radiation Heat Gain per Unit Area
k	$\left[W/m°C\right]$	Thermal Conductivity
K		Convection Correlation Coefficient
K_1	$\left[J/°C\right]$	Heat Balance Equation Parameter

K_2	$[W/°C]$	Heat Balance Equation Parameter
K_3	$[W]$	Heat Balance Equation Parameter
m	$[kg]$	Mass
$\dot{m}$	$[kg/s]$	Mass Flow Rate
M	$[J/°C]$	Thermal Inertia
n		Number of Walls
O		Actual Calculation Output
P	$[Pa]$	Air Pressure
P_s	$[Pa]$	Water Saturation Pressure
P_w	$[m]$	Wall Perimeter
$\dot{Q}$	$[W]$	Thermal Load
r		Pull-Down Time Ratio
R	$[\Omega]$	Electrical Resistance
R^2		Coefficient of Determination
R_h	$[m^2°C/W]$	Convection Thermal Resistance
R_k	$[m^2°C/W]$	Conduction Thermal Resistance
R_t	$[m^2°C/W]$	Total Thermal Resistance
RPM	$[rpm]$	Engine Speed
t	$[s]$	Time
t_c	$[s]$	Pull-Down Time Constant
t_p	$[s]$	Target Pull-Down Time
T	$[°C]$	Temperature
U	$[W/m^2°C]$	Overall Wall Surface Heat Transfer Coefficient
V	$[v]$	Voltage
Vel	$[m/s]$	Velocity

w	$[W/°C]$	Weight Factor
w_0	$[W]$	Bias Weight Factor
W_p	$[kg]$	Passenger Weight
x	$[m]$	Length Coordinate
X		Humidity Ratio
y	$[m]$	Width Coordinate
z	$[m]$	Height Coordinate

Greek Symbols

α		Surface Absorptivity
A	$[W/m^2]$	Radiation Calculation Parameter
β		Altitude Angle
β_T	$[1/°C]$	Coefficient of Thermal Expansion
B		Radiation Calculation Parameter
Γ		Radiation Calculation Parameter
ε		Convergence Threshold
ϕ		Relative Humidity
η		Training Learning Rate
μ	$[Ns/m^2]$	Dynamic Viscosity
M	$[W/m^2]$	Metabolic Heat Production Rate
θ	$[Radians]$	Angle Between Surface Normal and Sun Position
ρ	$[kg/m^3]$	Density
ρ_g		Ground Reflectivity Coefficient
τ		Surface Element Transmissivity
Σ	$[Radians]$	Surface Tilt Angle
ω		Number of Compressor Starts

Subscripts and Superscripts

0	Initial
a	Internal Air

AC	Air Conditioning
Amb	Ambient
c	Cooling
$comf$	Comfort
$comp$	Compressor
Dif	Diffuse
Dir	Direct
D	Temperature-Decreasing Process
ei	Evaporator Inlet
Eng	Engine
eo	Evaporator Outlet
Exh	Exhaust
h	Heating
H	High Set Point
i	Inside
I	Temperature-Increasing Process
j	Wall Number
k	Training Step Number
l	Calculated
L	Low Set Point
m	Mean
Met	Metabolic
n	Number of Walls
Net	Net Average
o	Outside
Rad	Radiation
Ref	Reflected
s	Wall Surface
S	Internal Sources
Tot	Total
V	Ventilation and Infiltration
Ven	Ventilation

w	Wall
W	Walls

Executive Summary

Motivation

Energy consumption by heating, ventilation, air conditioning, and refrigeration (HVAC-R) systems forms approximately 50% of the total energy usage in buildings and 20% of the total national energy usage in European and American countries. Vehicle fuel consumption and emissions are also significantly affected by air conditioning. Air conditioning (AC) can increase NOx emission by up to 100% in vehicles. The AC power consumption of mid-sized cars is estimated to be higher than 12% of the total vehicle power during regular commuting. HVAC-R is also a critical system for hybrid electric vehicles (HEVs) and electric vehicles (EVs), as it is the second most energy consuming system after the electric motor of the vehicle. As such, proper design and efficient operation of HVAC-R systems can significantly reduce the environmental impact and greenhouse gas emissions. Consequently, accurate calculation of thermal loads as well as appropriate design and selection of HVAC-R systems are crucial.

Common practice in HVAC-R engineering consists of a primary calculation of thermal loads followed by the selection of an HVAC-R system to provide the estimated cooling or heating load. A promising alternative design approach is one in which the thermal loads are not only calculated as the initial design step but are also calculated in real-time. Modern air conditioning systems are equipped with feedback controllers to allow the HVAC-R unit to sustain thermal comfort. The real-time calculation and prediction of thermal loads is beneficial for energy-efficient control of HVAC-R systems especially in mobile air conditioning (MAC) applications that experience highly dynamic load variations. The calculation procedure can be implemented in a load-based controller to provide thermal comfort with the most efficient energy consumption. This approach can optimize HVAC-R energy consumption while providing the required thermal load for current as well as future conditions. Furthermore, the proposed system can be readily implemented for retrofitting existing systems.

Objectives

The objective of the present research is to establish energy-smart and real-time thermal load calculation methods that can be used to develop energy-efficient HVAC-R control systems in both stationary and mobile applications.

Methodology and Contributions

A systematic approach is incorporated to achieve the objectives of this research. A combination of analytical methods, experiments, and numerical computations is used to develop comprehensive models for energy-smart thermal load calculations. The mathematical approaches are kept simple yet accurate to provide them with commercial attractiveness in the HVAC-R market. Extensive data collection is performed on 2 refrigerated trucks, a stationary walk-in freezer, and 2 lab-scale testbeds.

The models are primarily developed based on fundamental heat transfer equations. In the next step, the results are verified and validated with experiments. Finally, the packaging of the models is discussed for implementation in real-world HVAC-R applications. The developed methodology consists of the following milestones:

- Developed a new comprehensive heat balance method to simulate thermal loads in mobile applications.
- Built two testbeds in the lab to simulate and validate thermal loads in an electric vehicle. The testbeds included adjustable windshield angles, heater, humidifier, air distribution ducts, thermocouples, control system, and a data acquisition (DAQ) system.
- Collected extensive data on the thermal operation of the walk-in freezer room of a restaurant. The room temperature was measured at several locations. Refrigerant flow rate, pressure, and temperature were also measured during several months and the performance of the freezer room was deeply investigated accordingly.
- Developed an inverse mathematical model for simultaneous calculation of thermal inertia and thermal loads in real-time. The collected data from the walk-in freezer room were used to validate the model.

- Demonstrated a resistance-capacitance (RC) lumped modeling approach to simulate thermal loads in both stationary and mobile applications. The model was verified by the data collected from the freezer room and parametric studies were performed on various components of the heat load to investigate their contributions.
- Established a new self-adjusting algorithm to improve the thermal load calculations through real-time estimation of heat transfer coefficients. Implemented the model in the lab-scale testbed and demonstrated calculation improvements by experiments.
- Established a methodology for energy-efficient selection of temperature set points in on/off controllers. Proposed a data-driven approach for optimized selection of set point hysteresis based on exponential temperature correlations. Implemented the model in a controller and showed energy-efficiency improvements.
- Collected temperature data from the refrigerated trucks of a major dairy transportation company and established a data-driven method for duty cycle identification in mobile refrigerated cabins.

Chapter 1. Introduction

1.1. Research importance

A significant portion of the energy produced worldwide is consumed by heating, ventilation, air conditioning, and refrigeration (HVAC-R) systems. Energy consumption by HVAC-R systems is 50% of the total energy usage in buildings and 20% of the total national energy usage in European and American countries [1]. Predictions indicate a further increase of 50% from the current figure during the next 15 years in the European Union countries [1]. HVAC-R energy consumption can exceed 50% of the total energy usage of a building in tropical climates [2]. Furthermore, refrigeration systems also consume a substantial amount of energy. Supermarket refrigeration systems, as an example, can account for up to 80% of the total energy consumption in a supermarket [3]. Implementing opportunities to reduce energy consumption in HVAC-R systems can propagate to a large number of systems used in various applications. As such, efficient design of new HVAC-R systems and devising intelligent control methods for existing systems can lead to large-scale reductions in total energy consumption and greenhouse gas emissions.

Air conditioning (AC) is an important energy consuming unit in vehicles as well [4] and has a significant impact on emissions and fuel economy. AC energy usage in vehicles outweighs the energy dissipated due to rolling resistance, aerodynamic drag, and driveline losses for a typical vehicle. Studies have shown that AC systems can reduce the fuel economy of mid-sized vehicles by more than 20% while increasing CO emissions by 70% and NOx by up to 100% [5], [6]. The United States alone consumes an estimated 26.5 billion liters of fuel per year for the AC systems of light-duty vehicles [7]. The reduction of fuel consumption and tailpipe emissions are two crucial targets for the auto industry that can be addressed by improved AC systems.

AC is also a critical system for Hybrid Electric Vehicles (HEV) and Electric Vehicles (EV), as it is the second most energy consuming system after the electric motor [4]. In an electric vehicle AC power consumption can be as high as 12% of the total vehicle power during regular commuting [8] and the energy required to provide cabin cooling for thermal comfort can reduce the range of plug-in electric vehicles (PEV) by up to 50%, depending on outside weather conditions [4]–[6]. Thus, it is of both environmental and economic interest to seek new methods to improve the efficiency and performance of vehicle AC systems as less energy consumption by mobile air conditioning (MAC) systems directly results in higher mileage and better overall efficiency on the road.

1.2. Motivation

Calculating thermal loads is the primary step in designing HVAC-R systems. Any improvement in the calculation methods can result in a significant reduction of the total energy consumption and the greenhouse gas emissions. Proper design and efficient operation of any HVAC-R system require: i) accurate calculation of thermal loads, and ii) appropriate design and selection of the HVAC-R unit. Common practice in HVAC-R engineering is to start the design process by calculating the thermal loads in the space. This step consists of a careful study of the room characteristics such as wall properties, fenestration, openings, and air distribution. Additionally, room usage patterns, occupancy levels, geographical location, and ambient weather conditions need to be thoroughly investigated before a decision is made on the required thermal load. An HVAC-R unit is then selected to handle the required load. As such, detailed information about a number of parameters is required to properly calculate the thermal loads and select the HVAC-R system.

Innovative methods to calculate the thermal loads in real-time based on a minimal amount of data can be promising ways to add intelligence to HVAC-R controllers. The additional real-time knowledge of the loads encountered in the room can improve the overall performance and efficiency of the HVAC-R system. As a direct result, reduced energy consumption and emissions can be achieved by the present approach.

1.3. Scope

The objective of this thesis is to establish new intelligent real-time thermal load calculation methods. The proposed methods enhance the estimation of cooling and heating loads in order to improve energy efficiency and reduce emissions. These methods provide real-time estimations to load-based controllers in order to improve the control action towards increased energy efficiency.

The primary focus of this work is on comprehensive models, based on the conventional heat balance method, that were developed for calculations of thermal loads in mobile and stationary applications. Further, an intelligent method was established to estimate bulk thermal inertia and heat gain in real-time. In order to incorporate more detailed temperature measurements, another method was developed for automatic calculations of wall heat transfer coefficients. The automatic estimation of coefficients further improves the heat balance calculations. Finally, a study was performed on the opportunity for increasing energy efficiency in existing on/off controllers by optimizing the selection of the set points. The developed methods can remarkably benefit a wide range of HVAC-R systems.

1.4. Thesis Structure

Careful investigation of the pertinent literature shows that intelligent calculation of thermal loads can either be done by a law-driven (forward) approach or a data-driven (inverse) approach. Both methodologies are followed in this study and the thesis is also structured accordingly. Figure 1-1 shows a roadmap of the project steps.

Chapter 2 covers the developed models based on the law-driven method. Due to a lack of a comprehensive model for dynamic calculation of thermal loads in automotive applications, Section 2.1 is devoted to proposing such a model. In Section 2.2, the experimental setup in a stationary freezer room is described. This setup is used to develop another law-driven model in Section 2.3 based on RC modeling.

Chapter 3 covers the developed models based on the data-driven method. The same experimental setup of Section 2.2 is used to establish an inverse model for

estimating the thermal inertia and heat gain. An in-house experimental testbed is built as described in Section 3.2. In Section 3.3, a new method is developed for real-time load calculations based on automatic estimation of heat transfer coefficients. Section 3.4 proposes an optimized method for energy efficient selection of temperature set points in on/off controllers.

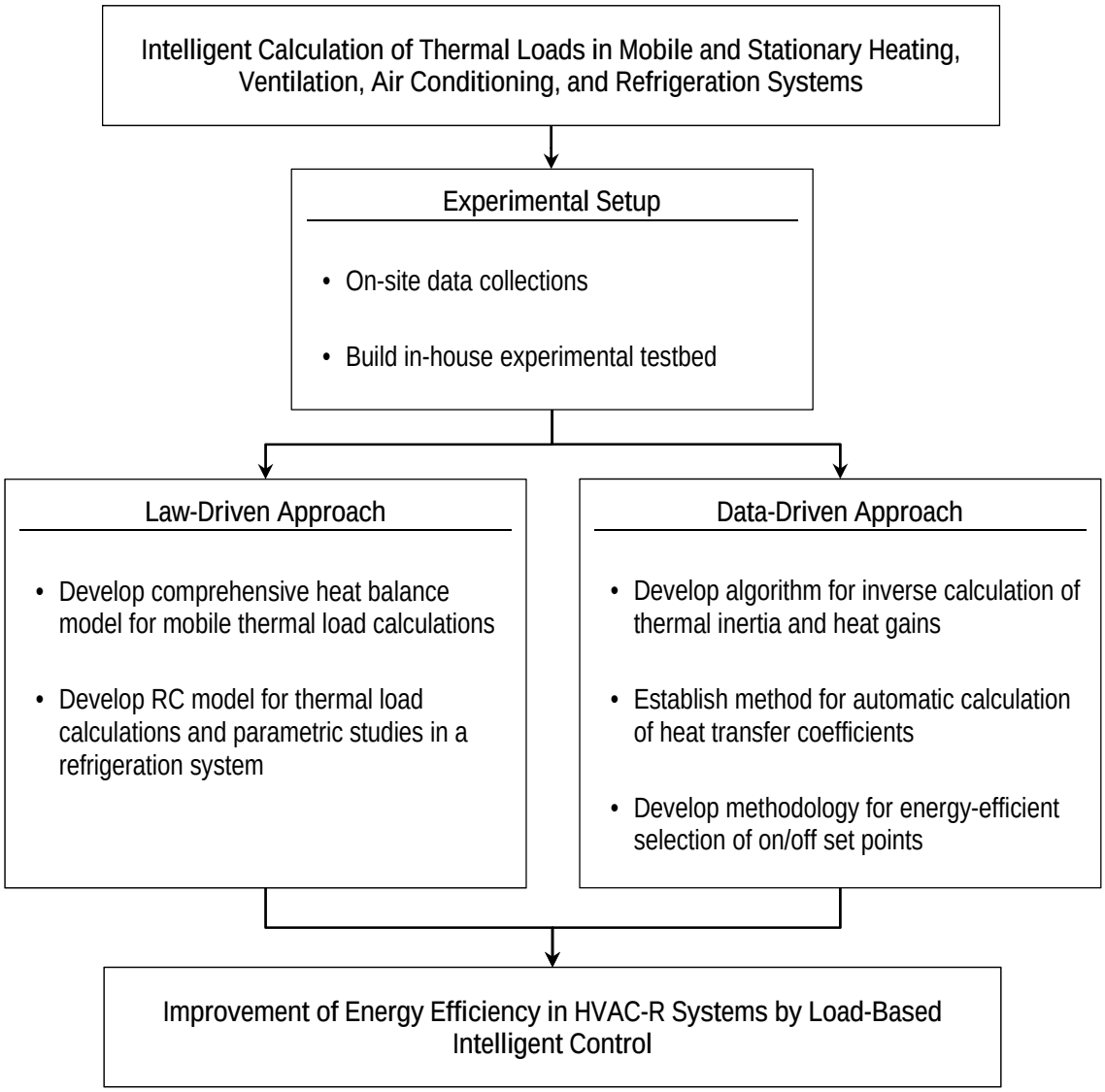

Figure 1-1: Thesis structure.

Chapter 4 concludes the major contributions of the thesis. Suggestions for future studies are also described in Chapter 4.

1.5. Literature Review

In this section, a review of the pertinent literature is presented. The various aspects of thermal load calculations and the methods used are collected herein. A lack of research in certain areas is identified, motivating the present study.

1.5.1. Conventional Load Calculation

The conventional methods of thermal load estimation are highly established. They can be categorized into methods for stationary applications and mobile applications.

Stationary Applications

The American Society of Heating, Refrigeration, and Air Conditioning Engineers (ASHRAE) has established extensive methodologies for calculating heating and cooling loads [9]. The heat balance method (HBM) [10] is an example of such a load calculation method. It is a straightforward and comprehensive method that involves calculating a wall-to-wall heat balance of the room through consideration of conduction, convection, and radiation heat transfer mechanisms. The method has been extensively used in stationary [11] as well as mobile [12] applications. The essence of the HBM is a calculation of the overall heat flow through the walls of a room. For every wall, heat flow encounters an outside convection resistance, a conduction resistance across the wall, and an inside convection resistance. Some heat is also stored in the wall, depending on its thermal inertia and temperature. After balancing the incoming energy, the overall heat balance calculation is carried out for the room air.

Among the heat transfer mechanisms involved in the heat balance method, calculation of convective heat transfer has a sophisticated nature and tends to be complicated. The convective heat transfer over a wall depends on the velocity and temperature of the air as well as the surface temperature. A common practice for the calculation of convective heat transfer is to evaluate the coefficients using analytical or empirical correlations. ASHRAE Standard 90.1 [13] offers comprehensive tables for the estimation of U-Factors. The U-Factor, or thermal transmittance, is defined as the “heat transmission in unit time through a unit area of a material or construction and the

boundary air films, induced by unit temperature difference between the environments on each side" [13]. However, finding the proper U-Factor requires extensive information to be gathered by the designer. Moreover, the estimated U-Factor may be inaccurate for varying air patterns and thermal conditions.

Besides ASHRAE, other attempts have been made to provide reliable estimations of the convection coefficient and a broad range of experimental, computational, and analytical methods appear in the literature. Loveday and Taki [14] used an experimental arrangement to find correlations for the external convection coefficient as a function of wind speed for a building wall. Kurazumi et al. [15] experimentally found the convective heat transfer coefficients of a seated human body during forced convection by downward flow from the ceiling using a thermal mannequin. Lei et al. [16] presented an inverse modeling strategy to determine the required wall boundary convective heat fluxes required in computational simulations. In several studies by Zhai et al. [16–21], they developed a methodology to couple computational fluid dynamics (CFD) simulations with energy simulations (ES) to improve the accuracy of the latter for different air distribution patterns. They concluded that an ES module coupled with a CFD simulation can benefit from more accurate convection coefficients, which improve the overall load calculation process [20]. However, Zhai and Chen [22] reported that one CFD simulation may take a long time to obtain a reasonable result even with steady-state conditions. This high computation cost associated with CFD tools is a drawback that hinders their usage in many typical applications.

Many reviews have attempted to outline the numerous formulas for convection coefficients. Khalifa [20,21] thoroughly reviewed available correlations for natural convection coefficient over flat surfaces. Sartori [25] reviewed the equations of forced convection coefficient for flow over flat surfaces. Palyvos [26] presented a survey of the correlations for wind convection coefficient to be used for energy modeling in building envelopes. Defraeye et al. [27] also collected the existing correlations for convection coefficients over exterior building surfaces and compared them with CFD simulations.

From the above reviews, it is evident that the convection coefficient can strongly affect heat balance calculations and an ultimate form that covers all conditions and scenarios is not available. Various suggested values of convection coefficients, even

varying by an order of magnitude, can be found in the literature for the same problem. Therefore, an intelligent approach for real-time estimation of the convection coefficients can improve heat balance calculations significantly.

Mobile Applications

The calculation of thermal loads in MAC systems follows the same concepts as in stationary applications. Considerable studies are devoted to thermal load calculations in MAC systems. Fanger's model of thermal comfort [28], which is extensively used in air conditioning design is, also recognized for MAC applications.

Based on Fanger's model, Ingersoll et al. [29] developed a human thermal comfort calculation model specific to automobile passenger cabins. Zheng et al. [30] devised a simple method to calculate vehicle thermal loads and validated it using wind tunnel climate control tests. Arici et al. [31] developed computer code for simulating the dynamic operation of a climate control system for a typical vehicle. Ding and Zito [32] also used a lumped model for vehicle cabins and solved the corresponding transient heat transfer differential equation analytically. Their analytical solution can be used as a benchmark for basic problems such as the cool-down test. Selow et al. [33] developed a virtual vehicle based on experimental correlations for each significant vehicle component. The virtual vehicle was divided into different modules, one of which was the cabin climate. Simultaneous operation of these modules could provide estimates without necessitating cumbersome and costly experiments. Khayyam et al. [34] collected a set of models to calculate the various types of thermal load encountered in a vehicle. These models were later used to estimate the overall cooling load, which was fed back to a coordinated energy management system to reduce the air conditioning energy consumption [35]. Wei and Dage [36] developed an intelligent cabin climate control system based on human-sensory response to comfort factors.

Numerical simulations are also used to improve MAC load estimations. Methods put forth by ASHRAE and in other literature often assume the vehicle cabin as a lumped system and do not take the three-dimensional distribution of temperature and flow parameters into account. Finding exact solutions for distribution of airflow, temperature, and humidity is often complex. Therefore, numerical methods are employed for such simulations. Alexandrov et al. [37] used two- and three-dimensional CFD simulations to

investigate the effect of various parameters such as car velocity and outside temperature on the performance of MAC systems. They simulated the flow in a typical vehicle and found a maximum temperature difference of about 7°C between two points in the car cabin. They concluded that issues such as low air circulation zones in the cabin can be resolved by designing better air inlet and outlet configurations.

The variation of thermal loads in vehicle cabins generally occurs more rapidly than in stationary applications. Vehicle movement adds dynamism to the radiation and convection mechanisms. The small size of a vehicle cabin also causes variations in the thermal phenomena to occur quickly. However, although the real-time estimation of cooling/heating loads in mobile systems can be complicated, it is beneficial for energy-efficient control of the MAC system.

1.5.2. Resistance-Capacitance (RC) Modeling

Thermal load calculations pertaining to the heat balance method are greatly facilitated by resistance-capacitance (RC) modeling. RC modeling allows for better understanding the physics of the problem and makes it possible to easily evaluate modeling hypotheses and sensitivity to different parameters [38].

RC modeling is a well-established approach based on the analogy between thermal systems and electric circuits [39]. In this approach, the thermal system under consideration is represented by an equivalent electric circuit that is mathematically identical to the thermal system. In this way, RC modeling helps visualize the HBM approach and solve the problem with better engineering insight. RC modeling is also widely used in other applications such as electronic cooling [40]–[44], mobile air conditioning [45], and phase change materials [46].

Bueno et al. [38] applied RC modeling to an urban canopy and evaluated their results in comparison to advanced simulation tools. They reported that the RC technique provides simplicity and computational efficiency, especially for studying the sensitivity of results to different parameters. Ogunsola et al. [47] deduced a time-series cooling load model from a simplified RC model to provide thermal load estimations with manageable

computational requirements. RC modeling is also used for studies on specific parameters related to HVAC-R load calculations.

In an RC model, the thermal system is often divided into: i) the room, and i) the envelope, i.e., the surrounding walls of the room. Each component can be modeled by a number of resistors and/or capacitors. For example, a 3R2C thermal model of a wall means that 3 resistors and 2 capacitors are used to represent it in its identical electric sub-circuit. Since one RC sub-circuit represents each wall or room, the complete model can become complicated with a large number of electrical components. Deng et al. [48] described a model reduction methodology used to obtain a simpler multi-scale representation of the RC network. The original RC network of a building application consists of a large number of coupled linear differential equations. The proposed technique by Deng et al. [48] retains the physical intuition of the original model, but is a simpler RC network. However, their model reduction methodology was not compared with experimental data.

RC modeling is also used for studies on specific parameters related to HVAC-R load calculations. Haldi and Robinson [49] developed a means for representing occupant presence and behavior through RC modeling. They discussed a comprehensive representation of occupants and their activities in buildings. They used regression parameters to predict the probabilities of actions such as window and blind opening by occupants. Implementing these types of parameters in the HVAC-R design is highly facilitated by using the RC modeling approach.

Alongside residential air conditioning, RC models are also used in MAC and thermal energy storage (TES) applications. Mezrhab and Bouzidi [45] studied the thermal comfort inside a passenger car compartment according to climatic conditions and materials that compose the vehicle. They developed a numerical model based on the nodal method and solved the network using the finite difference method. Zhu et al. [46] used RC modeling for analyzing the application of phase change materials (PCM) for demand compensation of air conditioning loads. They used a 3R2C model for the walls in series with a 4R2C model for the PCM layer.

An important issue regarding the usage of RC models in HVAC-R applications is the estimation of parameter values. Several thermal properties of the room and the envelope are often necessary and need to be acquired from a comprehensive collection of data. In some cases, complex mathematical algorithms are incorporated to estimate these properties instead of directly acquiring them. Ogunsola et al. [47] used building construction data for envelope thermal properties, while a genetic algorithm was used to estimate the internal thermal mass. Wang and Xu [50] obtained the RC parameters using a genetic algorithm and solved the integrated model numerically using Runge-Kutta classical methods. Oldewurtel et al. [51] performed an investigation of how model predictive control (MPC) and weather predictions can increase HVAC-R energy efficiency while maintaining occupant comfort. An RC network was constructed and employed for building climate control using MPC and weather forecasts. Maasoumy et al. [52] also used an MPC approach for energy efficient buildings. They used an RC representation of an office room to model the heat transfer paths and proposed a parameter-adaptive building model that facilitates the parameter tuning process in an online fashion in the MPC approach. Nevertheless, their approach adds to the complexity of the plain RC model. Platt et al. [53] focused on real-time HVAC-R zone model fitting and prediction techniques based on physical principles, as well as the use of genetic algorithms for optimization. They included supply air input in their model, but the thermal inertia of the walls was ignored.

Table 1-1 summarizes the recent RC models used in HVAC-R applications. The RC sub-circuit models used for the room and its envelope are also shown. Many of the methods depend on experimental measurements for acquiring the model parameters. Nevertheless, other approaches for estimating the RC parameters, instead of measuring, are also listed in Table 1-1.

Table 1-1: Summary of recent RC models in HVAC-R applications. Reprinted with permission [54]**.**

Reference	Envelope Model	Room Model	Parameters Estimation Method
Ogunsola et al. [47]	3R2C	2R2C*	Measurements and genetic algorithm
Maasoumy et al. [52]	4R1C	1C	Parameter adaptive building
Platt et al. [53]	1R	1C	Genetic algorithm
Bueno et al. [38]	3R2C	1C	Measurements

Oldewurtel et al. [51]	2R2C	1C	Stochastic model predictive control
Deng et al. [48]	3R2C	1C	Measurements
Mezrhab and Bouzidi [45]	2R2C	2R1C*	Measurements
Haldi and Robinson [49]	4R1C	1R1C*	Measurements
Zhu et al. [46]	3R2C**	1R1C*	Measurements
Wang and Xu [50]	3R2C	2R2C*	Genetic algorithm

* Resistance for room models is used to account for ventilation, convection, and radiation.
** A 4R2C model is added to the wall in series to account for the layer of phase change material.

1.5.3. Artificial Intelligence Methods

Due to significant advances in computational power, a number of intelligent approaches have been proposed in recent years for enhanced calculation of thermal loads in both stationary and mobile AC applications. Ansari et al. [55] demonstrated that a great deal of mathematical complexities can be avoided in cooling load calculations without sacrificing accuracy. They suggested that hefty procedural details might be avoided with negligible loss of accuracy. Nevertheless, more complex approaches for thermal load estimation are also used in literature, including neural networks, genetic algorithms, and fuzzy logic controllers. These approaches cover a range of simplified to rigorous methods and have different levels of accuracy and engineering usability. Few of these methods are both accurate and easy-to-use.

Kashiwagi and Tobi [56] proposed a neural network algorithm for prediction of thermal loads. Ben-Nakhi and Mahmoud [57] also used general regression neural networks and concluded that a properly designed neural network is a powerful tool for optimizing thermal energy storage in buildings based only on external temperature records. They claimed that their set of algorithms could learn over time and improve the prediction ability. Li et al. [58] presented four modeling techniques for hourly prediction of cooling loads. Yao et al. [59] used a case study to show that a combined forecasting model based on a combination of neural networks and a few other methods can be promising for predicting a building's hourly load for the future hours. Solmaz et al. [60] used the same concept of neural networks to predict the hourly cooling load for vehicle cabins. Methods that are purely based on neural networks are inherently unaware of the heat transfer mechanisms. Thus, they might prove unreliable in new scenarios and conditions for which they are not trained.

Fuzzy control algorithms are also proposed as load prediction methods. Among many, Sousa et al. [61] developed a fuzzy controller to be incorporated as a predictor in a nonlinear model-based predictive controller. They developed a fuzzy controller to be incorporated as a predictor in a nonlinear model-based predictive controller. Khayyam et al. [62] used a fuzzy logic air conditioning enhanced look-ahead system that estimated future road slope within a distance ahead of the vehicle. They showed that 12% energy consumption savings could be achieved using their enhanced fuzzy system. Wei and Dage [36] developed an intelligent cabin climate control system based on human-sensory response to comfort factors. They used passive remote infrared sensors to measure passenger skin temperatures. An intelligent climate controller then controlled parameters such as the blower speed to provide passenger thermal comfort.

Genetic algorithms are another artificial intelligence approach used for thermal load prediction. Wang and Xu [50], [63] used genetic algorithms to estimate the lumped internal thermal parameters of a building thermal network model using the operation data collected from site monitoring. They combined an RC model of the building envelope with a data-driven approach where their model parameters were corrected via real-time measurements.

Table 1-2 summarizes the recent literature devoted to various proposed methods for calculation of thermal loads. For each study, the corresponding application is demonstrated. Table 1-2 also reveals the method based on which each specific study was proposed. The disadvantage of some of these methods is their complexity of implementation in typical HVAC-R applications. While relying upon conventional design methods can cause inaccuracies in thermal load estimations, incorporation of artificial intelligence methods may require computational resources that are not available for typical systems. An accurate real-time load calculation method that is not computationally intensive can be beneficial for practical HVAC-R designs.

Table 1-2: Summary of relevant literature covering methods for thermal load calculation.

Authors	Application	Method
Khayyam et al. [34], [62], [64]	Automotive	Fuzzy Logic
Barnaby et al. [11]	Residential Building	Heat Balance Method
Fayazbakhsh and Bahrami [12]	Automotive	Heat Balance Method

Fayazbakhsh et al. [65]	Refrigeration Room	Heat balance method
Arici et al. [31]	Automotive	Analytical Energy Balance
Li et al. [58]	Office Building	Artificial Neural Network
Kashiwagi and Tobi [56]	Residential Building	Artificial Neural Network
Ben-Nakhi and Mahmoud [57]	Office Building	Artificial Neural Network
Yao et al. [59]	Office Building	Analytic Hierarchy Process
Solmaz et al. [60]	Automotive	Artificial Neural Network
Sousa et al. [61]	Generic Building	Fuzzy Logic
Wang and Xu [50], [63]	Office Building	Genetic Algorithm
Zhai et al. [17]–[22]	Generic Building	Computational Fluid Dynamics
Pedersen et al. [10]	Generic Building	Heat Balance Method
Zheng et al. [30]	Automotive	Heat Balance Method
Ding and Zito [32]	Automotive	Analytical Energy Balance
Selow et al. [33]	Automotive	Analytical Energy Balance
Alexandrov et al. [37]	Automotive	Computational Fluid Dynamics
Khayyam et al. [34]	Automotive	Analytical Energy Balance
Ogunsola et al. [47]	Generic Building	Genetic Algorithm
Maasoumy et al. [52]	Office Building	Parameter Adaptive Building
Platt et al. [53]	Office Building	Genetic Algorithm
Bueno et al. [38]	Generic Building	Experimental Analysis
Oldewurtel et al [51]	Generic Building	Model Predictive Control
Deng et al. [48]	Generic Building	Experimental Analysis
Mezrhab and Bouzidi [45]	Automotive	Experimental Analysis
Haldi and Robinson [49]	Generic Building	Experimental Analysis
Zhu et al. [46]	Office Building	Experimental Analysis
Wang and Xu [50]	Generic Building	Genetic Algorithm

1.5.4. Law-Driven Vs. Data-Driven Methods

A disadvantage of most existing load calculation methods is that they require a lot of information about the air-conditioned space to estimate the loads. For instance, the heat balance method requires knowledge of material properties, thickness of walls, geographical location, fenestration data, weather information, occupancy, appliances, and other detailed information. Such an approach may not rely on feedback information from the air-conditioned space. This type of methodology is called a “forward” approach, which makes the redesign and retrofit of existing HVAC-R systems a laborious and time-consuming task. However, with the availability of on-site sensors and computational

resources, new methodologies can focus on the incorporation of real-time data in the calculation process.

The original heat balance method is known as a “forward” or “law-driven” approach, i.e., it estimates the loads based on rigorous room details. Real-time feedback data are not incorporated in the formulations of this method. In contrast to the heat balance method, “inverse” or “data-driven” methods study existing HVAC-R systems and allow the thermal performance of the system to be inferred based on temperature measurements. Such approaches mathematically evaluate the loads through learning and testing rather than analyzing the heat transfer equations. Therefore, in an inverse method, the entire system, i.e., the conditioned space plus the HVAC-R unit, is considered as a black box that is investigated for a period of time.

The design methodology for HVAC-R controllers can be categorized with respect to their reliance on real-time measurements. White-box (purely law-driven), black-box (purely data-driven), and gray-box (combination of the two) modeling approaches are among the methods proposed in the literature [66]. White-box methods are purely based on predetermined physical laws and are unaware of the real-time performance of the system. Black-box methods are learning algorithms that are often designed as generic tools for intelligent control systems regardless of the actual application. Gray-box approaches offer a mix of the two. In gray-box methods, the governing equations of the specific control problem is incorporated in the design to some extent, while available operation data are also utilized to complement the approach with a degree of real-time intelligence.

1.5.5. HVAC-R Controllers

It has been shown that intelligent control of the HVAC-R operation based on thermal load predictions can help maintain air quality while minimizing energy consumption [62], [64]. Improving load calculation methods and the ability to estimate and predict the loads in real-time can improve the feedback information, which in turn results in a significant reduction in total energy consumption and greenhouse gas emissions. Furthermore, in applications where the room contents may vary over time, an

algorithm that can estimate the thermal inertia in an unsupervised manner can aid the HVAC-R system to adapt to the new conditions.

Controller design is a critical aspect of HVAC-R systems. Proper selection and design of the controller directly affects the overall energy consumption and thermal comfort. Air conditioning and refrigeration systems are often controlled by feedback systems that receive input signals from a temperature sensor, such as a thermocouple, installed inside the room. The controller compares the measured temperature to the desired (set point) temperature, and provides an output to the control element. The control element of the refrigeration system can be the compressor, the evaporator fan, or the condenser fan.

A wide spectrum of controller types is available for HVAC-R applications. Classic controllers include: on/off, proportional, and PID controllers. Mirinejad et al. [67] conducted a thorough review of the newer intelligent controllers used in HVAC-R systems. Although more sophisticated controllers are proposed, the industry often delays in adopting the new methods due to the associated cost, complexity, and lack of incentives. It is therefore important to consider approaches that can be adopted rather quickly with the utmost ease and a tolerable cost.

On/off and modulation controllers are widely used in HVAC-R systems that use the room temperature as the controlled variable [68]. On/off controllers are capable of switching the system on and off based on a comparison between the measured temperature and the desired set point.

By predicting the thermal loads in real-time, controllers are enabled to not only provide thermal comfort in the current conditions, but also adjust the system operation to cope with upcoming conditions in an efficient manner. Argüello-Serrano and Vélez-Reyes [69] stated that availability of thermal load estimations allows the HVAC-R controller to efficiently provide comfort regardless of the thermal loads. Afram and Janabi-Sharifi [70] showed that improved load estimations can lead to the design and testing of more advanced controllers. Zhu et al. [71] studied an optimal control strategy for minimizing energy consumption using variable refrigerant flow (VRF) and variable air volume (VAV) air conditioning systems.

Proportional and PID controllers are meant for systems that have the capability of varying the provided heating/cooling power. For instance, a PID controller not only switches a heater on or off, but can also control the amount of energy input to the room. Therefore, proportional or PID controllers are generally more desirable for variable-capacity systems. Many existing HVAC-R devices are equipped with constant-speed compressors and fans. Nevertheless, Qureshi and Tassou [72] reviewed the application of variable-speed capacity control in refrigeration systems. They argued that in order to compensate for half-load usage conditions, the option of variable-speed compressor consumes the least percentage of the full load power compared to other methods.

One issue with adopting a conventional PID controller is the selection of its coefficients, which are often determined through measurements. Wemhoff [73] proposed a simple calibration procedure for successive optimization of the proportional, integral, and derivative coefficients to reduce energy consumption. Similar optimization concepts are applicable to the set points in on/off controllers [74]. Due to the higher initial cost associated with variable-speed compressors and fans, on/off control and constant capacity components are more common in HVAC-R applications.

Table 1-3 summarizes various characteristics of the available control methods for HVAC-R systems. These approaches cover a variety of approaches, ranging from classic controllers to newer intelligent methods. In Table 1-3, “Simplicity” refers to the ease of implementation of each method; “Computational Intensity” determines the relative amount of on-site computational resources required for the algorithm to perform; and “Cost” is an indication of the relative cost of the method in relation to how commercially available the method is, which also indicated by “Commercial Availability”. Different methods require different extents of system data such as the room thermal characteristics and the refrigeration cycle performance information. The extent of such data required by each method is shown under “System Data Requirement”. Finally, “Prediction and Adaptability” suggests how much each method is able to predict the upcoming thermal conditions and adapt the refrigeration cycle performance to the new scenarios.

Table 1-3: Summary of the characteristics of available controller types for HVAC-R systems. Reprinted with permission [75]**.**

	On/Off Controller	PID Controller	Neural Network	Fuzzy Logic	Genetic Algorithm	Real-Time Load Estimation
Sample Reference	[74]	[73]	[58]	[61]	[50]	[70]
Simplicity	High	Medium	Low	Low	Low	Medium
Computational Intensity	Low	Low	High	Medium	High	Medium
Cost	Low	Low	High	High	High	Medium
Commercial Availability	High	High	Low	Low	Low	Low
System Data Requirement	Low	Medium	High	Medium	High	High
Prediction and Adaptability	Low	Medium	High	Medium	High	High

A major drawback of the intelligent approaches is that they often tend to be mathematically complex and their implementation can be commercially unattractive in a range of regular applications. The sensors and computational resources required for the proper implementation of intelligent methods may be unavailable for inexpensive systems. Furthermore, the usage of intelligent methods often presumes the availability of a variable-load refrigeration system that has variable-speed fans and compressor. Since many existing refrigeration systems are constant-load and only have on/off controllers installed, changing the set point values of the on/off controller, as a means of improving energy efficiency, can be a relatively effortless approach.

The output of an on/off controller is either on or off, with no middle state. To prevent damage to contactors and valves, an on/off “hysteresis” is added to the controller operation [76]. This hysteresis causes the controller to wait for the temperature to surpass the set point by a certain amount before the output turns off or on again. As a result, on/off controllers practically have a pair of set points that are called the “high set point” and the “low set point”. Thus, the on/off controller of a cooling system keeps the system on until the temperature reaches the low set point. When this occurs, the system is switched off until the temperature rises back up to the high set point level, when it is

switched on again. On/off hysteresis prevents the output from making fast, continual switches. With on/off controllers, a precise control of temperature is not achieved. However, the temperature keeps cycling or “swinging” around the desired set point, resulting in an average temperature close to the desired set point.

Chapter 2. Law-Driven Methods

The heat transfer phenomena in a room are governed by well-established energy conservation equations. A wide range of reliable and robust methodologies are developed in the literature based on these governing equations. However, the fundamental conservation equations are general and cannot be directly applied to every application. It is necessary to customize the form of these equations to match every specific application. In this chapter, the fundamental heat balance equation is customized to develop a comprehensive model for automotive thermal load calculation. Moreover, a proper representation of the equation is also provided using the electric circuit equivalent of the heat balance equation. These models which are based on the basic governing laws of heat transfer can be used for calculating the thermal loads in related applications.

2.1. Mobile Air Conditioning Loads

In this section, the Heat Balance Method (HBM) is used for estimating the heating and cooling loads encountered in a vehicle cabin. A load estimation model is proposed as a comprehensive stand-alone model which uses the cabin geometry and material properties as its inputs. The model is implemented in a computer code applicable to arbitrary driving conditions. Using a lumped-body approach for the cabin, the present model is capable of estimating the thermal loads in mobile applications. By using this model, the pattern of upcoming changes in the comfort level can be predicted in real-time in order to intelligently reduce the overall air conditioning power consumption while maintaining driver thermal comfort.

With the focus of most relevant studies being on load estimations in buildings, the literature lacks a comprehensive model for vehicle air conditioning applications. The

customized model developed in this section can be adopted by the automotive industry for improving the control action of vehicle air conditioning systems.

2.1.1. Model Development

A lumped model is developed for calculation of thermal loads in vehicle cabins. The net load of the cabin is classified under nine different categories. The total load as well as each load category depend on various parameters and can either be positive (heating up the cabin) or negative (cooling down the cabin). The summation of all thermal loads forms the instantaneous cabin thermal load. The mathematical model is thus formulated as:

$$\dot{Q}_{Tot} = \dot{Q}_{Met} + \dot{Q}_{Dir} + \dot{Q}_{Dif} + \dot{Q}_{Ref} + \dot{Q}_{Amb} + \dot{Q}_{Exh} + \dot{Q}_{Eng} + \dot{Q}_{Ven} + \dot{Q}_{AC} \quad (2\text{-}1)$$

where $\dot{Q}_{Tot}$ is the total thermal load encountered by the cabin. $\dot{Q}_{Met}$ is the metabolic load. $\dot{Q}_{Dir}$, $\dot{Q}_{Dif}$, and $\dot{Q}_{Ref}$ are the direct, diffuse, and reflected radiation loads, respectively. $\dot{Q}_{Amb}$ is the ambient load. $\dot{Q}_{Exh}$ and $\dot{Q}_{Eng}$ are the exhaust and engine loads caused by the high temperature of the exhaust gases and the engine. $\dot{Q}_{Ven}$ is the ventilation load, and $\dot{Q}_{AC}$ is the thermal load provided by the air conditioning system.

Figure 2-1 schematically shows the various thermal load categories encountered in a typical vehicle cabin. Some of these loads cross the vehicle body plates while others are independent of the cabin surface elements. Each thermal load is calculated assuming a quasi-steady-state condition. Based on Eq. (2-1), load calculations can be performed at time steps during a simulation period. After every time step, all the load categories are added to update the cabin air temperature and surface element temperatures according to:

$$\Delta T_a = \frac{\dot{Q}_{Tot}}{m_a c_a + DTM} \Delta t \quad (2\text{-}2)$$

$$\Delta T_s = \frac{\dot{Q}_s}{m_s c_s} \Delta t \tag{2-3}$$

where ΔT_a and ΔT_s are the change in cabin and surface element temperatures at the current time step. DTM is the sum of all deep thermal masses, *i.e.*, the overall thermal inertia of all internal cabin objects other than air. These objects include the seats, the dash, etc. which are combined with the cabin air in the lumped model. Δt is the time step, m_a is the cabin air mass and c_a is the air specific heat. m_s and c_s are the mass and specific heat of each of the surface elements and $\dot{Q}_s = \dot{Q}_{s,Rad} + \dot{Q}_{s,Amb}$ is the total heat gain by a surface element consisting of the heat gain by radiation, $\dot{Q}_{s,Rad}$, and the heat gain from ambient, $\dot{Q}_{s,Amb}$.

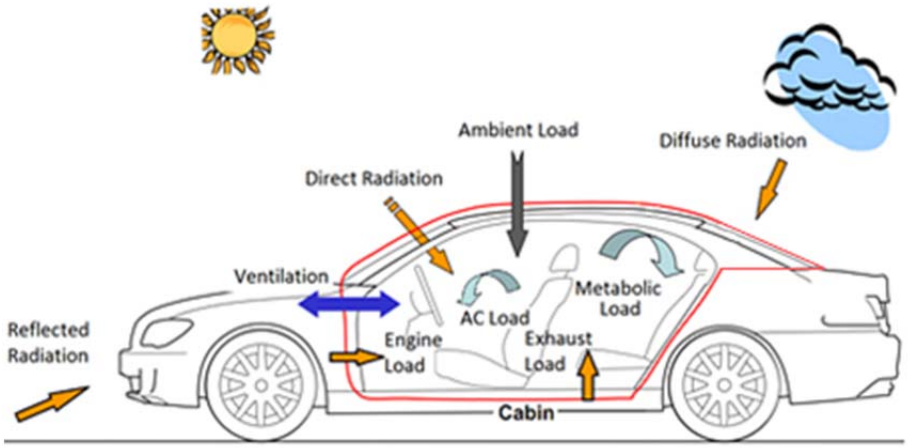

Figure 2-1: Schematic representation of thermal loads in a typical vehicle cabin. Reprinted with permission from SAE International [12]**.**

The detailed formulations for the calculation of each load category are described in the following:

Metabolic Load

Metabolic load is the heat generated by the human body. It is calculated by:

$$\dot{Q}_{Met} = \sum_{Passengers} \mathrm{M} A_{Du} \tag{2-4}$$

where M is the passenger metabolic heat production rate. It is found from the tabulated values in ISO 8996 [77] based on various factors such as occupation and activity level. For a driver and a sitting passenger, the values can be estimated as $85W/m^2$ and $55W/m^2$, respectively. The DuBois area A_{Du}, which is an estimation of the body surface area as a function of height and weight, is calculated by [77]:

$$A_{Du} = 0.202 W_p^{0.425} H_p^{0.725} \tag{2-5}$$

where W_p and H_p are the passenger weight and height, respectively.

Radiation Load

According to ASHRAE [9], the solar radiation heat can be categorized into direct, diffuse, and reflected. Direct radiation is the part of the incident solar radiation which directly strikes a surface element. It is calculated from:

$$\dot{Q}_{Dir} = \sum_{Surfaces} \tau A \dot{I}_{Dir} \cos\theta \tag{2-6}$$

where $\dot{I}_{Dir}$ is the direct radiation heat gain per unit area and θ is the angle between the surface normal and the sun position in sky. τ is the surface element transmissivity and A is the surface area, respectively. The direct radiation heat gain per unit area is found by:

$$\dot{I}_{Dir} = \frac{\mathrm{A}}{\exp\left(\frac{\mathrm{B}}{\sin\beta}\right)} \tag{2-7}$$

where A and B are constants tabulated in ASHRAE Handbook of Fundamentals [9] for every month. β is the altitude angle that is calculated based on position and time.

Diffuse radiation is the part of solar radiation which results from indirect radiation of daylight on the surface. During a cloudy day, most of the solar radiation is received in the form of diffuse radiation. The diffuse radiation heat gain is formulated as:

$$\dot{Q}_{Dif} = \sum_{Surfaces} \tau A \dot{I}_{Dif} \tag{2-8}$$

where $\dot{I}_{Dif}$ is the diffuse radiation heat gain per unit area which is calculated from:

$$\dot{I}_{Dif} = \Gamma \dot{I}_{Dir} \frac{1+\cos\Sigma}{2} \tag{2-9}$$

where Σ is the surface tilt angle measured from the horizontal surface and the values for Γ are tabulated in ASHRAE [9].

Reflected radiation consists of the part of radiation heat gain that is reflected from the ground and strikes the vehicle surface. The reflected radiation is calculated by:

$$\dot{Q}_{Ref} = \sum_{Surfaces} \tau A \dot{I}_{Ref} \tag{2-10}$$

$\dot{I}_{Ref}$ is the reflected radiation heat gain per unit area and is calculated from:

$$\dot{I}_{Ref} = \left(\dot{I}_{Dir} + \dot{I}_{Dif}\right) \rho_g \frac{1-\cos\Sigma}{2} \tag{2-11}$$

where ρ_g is the ground reflectivity coefficient. Based on the absorptivity of each particular surface element, a percentage of the incident radiation load is absorbed by that surface, hence increasing its temperature. The net absorbed heat of every surface element due to radiation is written as:

$$\dot{Q}_{s,Rad} = \alpha A\left(\dot{I}_{Dir}\cos\theta + \dot{I}_{Dif} + \dot{I}_{Ref}\right) \tag{2-12}$$

where α is the surface absorptivity.

Ambient Load

Ambient load is the part of heat transferred to the cabin air resulting from the temperature difference between the ambient and cabin air. External convection,

conduction through surface elements, and interior convection are involved in the total heat transfer between the ambient air and the cabin. The general form of the ambient load is calculated as:

$$\dot{Q}_{Amb} = \sum_{Surfaces} UA\left(T_s - T_a\right) \tag{2-13}$$

where U is the overall heat transfer coefficient of the surface element. T_s and T_a are the average surface temperature and average cabin temperature, respectively. U has different components consisting of the inside convection, conduction through the surface, and outside convection. The overall heat transfer coefficient is written as:

$$U = \frac{1}{R_{ti}} \quad , \quad R_{ti} = \frac{b}{2k} + \frac{1}{h_i} \tag{2-14}$$

for the internal side, and:

$$U = \frac{1}{R_{to}} \quad , \quad R_{to} = \frac{b}{2k} + \frac{1}{h_o} \tag{2-15}$$

for the external side. R_{ti} and R_{to} are the inside and outside total thermal resistances for a unit surface area. h_o and h_i are the outside and inside convection coefficients, k is the surface thermal conductivity, and b is the thickness of the surface element. The convection coefficients h_o and h_i depend on the orientation of the surface and the air velocity. Here, the following estimation is used to estimate the convection heat transfer coefficients as a function of vehicle speed [34]:

$$h = 0.6 + 6.64\sqrt{Vel} \tag{2-16}$$

where h is the convection heat transfer coefficient and Vel is the vehicle velocity. Despite its simplicity, this correlation is applicable in many practical automotive problems [29]. The cabin air is assumed stationary and the ambient air velocity is considered equal to the vehicle velocity.

Similar to radiation, a portion of the ambient load is absorbed by the vehicle body. Thus, the net absorbed heat is written as:

$$\dot{Q}_{s,Amb} = UA\left(T_o - T_s\right) - UA\left(T_s - T_a\right) = UA\left(T_o - 2T_s + T_a\right) \tag{2-17}$$

where T_o, T_a, and T_s are the ambient, cabin, and surface average temperatures, respectively.

Exhaust Load

Conventional and hybrid electric vehicles have internal combustion engines that create exhaust gases. The exhaust gas temperature can reach as high as $1000°C$ [78]. Because of this high temperature, some of the exhaust heat can be transferred to the cabin. Considering A_{Exh} as the area of the bottom surface in contact with the exhaust pipe, the exhaust heat load entering the cabin is written as:

$$\dot{Q}_{Exh} = UA_{Exh}\left(T_{Exh} - T_a\right) \tag{2-18}$$

where U is the overall heat transfer coefficient of the surface element in contact with the exhaust pipe and it is calculated by Eq. (2-14). A_{Exh} is the surface area exposed to the exhaust pipe temperature and T_{Exh} is the exhaust gas temperature. The temperature of the exhaust gases in Celsius degrees is estimated by [34]:

$$T_{Exh} = 0.138RPM - 17 \tag{2-19}$$

where RPM is the engine speed in revolutions per minute.

Engine Load

Similar to the exhaust load, the high-temperature engine of a conventional or hybrid vehicle can also contribute to the cabin heat gain. The following formulation is used for calculating the engine thermal load:

$$\dot{Q}_{Eng} = UA_{Eng}\left(T_{Eng} - T_a\right) \tag{2-20}$$

where U is the surface overall heat transfer coefficient in contact with the engine and A_{Eng} is the surface area exposed to the engine temperature. The overall heat transfer is calculated by Eq. (2-14). T_{Eng} is the engine temperature and is estimated in Celsius degrees using [34]:

$$T_{Eng} = -2\times10^{-6} RPM^2 + 0.0355 RPM + 77.5 \tag{2-21}$$

Ventilation Load

Based on psychrometric calculations, the ventilation heat gain consists of both sensible and latent loads. To account for both these terms given a known ventilation air flow rate, the amount of ventilation heat gain is calculated from:

$$\dot{Q}_{Ven} = \dot{m}_{Ven}\left(e_o - e_i\right) \tag{2-22}$$

where $\dot{m}_{Ven}$ is the ventilation mass flow rate and e_o and e_i are the ambient and cabin enthalpies, respectively. The enthalpies are calculated from [79]:

$$e = 1006T + \left(2.501\times10^6 + 1770T\right)X \tag{2-23}$$

where T is the air temperature and X is the humidity ratio. The humidity ratio is calculated as a function of relative humidity from:

$$X = 0.62198\frac{\phi P_s}{100P - \phi P_s} \tag{2-24}$$

where ϕ is the relative humidity, P is the air pressure, and P_s is the water saturation pressure at temperature T .

AC Load

The Air Conditioning (AC) system compensates for the heat gains so that the cabin temperature remains within the acceptable comfort range. In cold weather conditions, positive AC load (heating) is required for the cabin. Inversely, in warm

weather conditions, negative AC load (cooling) is needed for maintaining the comfort conditions. The actual load delivered by the AC system depends on the system parameters and working conditions. In this work, it is assumed that an AC (or heat pump) cycle is providing the thermal load calculated by:

$$\begin{aligned}\dot{Q}_{AC} = &-\left(\dot{Q}_{Met} + \dot{Q}_{Dir} + \dot{Q}_{Dif} + \dot{Q}_{Ref} + \dot{Q}_{Amb} + \dot{Q}_{Exh} + \dot{Q}_{Eng} + \dot{Q}_{Ven}\right) \\ &-\left(m_a c_a + DTM\right)\left(T_a - T_{comf}\right)\Big/ t_c\end{aligned} \tag{2-25}$$

T_{comf} is the target comfort temperature as described and widely used by ASHARE Standard 55 [80]. It is the target cabin temperature which is considered comfortable at the conditions under consideration. t_c is the pull-down time constant. Using Eq. (2-25) for the AC load, the pull-down time constant is calculated from:

$$t_c = \frac{t_p}{\ln\left|T_0 - T_{comf}\right|} \tag{2-26}$$

where T_0 is the initial cabin temperature and t_p is the target pull-down time indicating the time required for the cabin temperature to reach the comfort temperature.

In practice, the actual AC load depends on the system design and operating conditions. For a given system, the load also changes depending on the compressor speed and fan speed. Equations (2-25) and (2-26) are used in this study as a guideline for analyzing the performance of an AC system in a typical vehicle. It shows that analyzing different scenarios with the AC cycle can help the efficient sizing and control of the air conditioning cycle.

2.1.2. Results and Discussion

The model is implemented in an in-house computer code in the C++ language. The simulation model is flexible and can be used for different cabin geometries, driving scenarios, and ambient conditions. An important part of thermal load estimations is the underlying database used for cabin geometry, materials, weather conditions, and driving cycles. In the present simulations, a simplified version of the cabin of eVaro, shown in

Fig. 2-2, is used for the dimensions. The eVaro is a hybrid electric vehicle designed and built by Future Vehicle Technologies [81]. The eVaro has one driver and one passenger seat which are positioned in tandem. Figure 4 shows the simplified geometry and dimensions of the cabin, as used for the simulations of this work.

Figure 2-2: A picture of the eVaro hybrid electric vehicle made by Future Vehicle Technologies (FVT). Reprinted with permission [81]**.**

Table 2-1 summarizes the properties assigned to different surfaces of the body. Surfaces 1 and 2 are assumed to be glass with $3\,mm$ thickness, while the other surfaces are taken to be a typical vehicle body with $10\,mm$ thickness. 10% of surface number 5 (front) is subject to the engine temperature, while 1% of surface number 4 (bottom) is assumed to be subject to the exhaust temperature.

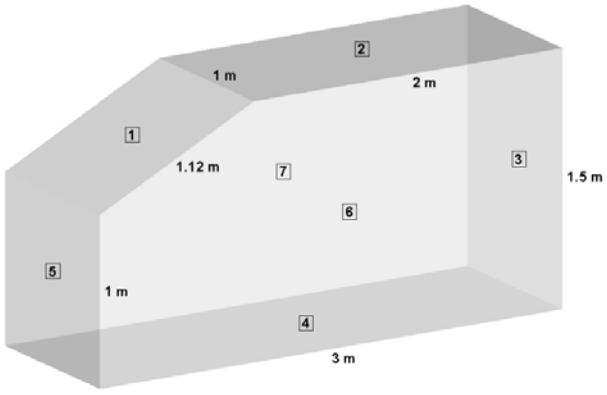

Figure 2-3: Schematic of the simulated cabin geometry. Reprinted with permission from SAE International [12]**.**

There are a number of standard driving cycles used in the auto industry as the basis for test and analysis. Among many, the Supplemental Federal Test Procedure (SFTP) or the US06 driving cycle [82] is used in this study. The driving cycle lasts 593 seconds. Therefore, it is repeated consecutively to cover longer driving ranges for the simulation period. Based on the gear changing according to the torque imposed on the wheels, the RPM values are estimated accordingly. The US06 driving cycle with the corresponding RPM values are provided in [12].

Table 2-1: Properties of the vehicle cabin body. Reprinted with permission from SAE International [12]**.**

Property	Glass	Body Plate
Thermal Conductivity, $k_w \left[W/mK\right]$	1.05	0.2
Density, $\rho_w \left[kg/m^3\right]$	2500	1500
Transmissivity, τ	0.5	0
Absorptivity, α	0.3	0.4
Specific Heat, $c_w \left[J/kgK\right]$	840	1000
Thickness, $b\left[mm\right]$	3	10

Two different driving conditions are simulated using the above-mentioned geometry and material properties. In both cases, the consecutively-repeated US06 driving cycle is used and actual weather data are collected and used for the specific date and time under consideration. The sky condition is assumed as mainly clear for both simulations. In real-time application of the model, the actual weather conditions can be obtained via wireless connection and a Global Positioning System (GPS) to determine more accurate results. In the following, the input parameters are shown for both simulated driving scenarios.

Driving Scenario 1

The specifications of driving scenario 1 are shown in Table 2-2. It is not efficient to use hot ambient air for ventilation when cooling is required. Therefore, a small amount of ventilation flow rate is assumed to account for the minimum fresh air requirements based on recommendations in [83] as well as the previously-mentioned leakages

calculated according to [84]. It should also be noted that this is an arbitrary scenario considered in this study to investigate the ventilation load. Realistically, the passenger has the option to change the ventilation rate.

The initial cabin temperature is selected at $80°C$ in this driving condition. This is because the soaked interior temperatures can reach very high values for a vehicle with closed windows parked under solar radiation. The vehicle is assumed to be driving approximately towards south. Figure 2-4 shows the random direction changes of the vehicle during the simulation time.

Table 2-2: Specifications for the first simulated driving condition. Reprinted with permission from SAE International [12]**.**

Specification	Value
Date	July 21, 2012
Local Time	13:00 to 16:00
Location	Houston, Texas
Driver Height, Weight	$1.7\ m$, $70\ kg$
Passenger Height, Weight	$1.6\ m$, $55\ kg$
Ventilation Flow Rate	$0.01\ m^3/s\ \ (21.2\ CFM)$
Ground Reflectivity	0.2
Ambient Temperature	$34.4°C$
Initial Cabin Temperature	$80°C$
Ambient Relative Humidity	70%
Cabin Relative Humidity	50%
Comfort Temperature	$23°C$
Pull-Down Time	$600\ s$
Deep Thermal Mass	$5600\ J/K$

Figure 2-5 shows the variation of cabin air temperature with time. The total heat gain in the cabin is also plotted. Negative heat values mean heat loss from the cabin, while positive values mean heat gains by the cabin. Figure 2-5 shows that the cabin temperature decreases from a soak temperature of $80°C$ to the comfort temperature after almost 10 minutes represented by the pull-down time. According to ASHRAE Standard 55 [80], the comfort level of the cabin temperature is within the range of $22°C$ to $24°C$ and the comfort range of relative humidity is between 40% and 60%. Thus, the

comfort temperature and cabin relative humidity are assumed to be $23°C$ and 50%, respectively. The cabin and ambient relative humidity values are assumed constant during the simulation period.

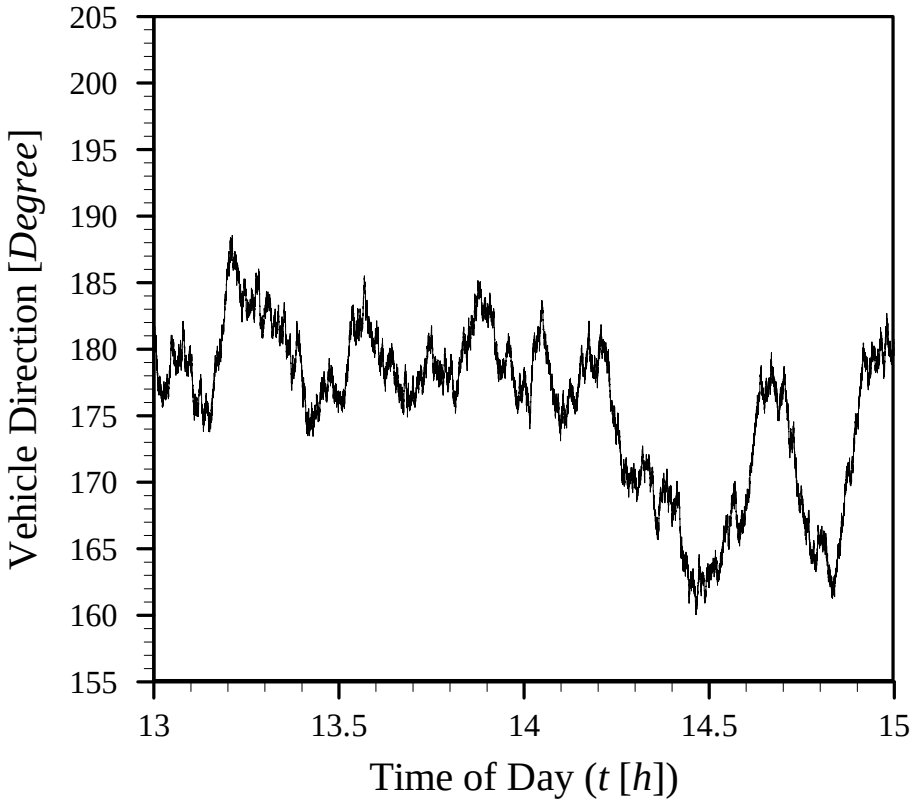

Figure 2-4: Driving direction for the simulated driving scenario 1. The directions are measured counter-clockwise from north. Reprinted with permission from SAE International [12]**.**

Without air conditioning, high cabin temperature is anticipated because of the small cabin volume, high metabolic heat generation, high radiation, and hot ambient conditions. During the pull-down period, the air conditioning system consumes more power and imposes a negative load on the cabin air to decrease the temperature down to $23°C$. After the pull-down period, a steady-state situation is achieved where the loads are balanced and a zero net load is maintained in the cabin for the rest of the simulation period.

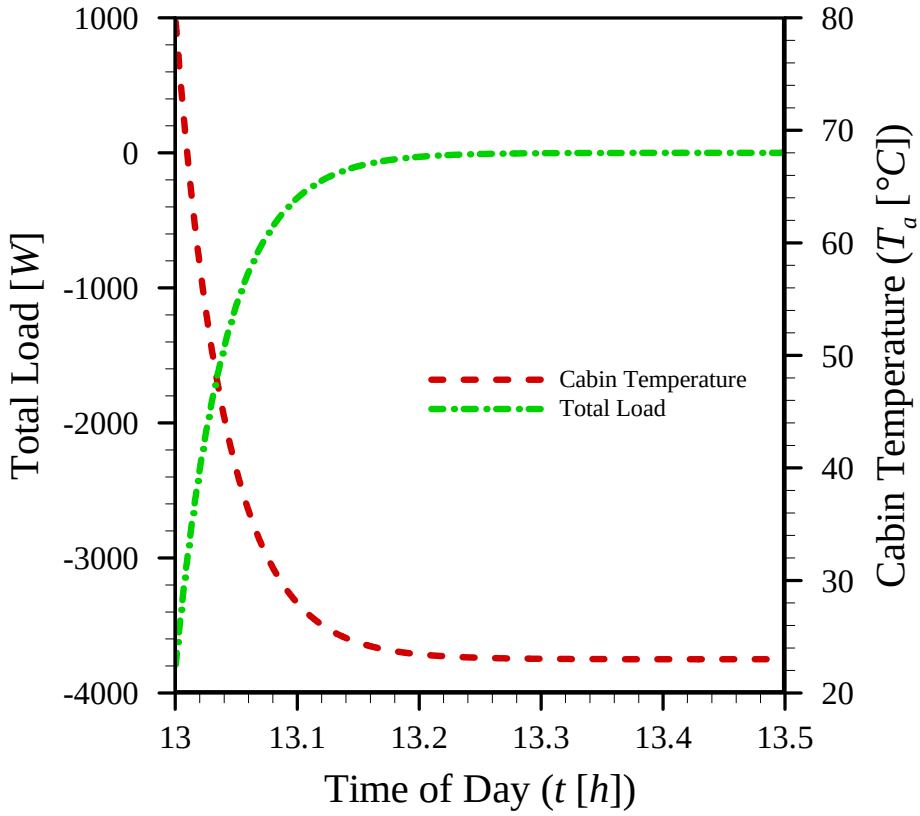

Figure 2-5: Total load and cabin temperature for the first half hour of driving scenario 1. Reprinted with permission from SAE International [12]**.**

Figure 2-6 shows the contribution of each load category on the net thermal load gained by the cabin. The engine, exhaust, and reflected radiation loads are negligible. It is concluded that, when seeking guidelines for reducing cabin heat gains in this driving condition, the engine, exhaust, and reflected radiation loads may be neglected from consideration. Khayyam et al. [35] also concluded that since proper insulation is used in most vehicles, the heat load from the engine and exhaust can be neglected in many cases. In such cases, the driving cycle will have an insignificant effect on the overall load estimation inside the cabin.

The direct and diffuse radiation loads, on the other hand, are important load categories that tend to impact the cabin temperature. It is observed that the direct radiation load decreases due to the decrease in the sun elevation angle for the simulation period, which happens after midday. Metabolic load is another positive load that is constant due to no change in the number of passengers. Ventilation and ambient loads are functions of the temperature difference between the cabin and ambient air.

During the first 5 minutes of simulation, the cabin temperature is higher than the ambient. This results in the negative starting values of these load categories. Once the cabin temperature reaches the steady condition, the warmer ambient air imposes almost constant positive ventilation and ambient loads.

The formula for the assumed AC load, Eq. (2-25), reaches a peak absolute value of around $3000\,W$ at the beginning of the scenario. After this time, the pull-down process of the cabin temperature finishes and the AC load reaches a balance with the rest of the loads. Then, the absolute AC load value gradually decreases since no more temperature pull-down is required and the contribution of the direct radiation load as a positive heat gain is decreasing as well.

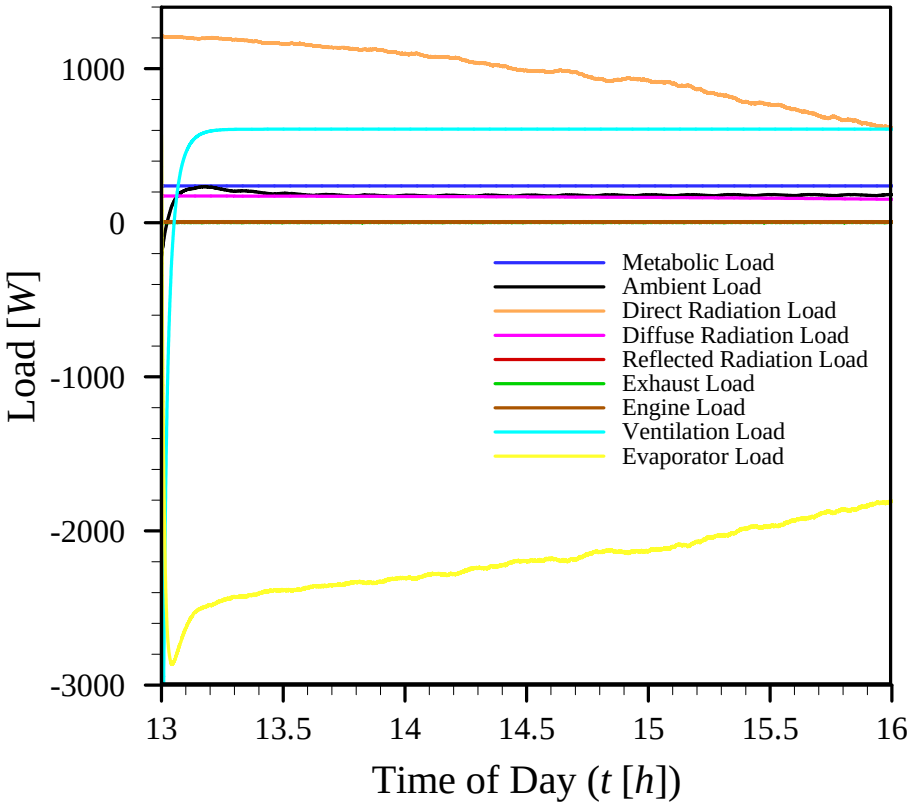

Figure 2-6: Simulated thermal load categories for driving scenario 1. Reprinted with permission from SAE International [12]**.**

Stegou-Sagia et al. [85] showed that there is room for saving AC energy in residential areas by using carefully selected glazing material. For a vehicle cabin, a predictive algorithm can be implemented in the vehicle AC controller to calculate the

loads in real-time. When the thermal loads are being estimated, the decision to decrease glazing transmissivity can be made and the cabin can be cooled down intelligently by keeping the radiation load from entering the cabin.

Figure 2-7 shows the advantage of using glazing transmissivity control on the vehicle glass within the accepted range of driving safety. The same driving condition is assumed, but with different glass transmissivity constants. Figure 2-7 reveals that by decreasing transmissivity from 0.8 to 0.5, the required AC power consumption can be reduced by up to 30%. This shows that, in a hot and sunny ambient condition, much of the AC fuel consumption can be saved by using an intelligent glazing system. In a cold and sunny weather condition, where the cabin should be heated up, solar radiation helps the AC loads. In that case, the AC controller should intelligently decide to increase glazing transmissivity, so the heating energy consumption is minimized by taking advantage of the free solar energy.

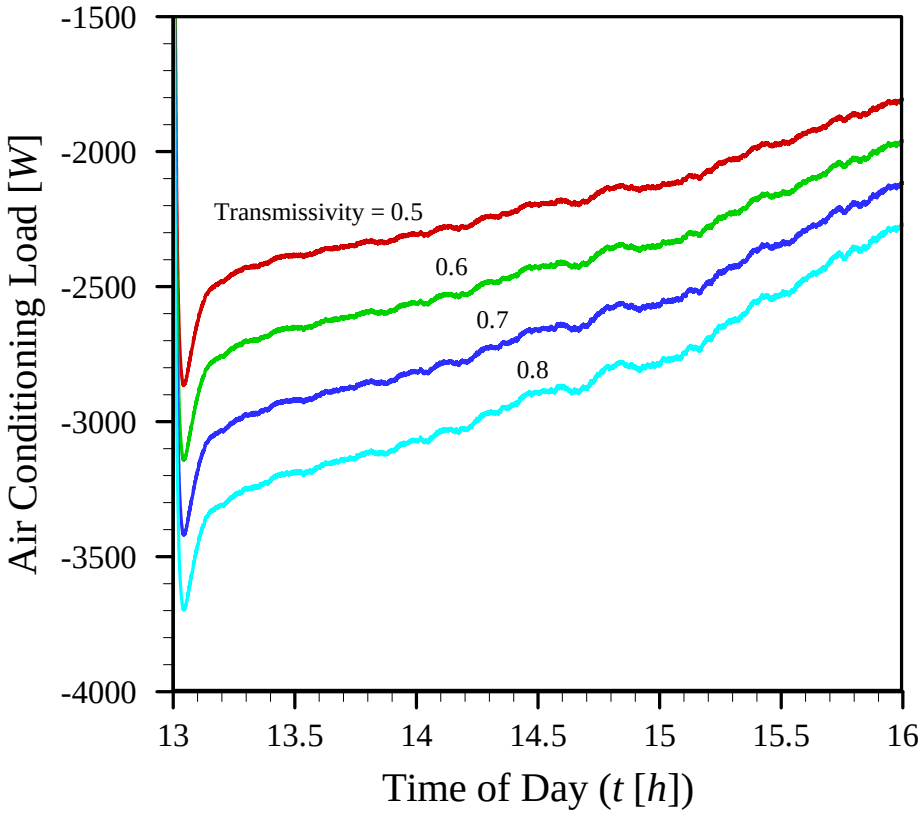

Figure 2-7: The required air conditioning load for maintaining comfort in driving scenario 1 with different glazing transmissivity values. Reprinted with permission from SAE International [12]**.**

Driving Scenario 2

Table 2-3 lists the specifications for driving scenario 2. Also in this scenario, it is not suitable to use cold ambient air for ventilation when heating is required. A small ventilation flow rate is thus assumed to supply the minimum fresh air requirement and leakages identified in the ventilation load model described above.

Table 2-3: Specifications for the second simulated driving condition. Reprinted with permission from SAE International [12]**.**

Specification	Value
Date	January 8, 2012
Local Time	4:00 to 7:00
Location	Toronto, Ontario
Driver Height, Weight	$1.8\,m$, $76\,kg$
Passenger Height, Weight	No Passenger
Ventilation Flow	$0.01\,m^3/s$ $\left(21.2\,CFM\right)$
Ground Reflectivity	0.2
Ambient Temperature	$-3.5°C$
Initial Cabin Temperature	$3°C$
Ambient Relative Humidity	85%
Cabin Relative Humidity	60%
Comfort Temperature	$23°C$
Pull-Down Time	$600\,s$
Deep Thermal Mass	$5600\,J/K$

In this driving scenario the vehicle is assumed to be driving approximately east. Figure 2-8 shows the random changes in the vehicle direction used as the simulation input. Figure 2-9 shows the variation of the cabin air temperature and net cabin load for driving scenario 2. In this driving scenario, the initial cabin temperature is below the comfort level of $23°C$. In this cold scenario, a positive net cabin load is provided to the cabin in order to increase its temperature up to the comfort level. After 10 minutes, the net heat load reaches zero, which means a balance has been reached between the AC load and the rest of the load categories. After that time, the cabin temperature is maintained at the comfort level.

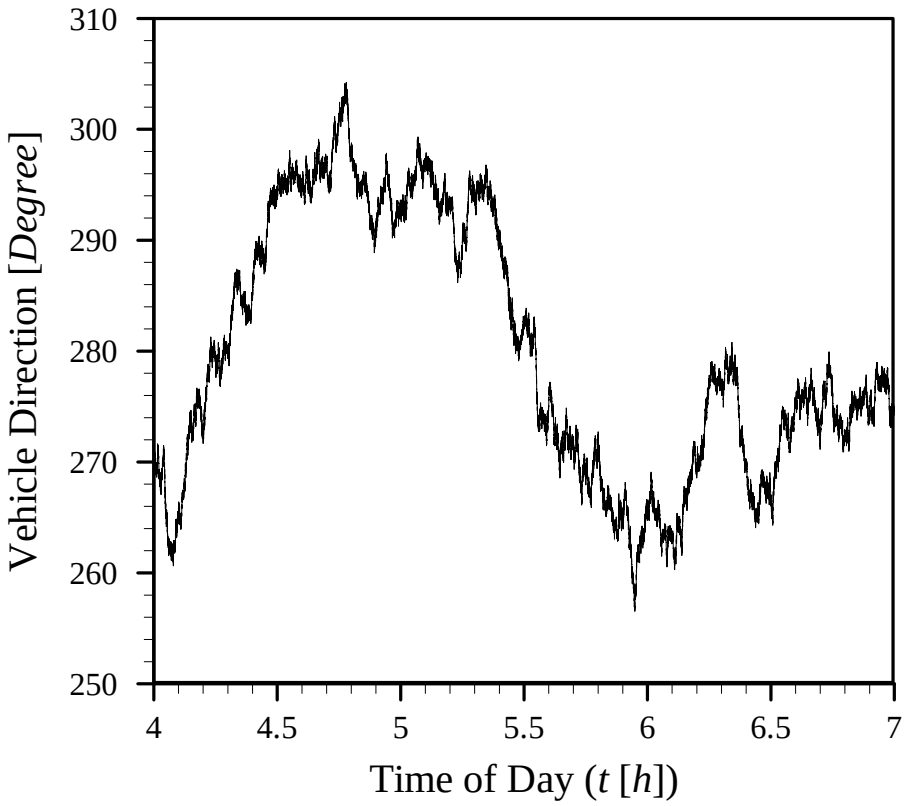

Figure 2-8: Driving direction for the simulated driving scenario 2. The directions are measured counter-clockwise from east. Reprinted with permission from SAE International [12]**.**

Figure 2-10 compares the contribution of each load category during the simulation period. Negative and positive loads are cabin heat losses and gains, respectively. In this driving scenario, the simulation period is before the local sunrise and thus, there is no contribution by the direct, diffuse, or reflected radiations. Also, the engine and exhaust loads are negligible as discussed in driving scenario 1.

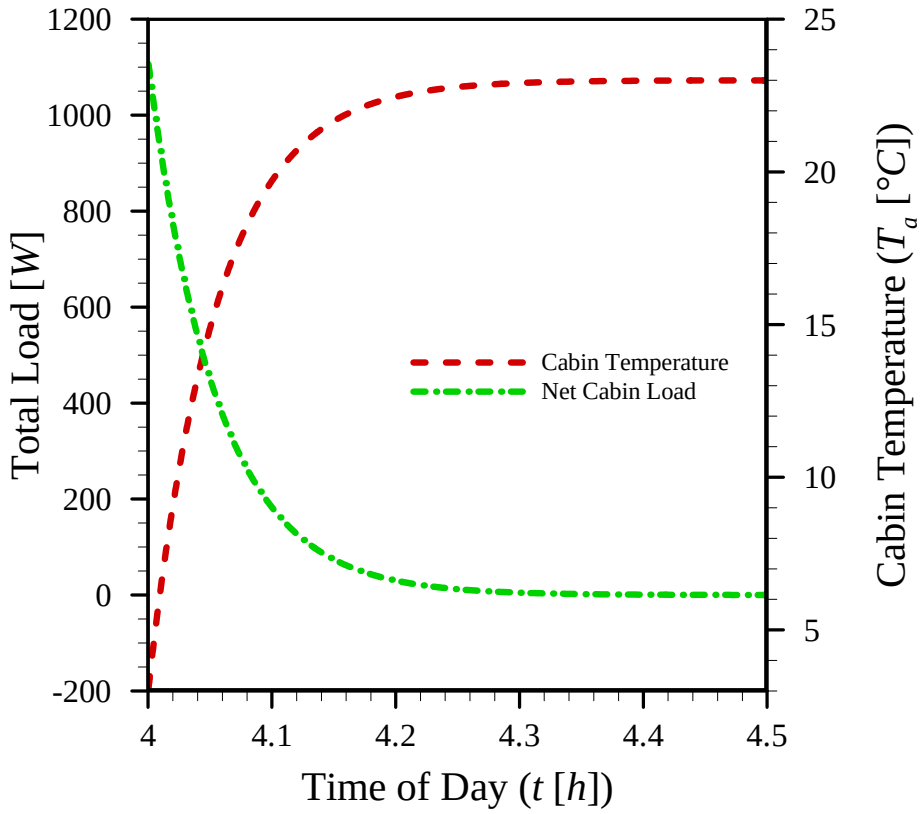

Figure 2-9: Total load and cabin temperature for the first half hour of driving scenario 2. Reprinted with permission from SAE International [12]**.**

Due to the cold ambient temperature of driving scenario 2, the ventilation and ambient loads have negative contributions to the cabin loads. This means that the cabin loses heat to the ambient air through these mechanisms. The positive metabolic load is not able to provide enough heat to keep the cabin temperature at the comfort level. Thus, a positive AC load of about $600\,W$ is required to maintain the comfort level.

As observed here, ventilation is causing a heat loss of more than $500\,W$ from the cabin in these cold conditions. This is definitely undesirable in terms of thermal comfort, but may be unavoidable due to leakages, fresh air requirements, or defogging.

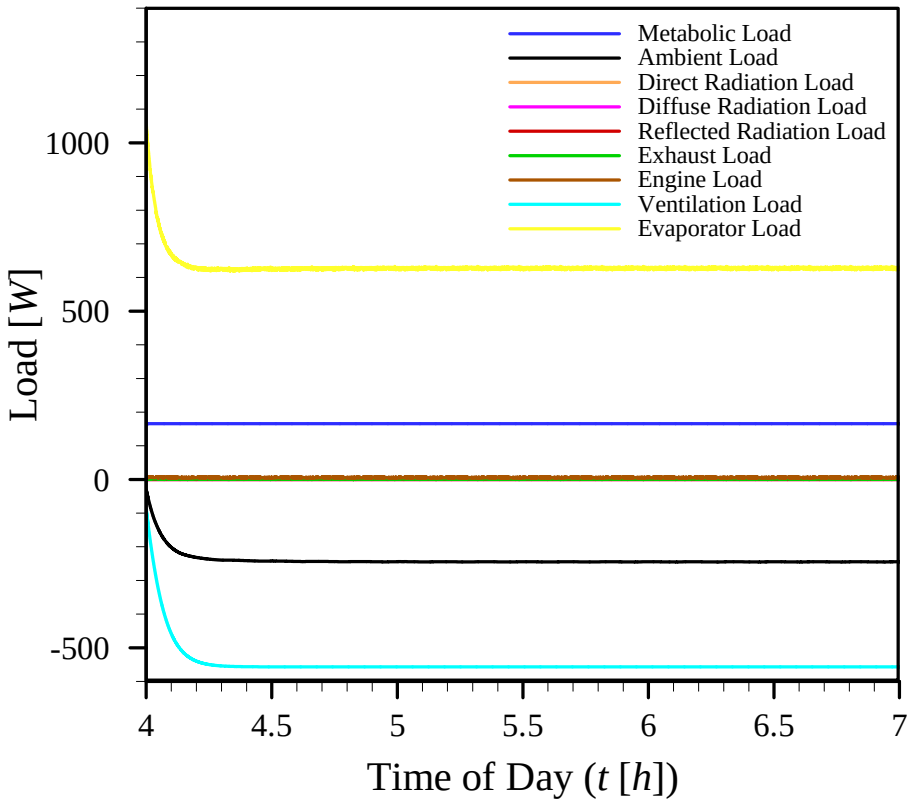

Figure 2-10: Simulated thermal load categories for driving scenario 2. Reprinted with permission from SAE International [12]**.**

2.1.3. Conclusions

In this section, the heat balance method was applied to a vehicle cabin to model the various heating and cooling loads transferred to the cabin via radiation, convection, and conduction. Mathematical models of the heat transfer phenomena were used to calculate the different load categories.

A comprehensive heat balance model was developed for usage in mobile air conditioning design. Mathematical load calculation models were devised and collected from various sources in the literature to create a comprehensive stand-alone model of load estimation. Quasi-steady-state and lumped-body assumptions were made and a constant time-stepping was performed by the computer simulation code. To perform case studies, specific material properties and the simplified geometry of a hybrid electric vehicle were considered. Two different scenarios were simulated to find the contribution of each load category to the overall heat gain. A standard driving cycle was applied in

the simulations for two different North American cities and the results were compared. Simulations of different driving scenarios showed that some load categories such as the engine, exhaust, and reflected radiation are often negligible, while others such as the ambient or ventilation load can play important roles in the variation of the cabin temperature.

The developed algorithm for load calculations in vehicles can be implemented in controllers to provide accurate feedback information. The knowledge of upcoming load variation patterns gives the controller the ability to adapt the system to future conditions. This adaption can lead to considerable improvements in the system's overall energy efficiency.

2.2. Walk-In Freezer Experimental Setup

In order to validate and implement the developed models of this thesis, an actual working freezer room was selected for experimental data collection. Since the selected setup is an actual working freezer, it was considered as a realistic testbed for validation and implementation of the models.

A freezer room of a restaurant in Surrey, British Columbia, Canada was studied during more than 5 months of normal operation. Figure 2-11 shows an inside view of the walk-in freezer as well as its schematic with inside dimensions. Information about the room dimensions, insulation properties, and stored products were carefully gathered for validating the models developed in this study and are listed in Table 2-4.

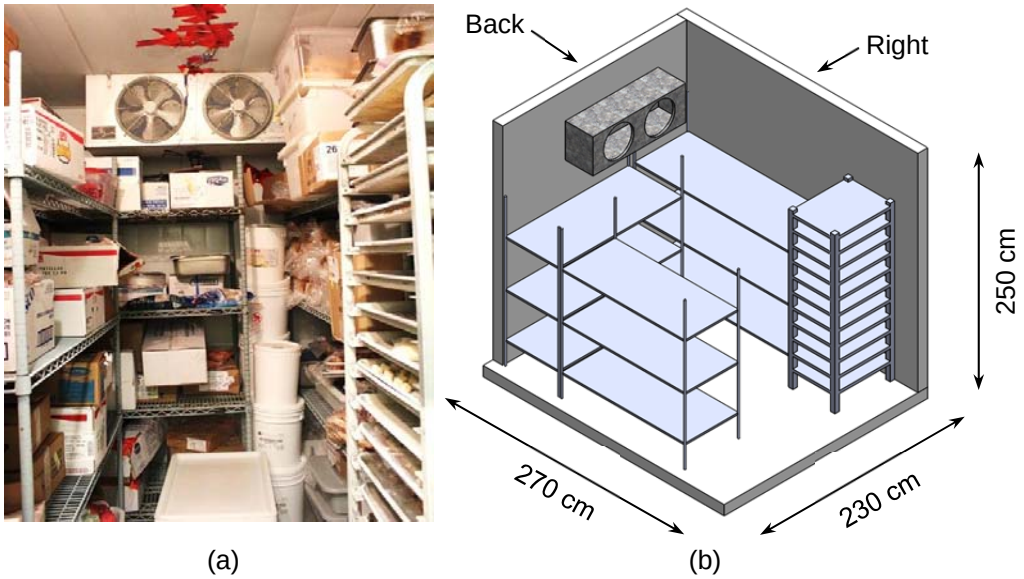

Figure 2-11: (a) Walk-in freezer room. (b) Freezer schematic with inner room dimensions. The front wall, left wall, and roof are omitted for clarity. Reprinted with permission [54], [65]**.**

The freezer temperature was measured over time using two different types of wireless temperature data loggers. For some measurements, high-accuracy temperature sensors (LOG-HC2-RC-US, Rotronic) with measurement accuracy of $\pm 0.1\,°C$ were installed in the freezer. For most measurements, low-accuracy temperature sensors (Track-It, Monarch Instruments) with measurement accuracy of $\pm 1.0\,°C$ were installed in several random locations on the freezer shelves.

It was observed that a non-uniformity of less than $\pm 2.5°C$ existed inside the room. Thus, either the measurements of one temperature sensor or the average of all sensors was assumed as the room bulk temperature.

Table 2-4 shows the dimensional, material, and thermal properties of the freezer room. Convection heat transfer coefficients were estimated using correlations from ASHRAE [9] for turbulent natural convection on the vertical and horizontal walls of the room. The ASHRAE coefficient of natural convection for air over a vertical wall is calculated from

$$h = 1.33\left(\frac{T_a - T_w}{H}\right)^{1/4} \tag{2-27}$$

where H is the wall height, T_a is the air temperature, and T_w is the wall surface temperature. The coefficient of natural convection for air over a horizontal surface is calculated from

$$h = K\left(\frac{g\beta_T \rho_a^2 k_a^3 c_a P_w}{\mu_a A}\left(T_a - T_w\right)\right)^{1/4} \tag{2-28}$$

where g is the gravitational constant, β_T is the volumetric coefficient of thermal expansion, ρ_a is the air density, k_a is the air thermal conductivity, c_a is the air specific heat, P_w is the wall perimeter, μ_a is the air dynamic viscosity, and A is the wall surface area. $K = 0.54$ for a cold surface facing down and $K = 0.27$ for a cold surface facing up.

Table 2-4: Dimensional, material, and thermal properties of the freezer room. Refer to Fig. 2-11 for wall locations. Reprinted with permission [54], [65]**.**

Quantity	Units	Wall No.					
		1	2	3	4	5	6
Location	-	Left	Back	Right	Front	Roof	Floor
Area, A	$\left[m^2\right]$	6.7	5.7	6.7	5.7	6.2	6.2
Outside convection coefficient, h_o	$\left[W/m^2°C\right]$	2.8	2.8	2.8	2.8	0.6	3.1
Inside convection coefficient, h_i	$\left[W/m^2°C\right]$	2.8	2.8	2.8	2.8	0.6	3.1
Total wall thickness, b	$\left[mm\right]$	110					
Insulation material	-	Polyurethane foam					
Wall thermal conductivity, k	$\left[W/m°C\right]$	0.05					
Wall density, ρ_w	$\left[kg/m^3\right]$	22					
Wall specific heat, c_w	$\left[kJ/kg°C\right]$	2.6					

The measured freezer room temperature for a period of 7 days is shown in Fig. 2-12. The freezer room is controlled by an on/off controller based on a pair of temperature set points, a low set point and a high set point. Consequently, the system produces cooling until the room temperature reaches the low temperature set point. Once the minimum temperature is reached, the thermostat shuts the refrigeration unit down. At this point, the decrease of the room temperature stops and the temperature begins to increase as a result of heat gains. Consequently, the temperature increases until it reaches the high temperature set point. Once the high set point is reached, the thermostat triggers the refrigeration unit to switch back on. The low and high temperature set points are settings of the room thermostat and they can also be inferred from the temperature measurements. By using the measured temperature at a location other than the thermostat, there can be a discrepancy between the actual thermostat set points and the apparent set points observed from the measurements. This is due to the temperature non-uniformity within the freezer, and, as a result, the set points may seem to vary. To keep the approach general for systems with the least available information, the apparent set points observed in the temperature data are used herein.

Investigating the temperature graph shown in Fig. 2-12, three patterns are noticeable: temperature swings, defrost cycles, and door openings.

Temperature Swings

Temperature oscillations or swings occur mainly due to the starts and stops of the refrigeration unit. The period of these oscillations in the freezer room is observed as approximately 20 minutes. Arrows point to regions with temperature swings in Fig. 2-12.

Defrosts Cycles

Rapid temperature increases are noticeable in some areas of Fig. 2-12. They are due to the occurrence of defrost cycles in the freezer. Defrosting is a process that melts the frost away from evaporator coils and is unavoidable for most systems. The defrost system can work either by heating the evaporator coils or turning off the system [86]. An automatic defrost system exists in the freezer room, which kicks in every 6 hours and heats up the evaporator coils to melt the frost. The defrost events, even though a

necessity, impose a huge amount of heat load on the freezer room, as seen by the sharp temperature increases in Fig. 2-12.

Door Openings

Also visible in the data are times when the freezer room door was open for significant periods of time. In Fig. 2-12, they are denoted by irregular and random-looking variations in the room temperature. Since the temperature is mostly above the set points, the condensing unit is constantly on during these periods. Door openings depend on the freezer usage pattern and are demarcated using brackets in Fig. 2-12. It is observed in Fig. 2-12 that the irregularities in the temperature pattern mostly occur during daytimes of the first 4 days of measurements, while the next 3 days mostly show swinging regimes and defrost spikes. It can be concluded that door openings and loading/unloading of goods in the freezer room considerably contribute to changes in the heat gain.

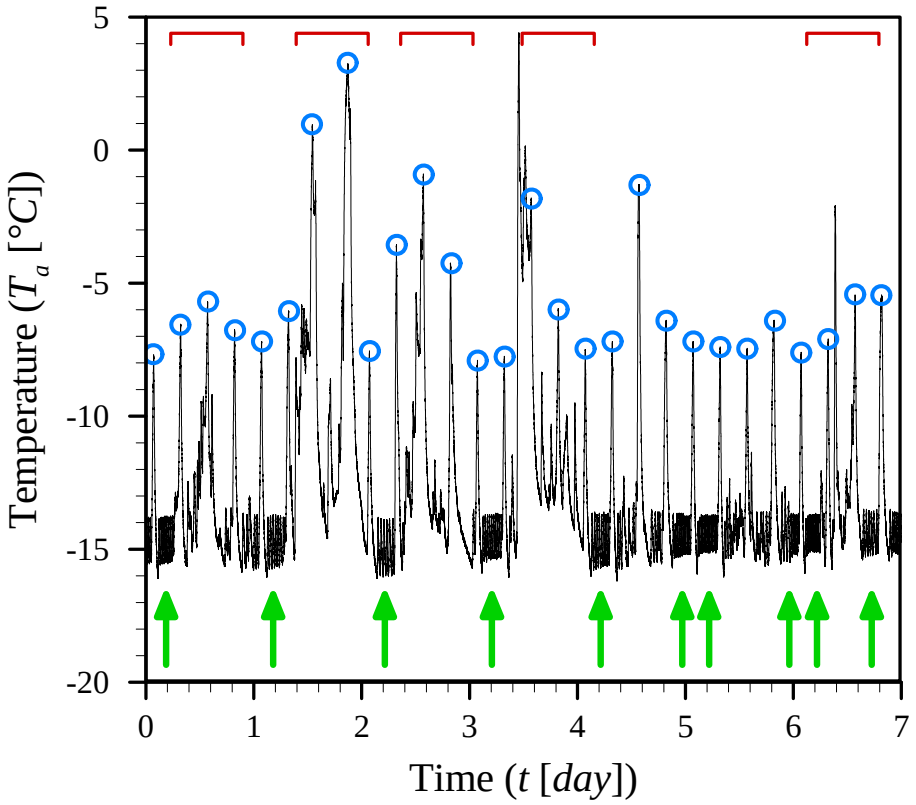

Figure 2-12: Average temperature in the freezer room. Arrows point to regions with noticeable temperature swings between the low and high set points. Brackets show door opening instances. Circles denote temperature spikes due to defrosts. Reprinted with permission [65]**.**

The experimental study presented above is used as the basis for validating and analyzing the models proposed in the following sections.

2.3. Resistance-Capacitance (RC) Modeling

Resistance-Capacitance (RC) modeling is a well-established concept used in heat transfer problems. In this section, an RC circuit representation of the freezer room of Section 2.2 is developed to simulate the thermal behavior of the room. Using the RC model, a parametric study is performed on various properties of the system. The effect of set points on the number of compressor starts per hour is also studied. The proposed technique provides an effective tool for facilitating the thermal modeling of air conditioned and refrigerated rooms. Using this approach, engineering calculations of cooling load can be performed with outstanding simplicity and accuracy.

2.3.1. Model Development

A lumped thermal model is developed based on the heat balance method applied to the freezer room of Section 2.2. The thermal model and its equivalent RC circuit are described in the following. The effectiveness of the RC modeling approach for simulating the thermal loads is presented through this study.

Thermal model

Following ASHRAE [9], the general equation of heat balance for the room temperature is

$$\dot{Q}_c + \dot{Q}_h = M \frac{dT_a}{dt} \tag{2-29}$$

where M is the room thermal inertia, T_a is the average room temperature, t is time, $\dot{Q}_c$ is the cooling power provided by the refrigeration system, and $\dot{Q}_h$ is the room heat gain. In general, the heat gain may consist of different components as follows:

- Direct heat gain: from electric equipment, human metabolic load, etc.
- Ambient heat gain: from heat transfer across walls
- Ventilation heat gain: from infiltration/exfiltration of room air
- Solar heat gain: from solar radiation on walls

The summation of the above heat gains equals the total heat gain. The instantaneous cooling power $\dot{Q}_c$ depends on various characteristics of the cooling cycle as well as the room. Assuming the ambient heat gain as the only available mechanism, the total heat gain is the summation of heat transfer across all walls:

$$\dot{Q}_h = \sum_{walls} \dot{Q}_w \tag{2-30}$$

where $\dot{Q}_w$ is the heat transfer rate across each wall. Applying the heat balance method, the heat flow across a wall crosses an outside convection resistance, a wall conduction resistance-capacitance, and an inside convection resistance. Thus, the following relationships hold:

$$\dot{Q}_w = h_o A\left(T_o - T_{wo}\right) = \frac{k}{b} A\left(T_{wo} - T_{wi}\right) + \rho_w bAc_w \frac{d\left(T_{wo} - T_{wi}\right)}{dt} = h_i A\left(T_{wi} - T_i\right) \qquad (2\text{-}31)$$

where h_o and h_i are the outside and inside convection coefficients, respectively. A is the wall surface area, k is the wall thermal conductivity, b is the wall thickness, ρ_w is the wall density, and c_w is the wall specific heat. T_o and T_i are the outside and inside temperatures, respectively. T_{wo} and T_{wi} are the temperatures on the outside and inside wall surfaces, respectively.

Thermal convection and conduction resistances are defined as $R_h = 1/hA$ and $R_k = b/kA$, respectively. Thermal inertia is defined as $M = mc$ where m is mass and c is specific heat. Specifically, thermal inertia is defined as $M_w = \rho_w bAc_w$ for the walls. Using these conventions, Eq. (2-31) is rewritten as:

$$\dot{Q}_w = \frac{T_o - T_{wo}}{R_{ho}} = \frac{T_{wo} - T_{wi}}{R_k} + M_w \frac{d\left(T_{wo} - T_{wi}\right)}{dt} = \frac{T_{wi} - T_i}{R_{hi}} \qquad (2\text{-}32)$$

Equation (2-29) should be solved for the heat balance analysis of the room using Eqs. (2-30) and (2-32) for the calculation of heat gains. The solution process is facilitated by considering the identical electric circuit described in the following.

RC Model

Simulating a thermal system using an RC model involves finding its equivalent electric circuit. Once the circuit is set up, the values of its components are found according to their corresponding thermal quantities. The temperature (T) in a thermal system is equivalent to the voltage (V) in an electric system while the heat flow rate ($\dot{Q}$) is the equivalent of the current (I). The thermal resistances (R_h and R_k) are equivalent to the electric resistance (R) and the thermal inertia (M) is equivalent to the electric capacitance (C). By appropriate selection of parameters, the governing equations of both thermal and electric systems are the same. Thus, the solution to the electric circuit is the same as the solution to its identical thermal problem. Using the following identities:

$$\dot{Q} = \frac{\Delta T}{R_h \text{ or } R_k} \quad \equiv \quad I = \frac{\Delta V}{R} \tag{2-33}$$

$$\dot{Q} = M_w \frac{dT}{dt} \quad \equiv \quad I = C_w \frac{dV}{dt} \tag{2-34}$$

we obtain the following equation:

$$I = \frac{V_o - V_{wo}}{R_o} = \frac{V_{wo} - V_{wi}}{R_w} + C_w \frac{d\left(V_{wo} - V_{wi}\right)}{dt} = \frac{V_{wi} - V_i}{R_i} \tag{2-35}$$

Equation (2-35) is the governing equation of the circuit shown in Fig. 2-13. Thus, Fig. 2-13 shows the equivalent electric circuit of a wall in a thermal system.

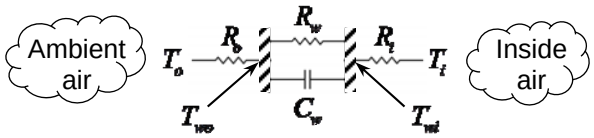

Figure 2-13: Analogous electric circuit of a wall heat balance using RC modeling. Reprinted with permission [54]**.**

The sub-circuit shown in Fig. 2-13 is a 3R1C representation of a wall. In this work, a 1C model is considered for the room air. Hence, the aggregate of the room air and the products stored in it are assumed to have a bulk thermal inertia represented by an analogous capacitance.

As demonstrated here, the methodology associated with RC modeling is general and can be applied to a wide range of HVAC-R applications. Once the RC network of a specific application is generated, it can be easily used for design, retrofit analysis, and parametric studies of the thermal system, with considerable ease and accuracy. In the following section, a case study is performed on a refrigeration application and the RC modeling results are compared with experimental measurements.

2.3.2. Results and Discussion

The proposed RC modeling technique is demonstrated based on experiments on the walk-in freezer room of Section 2.2. In this study, the focus is on the temperature swings of the freezer and a model is developed for cooling load simulation during these periods. The studied freezer is indoors and there is negligible solar radiation on it. There is no significant source of direct heat in the room and human metabolic load is only imposed to the system during door openings. During temperature swings, the freezer door is closed and the amount of infiltration/exfiltration of air is negligible. Hence, the only available heat source in the studied time periods is the ambient heat gain, which is in compliance with the assumption made in the model development. Other heat gain mechanisms can later be added to the model in order to include the door opening and defrost loads.

An RC model of the freezer room is prepared as demonstrated in Fig. 2-14. Figure 2-14 also shows the value of the circuit components according to their definitions and the properties presented in Table 2-4. In the main body of the circuit, 6 parallel wall blocks (Fig. 2-13) are considered. Each of the 6 wall branches in the circuit represents one of the freezer walls. In series to the 6-layer block, a capacitor C is inserted that represents the overall thermal inertia M of the air and products in the freezer.

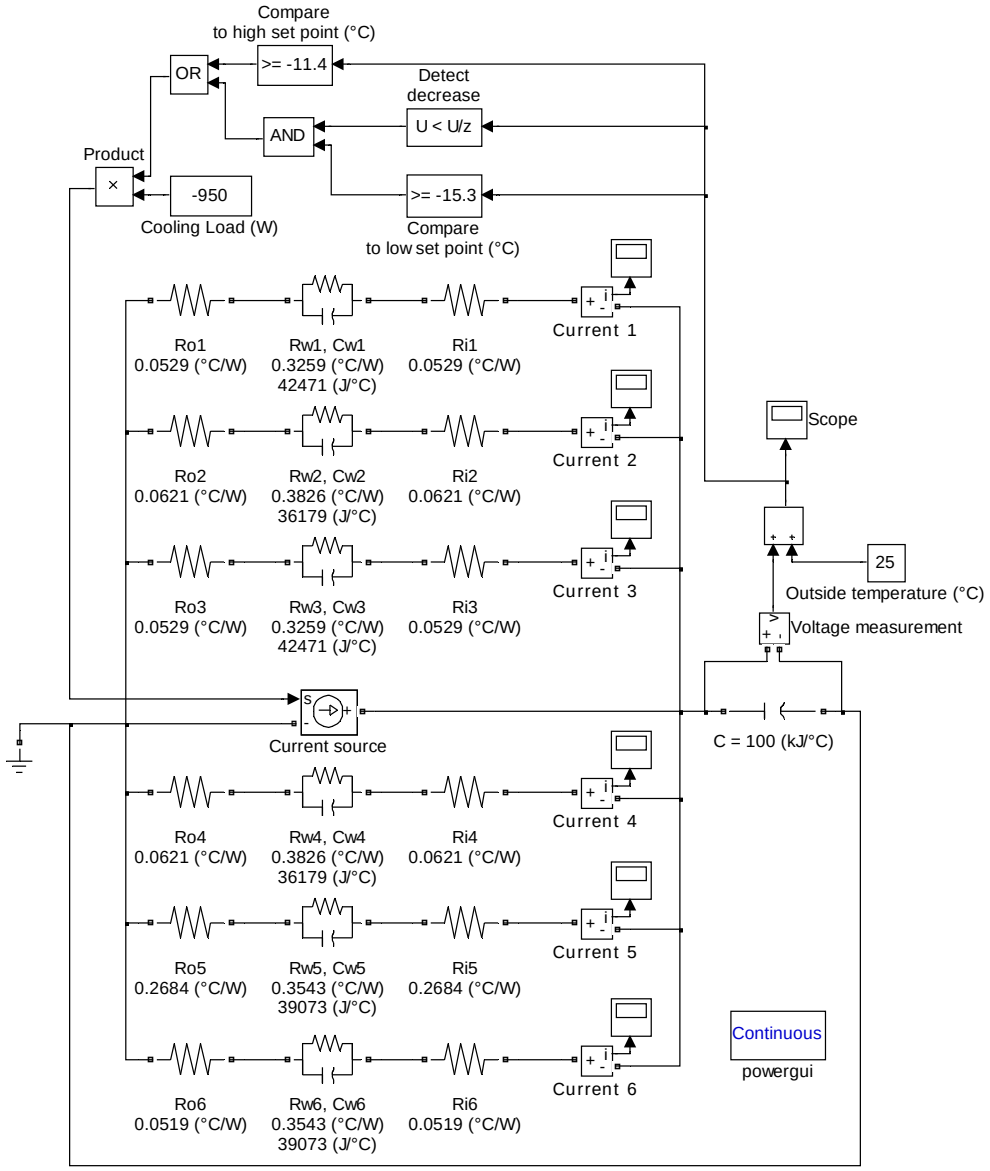

Figure 2-14: RC model of the refrigeration system. 3R1C and 1C models are used for the walls and the room, respectively. Reprinted with permission [54]**.**

The room air and its products have an estimated overall thermal inertia of $100 kJ/°C$. This value is calculated based on the controlled quantity of the products left in the freezer during the experiments pertaining to this model. By multiplying the mass of each product by its estimated specific heat and summing up all of the freezer contents, the total thermal inertia is estimated. The thermal inertia of the room envelope is not included in this value, since it is considered in the corresponding wall capacitors.

Assuming a combined mass of $100\,kg$ for the miscellaneous objects including the evaporator coils and shelves, and using an average specific heat of $0.6 kJ/kg°C$ for the metallic components, the total miscellaneous thermal inertia is calculated as $60 kJ/°C$.

The voltage difference between the two sides of the capacitor C represents the difference between the freezer and ambient temperatures. According to the measurements, the ambient temperature is kept at a value of $25 \pm 1°C$ during the period under consideration. This value is added to the aforementioned temperature difference in the circuit. According to the manufacturer information and analysis of the refrigeration unit, it is estimated that the refrigeration cycle provides an average amount of $\dot{Q}_c = 950W$ cooling capacity to the room when the temperature is near the set point values.

Because of the mostly uniform temperature inside the freezer, the temperature measurements of one of the sensors are assumed as the room bulk temperature. Therefore, the apparent low and high set points are deduced based on the measurements at that sensor's location. Based on the measurements, the low set point is perceived as $-15.3°C$, while the high set point is found approximately equal to $-11.4°C$.

Between the 6 parallel RC blocks, a current source that represents the cooling load provided by the refrigeration system is inserted. Since the cooling load does not cross any wall and is directly transferred to the room, this heat source is implemented parallel to the walls. The current direction is shown towards the room. Therefore, a negative cooling load is considered for this source.

In this study, the ventilation load due to door openings is not considered. In a future study, further information on the occurrence of door openings and their duration can be incorporated in the model. Those data can be inserted in appropriate correlations to find the total ventilation heat gain imposed to the system in each door opening occurrence. Furthermore, the radiation loads can also be incorporated in the model as another mode of heat gain into the room. In that case, the ventilation and radiation heat gains can be simply added to the "current source" included in the middle of the RC model of Fig. 2-14.

The operational logic of the cooling cycle is implemented in the RC model shown on the top part of Fig. 2-14. MATLAB Simulink [87] is used to implement and solve the RC model. The transient solution is solved using the software and the results are compared to measured freezer temperatures.

The transient solution of the RC model shown in Fig. 2-14 is compared to the temperature measurements inside the freezer room. Figure 2-15 shows a comparison between the present model and the measured temperature during 200 minutes of the freezer operation. During the simulated period of Fig. 2-15, the freezer door is not open and the temperature is already within the range of the set points. This condition covers most of the service period of many refrigeration rooms.

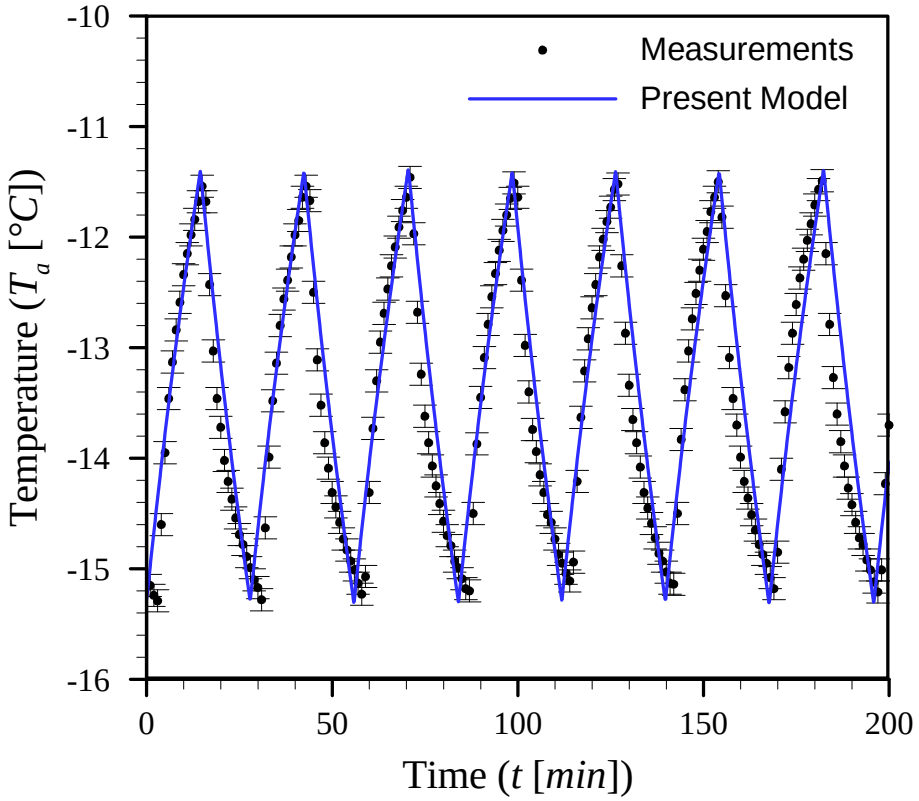

Figure 2-15: RC model results compared to the measured freezer temperature during 200 minutes of its operation. A maximum discrepancy of less than $1°C$ between the measurements and the RC model is observed. Reprinted with permission [54]**.**

The uncertainty of the experimental results shown in Fig. 2-15 is less than $0.1°C$ according to the manufacturer's datasheet of the temperature sensors (LOG-HC2-RC-

US, Rotronic). The maximum discrepancy between the measurements and the RC model is less than $1°C$. Therefore, the RC model shows a good agreement with the freezer temperature measurements.

Degradation of thermal insulation materials is a serious issue in long-term applications. Polyurethane insulators are prone to degradation, which decreases their thermal resistivity over time. The present model is used to study the effect of thermal degradation on the overall energy consumption of the freezer. Figure 2-16 shows the freezer temperature during 40 minutes of its operation. The walls thermal conductivity is varied from $k = 0.05 W/m°C$ to $k = 0.10 W/m°C$. As demonstrated in Fig. 2-16, an instant of temperature swing can be divided into a heat-gain portion when the temperature increases due to heat gains and a pull-down portion when the temperature decreases due to the cooling system's operation. During the heat-gain period, the cooling cycle is off and it consumes no energy. On the other hand, during the pull-down period, the cooling cycle is on and provides a cooling load of $\dot{Q}_c = 950W$ to the freezer. The ratio of the pull-down time to the total swing time is defined as:

$$r = \frac{\text{Pull-down time}}{\text{Swing time}} \tag{2-36}$$

where r is the pull-down time ratio. The swing time is defined as the total time between two consecutive low set points in the temperature diagram, as indicated in Fig. 2-16. The cooling time ratio r represents the portion of time that the refrigeration cycle is on and produces cooling effect. By multiplying the cooling time ratio by the instantaneous cooling load, the net cooling effect $\dot{Q}_{Net}$ is calculated as:

$$\dot{Q}_{Net} = r\dot{Q}_c \tag{2-37}$$

The net cooling effect $\dot{Q}_{Net}$ is the average cooling power provided by the refrigeration cycle during temperature swings. Since the overall power consumption of the cooling cycle is directly proportional to the provided net cooling effect, higher values of $\dot{Q}_{Net}$ result in higher energy consumption by the entire system.

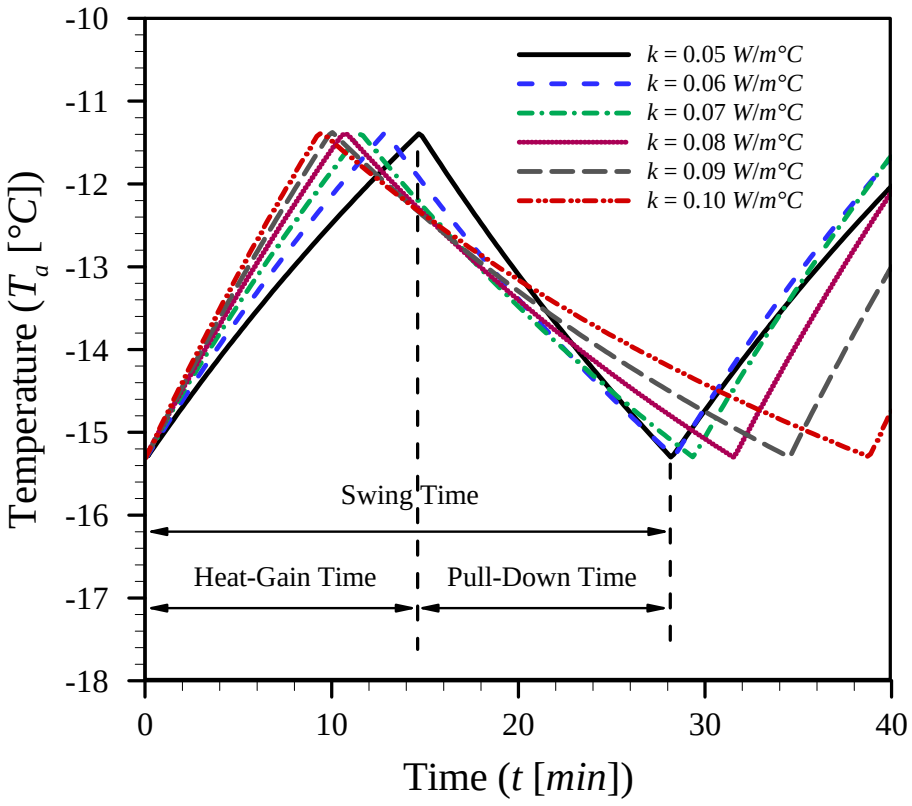

Figure 2-16: Effect of wall thermal conductivity (k) degradation on temperature swings in the freezer room. Reprinted with permission [54]**.**

Table 2-5 shows the cooling time ratio (r) for different wall conductivities (k) and their corresponding net cooling effects ($\dot{Q}_{Net}$). The power consumption increase in Table 2-5 shows the percentage of increase in the average refrigeration power due to insulation degradation compared to the current condition, i.e., walls with $k = 0.05 W/m°C$. As shown in Table 2-5, a reduction of 20% in the walls' thermal resistivity from the current value can increase the energy consumption rate by 14.87%. When the walls thermal resistivity reduces to half, a considerable power consumption increase of 57.05% is expected. Thus, there is a tremendous opportunity in replacing the wall insulation regularly and the insulation cost can be paid off by the decrease in wasted energy during freezer operation. The RC model is beneficial for estimating the power loss which can be used as a criterion for the timing of insulation renewals.

Table 2-5: Comparison of the required net cooling effect for different freezer wall thermal conductivity values. Reprinted with permission [54]**.**

Wall Thermal Conductivity $k\,[W/m°C]$	Pull-Down Time Ratio r	Net Cooling Effect $\dot{Q}_{Net}\,[W]$	Power Consumption Increase $[\%]$
0.05	0.48	457	0
0.06	0.55	525	15
0.07	0.61	576	26
0.08	0.66	628	37
0.09	0.71	674	48
0.10	0.76	717	57

Figure 2-17 shows the effect of different set point values on the temperature swing pattern of the freezer during 40 minutes of its operation. When the set points are narrow, i.e., the values of the high and low set points are close to each other, the frequency of the oscillations is high and the swing time is low. As shown in Fig. 2-17, 3 different set point pairs are studied. All set point pairs are mirrored around the same average temperature, $T_a = 13.35°C$. The swing time is again defined as the total time between two consecutive low set points in the temperature diagram. The maximum temperature deviation for each set point pair is defined as the absolute difference between the average temperature and the high or low set point.

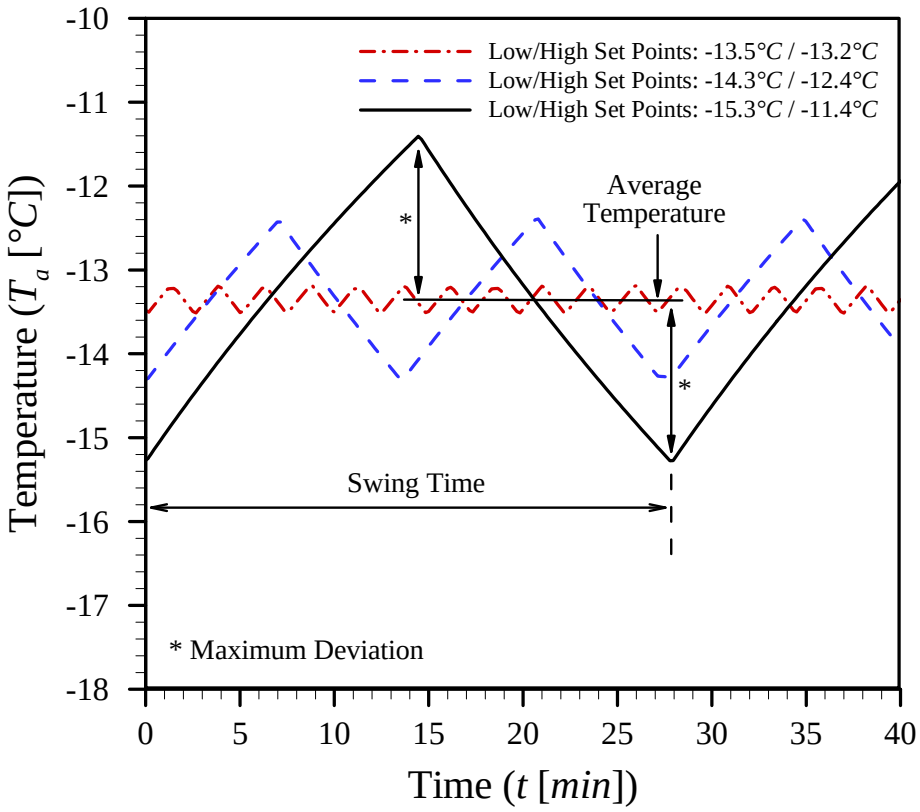

Figure 2-17: Effect of set points on temperature swings in the freezer room. Reprinted with permission [54]**.**

Table 2-6 demonstrates a comparison of the swing time for different set points. The maximum temperature deviation is also shown in Table 2-6. Generally, it is required that the product temperatures remain constant at the design level and deviations from the average value are not desirable. To achieve lower temperature deviations, narrower set point pairs can be implemented in the freezer thermostats and the products will experience less temperature variation as a result. A drawback of using narrow set point pairs is that the swing time decreases as well. This results in an increased number of compressor starts per hour. Compressor manufacturers normally recommend a limited number of starts per hour to assure proper operation during the designed lifetime of the compressor. Furthermore, compressors draw a high amount of energy at every start-up. This increased power draw also increases the overall power consumption of the refrigeration system. Thus, it is required to keep the number of compressor starts within a certain limit.

Table 2-6 shows that by changing the set points, the maximum temperature deviation can be reduced to $0.3°C$, but the swing time would decrease to 2.59 minutes and an average of 24 compressor starts per hour would be required. Nevertheless, the system can be allowed to have 14 compressor starts per hour to provide a maximum temperature deviation of less than $1°C$. The RC model can be an advantageous tool for predicting the temperature variation pattern for various set point pairs and helps estimate the trade-off between the maximum temperature deviation and the number of compressor starts per hour.

Table 2-6: Comparison of swing time and temperature deviation for various set points. Reprinted with permission [54]**.**

Low/High Temperature Set Points $[°C]$	Swing Time $[min]$	Compressor Starts per Hour $[1/h]$	Maximum Temperature Deviation $[°C]$
-13.5 / -13.2	2.59	23.17	0.3
-14.3 / -12.4	13.5	4.44	0.95
-15.3 / -11.4	27.86	2.15	1.95

2.3.3. Conclusions

In this section, an RC model was developed that used a representative network of electric resistors and capacitors to accurately simulate the thermal behavior of HVAC-R systems in real-time. The freezer room of Section 2.2 was used as the validation testbed. Corresponding thermal parameters were introduced and combined to design the analogous RC circuit. The model was validated by actual freezer temperature measurements. The present RC model has the following features:

- Real-time simulation capability
- Unsophisticated mathematical algorithms
- One RC circuit for an entire system
- Validated with experimental data
- Usable for retrofit analysis

The proposed RC model proved to be an effective tool for facilitating thermal modeling as well as acquiring accurate predictions of the system behavior in real-time.

The room heat gain was estimated using the model. A parametric study was performed on the effect of insulation degradation on the net power consumption by the refrigeration cycle. It was shown that 20% degradation of the insulation can result in around 15% of increase in the net power consumption by the cooling cycle. The effect of set points on the number of compressor starts per hour was also studied and it was shown that narrow set points can result in a steady temperature pattern in exchange for a high number of compressor starts per hour. Using the RC modeling methodology, engineering calculations of cooling load in HVAC-R applications can be performed with outstanding simplicity and accuracy.

Chapter 3. Data-Driven Methods

Conventional methods of thermal load calculation and control have pushed engineering designs forward for the best part of the last century. However, as inexpensive sensors and on-site computational resources are becoming available in recent years, more innovative methods are being put in to practice for overcoming the difficulties associated with the conventional methods. An important category of such innovative methods is called data-driven methods. These models acquire the system's operational data by various sensors and provide thermal load and comfort calculations accordingly. Intuitively, since real-time data are fed to such algorithms, they are able to provide more reliable estimations compared with law-driven calculations that are performed before the system's design and installation. Using such data-driven methods, the overall energy efficiency of air conditioning and refrigeration systems can be improved while the same level of thermal comfort is provided.

In this chapter, a method is proposed for real-time estimation of a room's thermal inertia and heat gain. Furthermore, a detailed thermal analysis of the room with an increased number of sensors is considered and a method is proposed for automatic estimation of wall heat transfer coefficients. Finally, the opportunities for increasing the energy efficiency of conventional on/off controllers, by merely changing the high and low set points to optimized values, are investigated. The technologies developed in this chapter can be used to intelligently acquire real-time thermal load estimations and improve the overall energy efficiency of HVAC-R systems accordingly.

3.1. Thermal Inertia and Heat Gain Calculation

In this section, an inverse method is proposed for acquiring an estimation of thermal inertia and heat gains in air conditioned and refrigerated systems. The developed model is validated by measurements in a freezer room. The simplicity of the

model together with its small number of required sensors is a major advantage of the proposed method for adoption in novel air conditioning and refrigeration systems.

3.1.1. Model Development

A lumped thermal model of the freezer room of Section 2.2 is used to develop an inverse model for estimating the thermal inertia and heat gain. Following a data-driven approach, the freezer room is assumed to be a black box about which little information is available. In contrast to forward approaches, the objective in an inverse method is to determine the thermal characteristics of the freezer room based on available experimental data. A lumped or zero-dimensional thermal model can be described by two characteristics of the freezer enclosure: 1) total thermal inertia, and 2) total instantaneous heat gain. The net thermal energy transferred to the room contributes to its temperature variation. Therefore, the cooling load provided by the refrigeration system satisfies the following heat balance equation:

$$\dot{Q}_c + \dot{Q}_h = M \frac{dT_a}{dt} \tag{3-1}$$

where $\dot{Q}_h$ is the instantaneous total heat gain, $\dot{Q}_c$ is the instantaneous cooling load provided by the refrigeration unit, M is the overall thermal inertia of the freezer room, T_a is the average room temperature, and t is time.

If a forward method were to be adopted for calculating the thermal inertia M and overall heat gain $\dot{Q}_h$, detailed information of the room and stored goods would be required. On the other hand, in the inverse method an estimation of these two parameters is made based on measurements of the room temperature and an analysis of the refrigeration system's performance. Figure 3-1 summarizes the steps of the proposed analysis approach from data collection to the estimation of instantaneous thermal inertia and total heat gain.

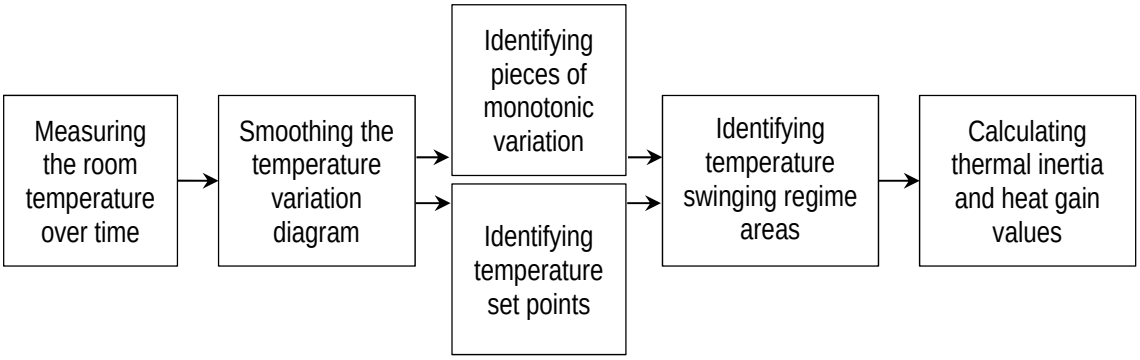

Figure 3-1: Summarized algorithm of the proposed inverse method for calculation of thermal inertia and heat gains. Reprinted with permission [65]**.**

In the first step, the room temperature is measured. Averaging and noise in temperature measurements can lead to a non-smooth temperature variation pattern. To ensure robust computations, it is important to first smooth the temperature fluctuations. Many noise reduction and smoothing algorithms are available in the literature. In this work, weighted averaging techniques similar to the one used in smoothed particle hydrodynamics [88] are used. The same technique is used to calculate the time derivative of the average temperature. The smoothing process may create inaccuracies, but is necessary for future steps where calculation of time derivatives is needed. Figure 3-2 shows the smoothed temperature as well as its calculated time derivative for a sample piece of data.

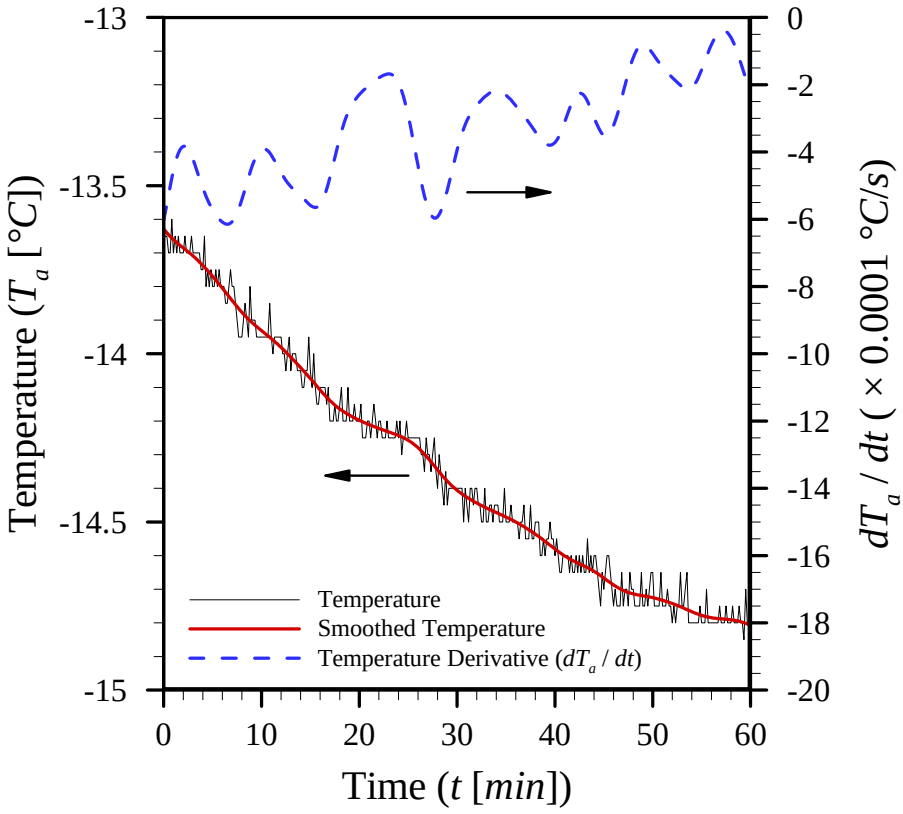

Figure 3-2: An instance of the smoothing process applied on raw temperature measurements and the calculated temperature derivative. Reprinted with permission [65]**.**

Figure 3-3 shows a zoomed view of temperature swings as described in Section 2.2. One of the temperature sensors (Track-It, Monarch Instruments) installed in the freezer is arbitrarily selected to represent the room bulk temperature. The apparent low and high temperature set points at the selected sensor are identified from Fig. 3-3 to be $-15.1°C$ and $-13.8°C$, respectively.

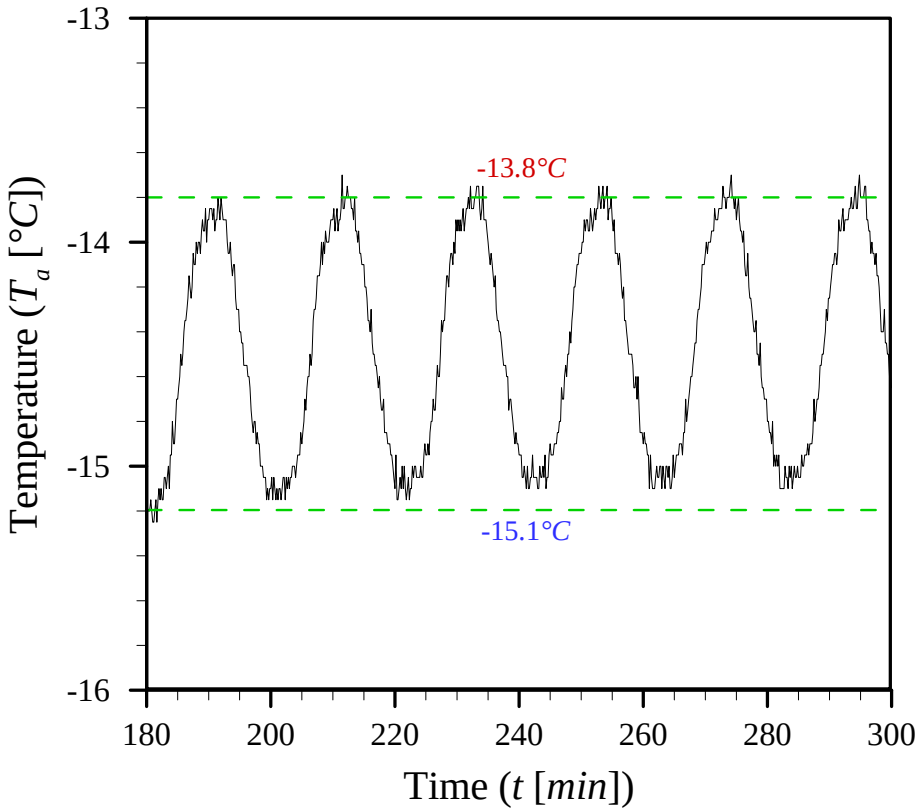

Figure 3-3: Sample temperature swings between low and high set points. Apparent low and high temperature set points are identified as $-15.1°C$ and $-13.8°C$, respectively. Reprinted with permission [65]**.**

A numerical algorithm is developed that sweeps the data to find the time steps where the temperature derivative approaches zero. These time steps signify a change in the increasing or decreasing trend of the smoothed temperature. Once these extrema are found, the algorithm divides the temperature diagram into the "pieces" which fall between them. The temperature within each piece is either monotonically increasing or decreasing. Figure 3-4 shows a few of these data pieces identified by the algorithm. In order to present the piece-identification process more clearly, an exponential curve fit is provided over each of the pieces shown in Fig. 3-4. The specific period shown in Fig. 3-4 contains 16 pieces outlined by exponential correlations. The pieces can be categorized into the following pull-down processes and heat-gain processes.

Pull-Down Process

The data pieces where the temperature is decreasing are called pull-down processes. During pull-down processes, cooling is provided by the refrigeration cycle to

compensate for the instantaneous heat gains and the thermal inertia of the freezer room. Therefore, the room temperature is pulled down.

Heat-Gain Process

The data pieces in which temperature is increasing are called heat-gain processes. Note that during a heat-gain period, the refrigeration cycle can be on or off depending on the room temperature compared to the set points. During this process, the heat gain surpasses the potential cooling provided by the refrigeration unit, which in turn results in an increase in the average room temperature.

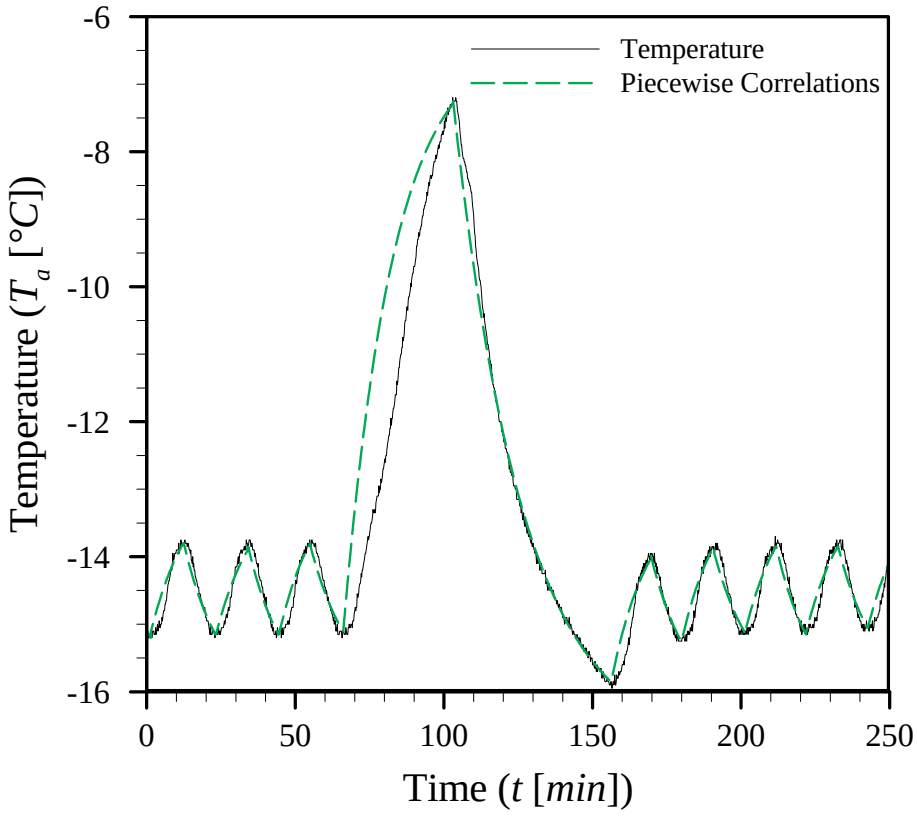

Figure 3-4: Sample temperature diagram demonstrating the pull-down and heat-gain processes. The data are divided into pieces as demonstrated by piecewise correlations. The correlations are selected to have exponential form. Reprinted with permission [65]**.**

Considering a consecutive pair of heat-gain and pull-down processes within a temperature swinging period, the heat balance in Eq. (3-1) for the heat-gain process can be simplified to:

$$\dot{Q}_h = M \left. \frac{\Delta T_a}{\Delta t} \right|_{Heat-gain} \tag{3-2}$$

In this condition, the refrigeration unit does not provide any cooling effect during the heat-gain period. Meanwhile, during the pull-down processes of the swinging regimes, cooling load is also provided to the freezer room. Therefore, the heat balance equation for any pull-down process takes the following form:

$$\dot{Q}_c + \dot{Q}_h = M \left. \frac{\Delta T_a}{\Delta t} \right|_{Pull-down} \tag{3-3}$$

where $\dot{Q}_c$ has a negative value for cooling. Averaging over the time period of each piece, the time derivative dT_a/dt of Eq. (3-1) is replaced by $\Delta T_a/\Delta t$ in Eqs. (3-2) and (3-3). Thus, a constant overall heat gain value can be calculated by simultaneously solving Eqs. (3-2) and (3-3). $\Delta T_a = T_2 - T_1$ and $\Delta t = t_2 - t_1$ are the bulk changes in temperature and time during the process, respectively. Based on the definition, it is evident that $\Delta T_a/\Delta t > 0$ for heat-gain processes and $\Delta T_a/\Delta t < 0$ for pull-down processes.

Considering that the swings occur mostly at times when there is no change in the freezer room constituents (usually during nights when the door is shut and no goods are loaded or unloaded), it can be assumed that the thermal inertia of the system remains constant during the two consecutive heat-gain and pull-down processes. Since the door remains shut, the ventilation load is negligible during swinging regimes. The variation of temperature difference between the freezer room and the ambient air is also negligible, since both the inside and outside temperatures are almost constant. This results in a relatively constant heat gain due to direct and ambient heat loads. Therefore, it can be reasonably assumed that the heat gain is constant between every two consecutive heat-gain and pull-down processes of a swing. Thus, knowing the cooling effect provided by the refrigeration system, one can solve Eqs. (3-2) and (3-3) to arrive at the following relationship for the lumped thermal inertia of the freezer room:

$$M = \frac{\dot{Q}_c}{\left.\frac{\Delta T_a}{\Delta t}\right|_{Pull-down} - \left.\frac{\Delta T_a}{\Delta t}\right|_{Heat-gain}} \tag{3-4}$$

Once the thermal inertia is known for a specific time, it is further used to find the average heat gain using Eq. (3-2) for heat-gain processes and Eq. (3-3) for pull-down processes.

The data required for the proposed inverse method only includes the real-time temperature measurements and the instantaneous cooling power provided by the refrigeration system. As it was discussed in the previous chapter, law-driven methods require much more information including wall thickness, material properties, and room thermal capacity. Therefore, the inverse approach is stronger for retrofit applications where little information may be available from the system.

3.1.2. Results and Discussion

The analysis approach and the temperature data shown in Fig. 2-12 are implemented in a computer program to calculate the thermal inertia and heat gain. The algorithm detects periods of temperature swings. Once these periods are identified, the algorithm calculates the room thermal inertia.

In order to use Eq. (3-4), it is necessary to know the cooling load $\dot{Q}_c$ provided by the evaporator. In general, the provided cooling load varies with both the evaporator and condenser coil temperatures. Nevertheless, Eq. (3-4) is only applied during temperature swings when the evaporating temperature is swinging within a narrow range between the set points. As a result, whenever the value of $\dot{Q}_c$ is used in the present method, it merely represents the average cooling capacity of the system operating between the high and low set points.

Jabardo et al. [89] and Wang et al. [90] showed that the cooling capacity varies by less than 5% from $1°C$ of evaporating temperature increase. Both studies show the same behavior for the dependence of the cooling capacity on the condensing temperature. Thus, although the cooling capacity is a function of the evaporating and

condensing temperatures, the variation can be neglected for small changes in those temperatures.

Based on on-site measurements, the approximate cooling capacity provided by the studied refrigeration cycle is $\dot{Q}_c = -950W$ while the freezer temperature is swinging within the high and low set points. The negative sign shows the direction of heat transfer from the room to the ambient air.

To verify the assumption of constant cooling load, further measurements are performed on the studied refrigeration cycle. Figure 3-5 shows the air temperature at the inlet and outlet of the evaporator fan as measured by T-type thermocouples (5SRTC-TT-T-30-36, OMEGA®) during the same period of study. The thermocouples have an accuracy of $\pm 1°C$ and are installed at the inlet and outlet of the evaporator fan. Figure 3-5 shows the measured evaporator temperatures for an arbitrary instance of the swings demonstrated in Fig. 3-3. When the cooling system is turned off, the inlet and outlet evaporator temperatures are almost equal and a heat-gain process occurs. During the pull-down processes, on the other hand, there is almost a constant gap between the temperatures, which hints at an almost constant cooling load.

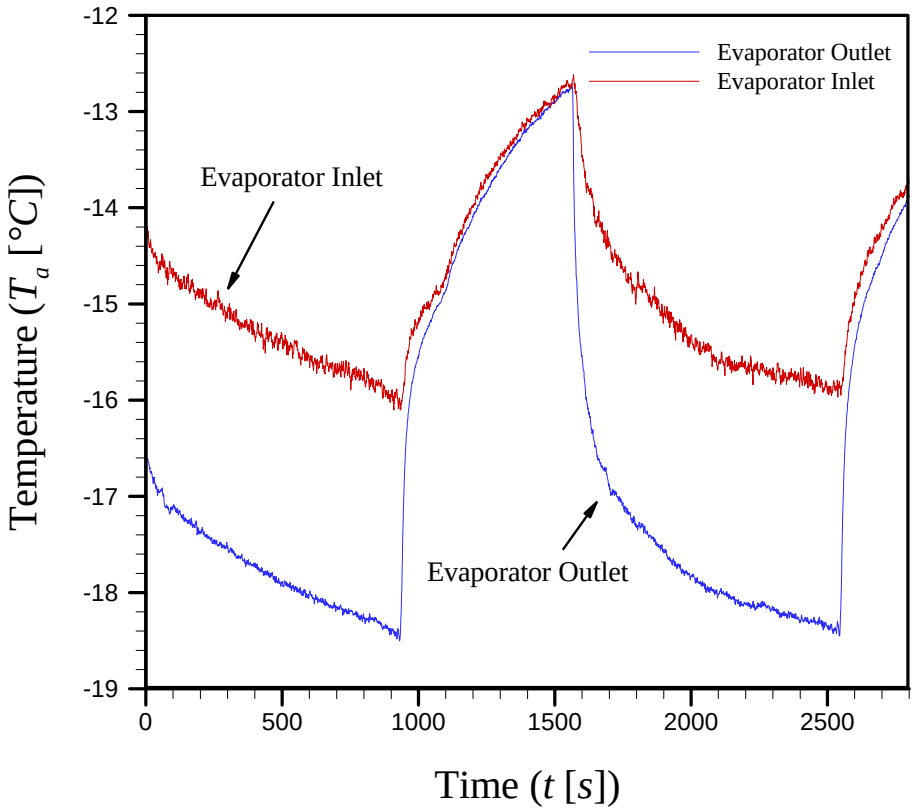

Figure 3-5: Air temperatures at the inlet and outlet of the evaporator during an instance of temperature swing between the high and low set points. Reprinted with permission [65]**.**

The volumetric flow rate of the evaporator fan is measured to be $600CFM$, which is equivalent to a mass flow rate of $0.38kg/s$ in the corresponding temperature range shown in 3-5. The sensible cooling capacity is thus calculated as:

$$\dot{Q}_c = \dot{m}_c c_c \left(T_{eo} - T_{ei}\right) \tag{3-5}$$

where $\dot{m}_c$ is the cooling air mass flow rate, c_c is the cooling air specific heat, T_{eo} is the evaporator outlet air temperature, and T_{ei} is the evaporator inlet air temperature.

Figure 3-6 shows the cooling capacity calculated based on the data shown in Fig. Figure 3-5 and Eq. (3-5). As observed in Fig. 3-6, the cooling capacity is negligible during the heat-gain processes. But during the pull-down processes, the cooling capacity oscillates around a constant value of about $\dot{Q}_c = -950W$. The cooling capacity in Fig. 3-6

does not show a significant trend or variation during the swing regime. Accordingly, the excessive calculations and measurements required for the instantaneous cooling load can be avoided and a constant cooling capacity can be used in relevant applications of the proposed method without remarkable loss of accuracy. The same assumption is used in the rest of this study.

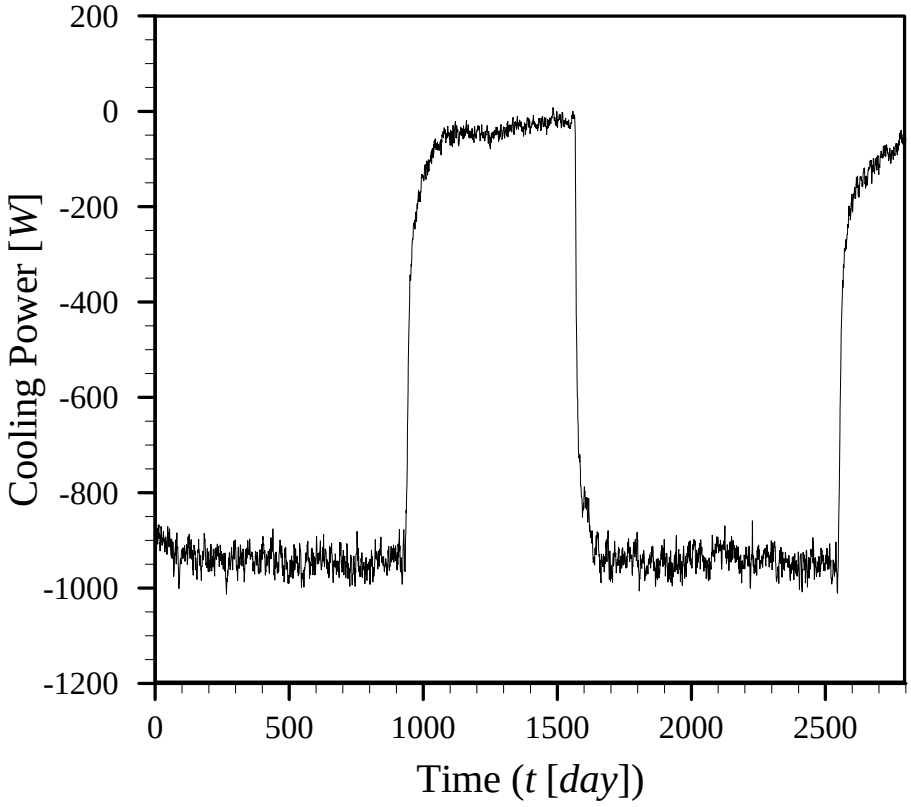

Figure 3-6: Cooling power provided by the refrigeration system during an instance of temperature swing between the high and low set points. Reprinted with permission [65]**.**

Figure 3-7 shows the calculation results for the room thermal inertia during the period under consideration. Since the freezer is regularly used for storing foodstuff, the contents of the room vary during the daytime. It can be inferred from the temperature variations of Fig. 3-7 that during daytime the freezer room experiences several events of door opening, which results in random temperature values far above the set points. Therefore, the swinging heat-gain and pull-down processes, occurring during night times, are used to estimate the thermal inertia until the next occurrence of temperature swing pattern.

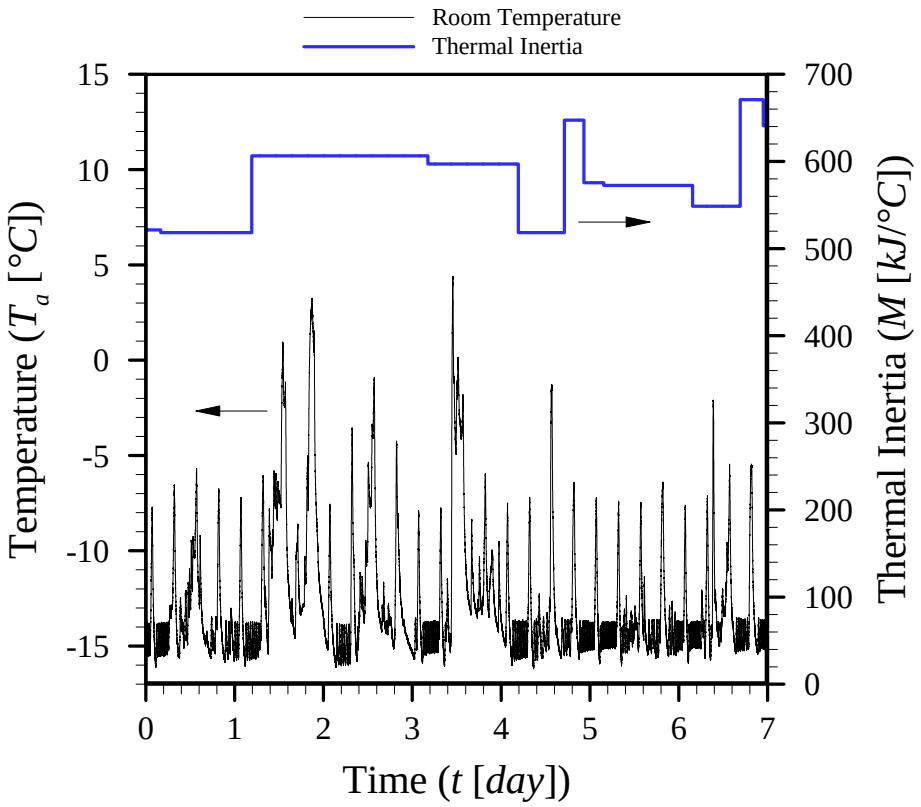

Figure 3-7: Thermal inertia calculation results for the freezer room during one week of its operation. Reprinted with permission [65]**.**

Figure 3-8 shows the estimated heat gain values. The heat gains are calculated for every time step based on the thermal inertia information inferred from Fig. 3-7 and Eqs. (3-2) and (3-3). For the sake of clarity, only results covering 12 hours of the system's operation are shown in Fig. 3-8. As mentioned in Fig. 2-12, there are 3 distinct temperature variation regimes: temperature swings, defrost spikes, and door openings. The data shown in Fig. 3-8 are chosen so they contain the 3 different patterns in order to show the capability of the present method for handling all of them.

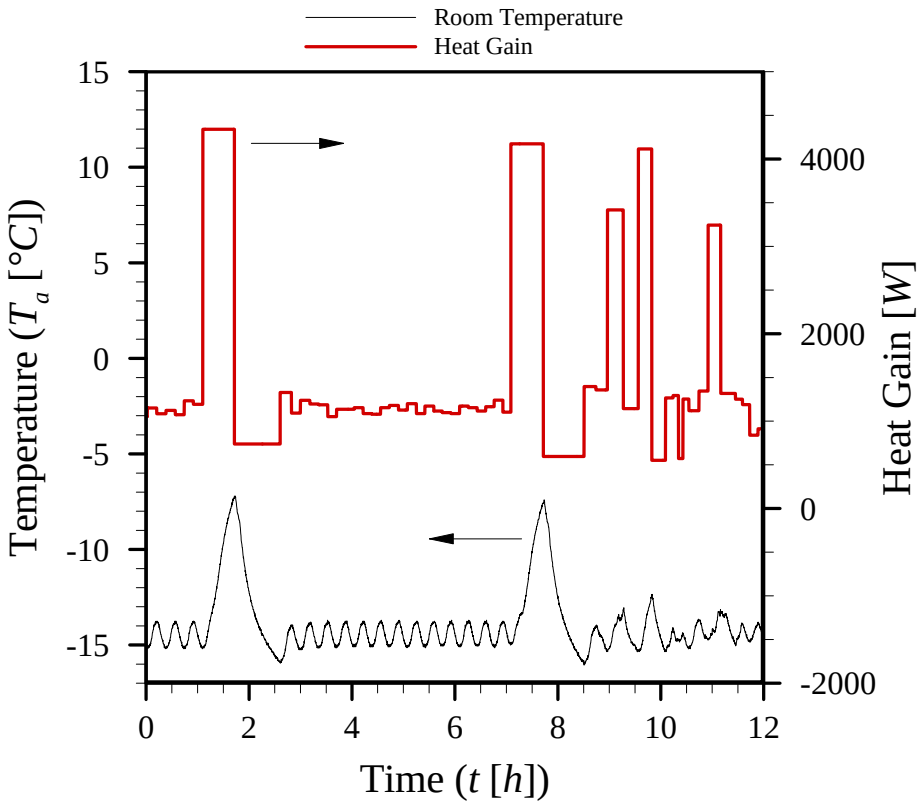

Figure 3-8: Heat gain calculation results for the freezer room during half a day of its operation. Reprinted with permission [65]**.**

It is noticeable in Fig. 3-8 that the defrost events that occur at hours 1 and 7 impose significant heat loads on the room. The instantaneous heat gain values jump to above $4kW$ during defrosts which result in a quick increase of temperature in the freezer room. As previously mentioned, the defrost events are set to automatically occur every 6 hours with no monitoring and sensing of ice formation on the evaporator coils. Nevertheless, previous studies show that there is a considerable energy-saving potential in using intelligent defrost units [91].

According to Fig. 3-8, during the temperature swings of hour 1 as well as hours 3 to 7, the heat gain is estimated to be at almost the same level as the cooling power provided by the refrigeration cycle. As a result, the temperature is kept at a constant average level in a swinging manner. During the defrost spikes of hours 2 and 8, there are two distinct heat-gain and pull-down processes. In the heat-gain section of defrost events, there is a large $4kW$ heat load imposed on the freezer from the heater-based defrost system. On the other hand, during the pull-down section of defrost events, there

is less heat gain imposed on the freezer, since the defrost heater is off. Furthermore, the heat gain directly depends on the temperature difference between the freezer air and ambient air. At the peak of a defrost spike, the difference between the inside and ambient air temperatures is at a minimum. As a result, the amount of heat gain in the pull-down section of a defrost event is even less than the steady heat gain of the swinging period.

The door opening event in Fig. 3-8, covering hours 8 to 12, demonstrates random variations in the heat gain level. During this time period, several cases occur when the restaurant personnel open the freezer door and allow large heat transfers from the ambient air into the freezer through a convection mechanism. Nevertheless, whenever the door is closed, the temperature decreases and the amount of heat gain is also reduced to the levels governed by wall heat fluxes.

Table 3-1 lists the daily-averaged thermal inertia and heat gain values of the freezer room. The present inverse method allows the identification of the usage pattern in the freezer room based on temperature measurements. For instance, as listed in Table 3-1, some goods are added to the freezer room on day 2 resulting in an increase of the overall room thermal inertia by $70 kJ/°C$ compared to the previous day. Such information that is inferred from temperature measurements can help retrofit existing systems in real-time while knowing little else about the freezer. Daily-averaged heat gain values are also reported in Table 3-1. It is apparent that relatively higher lumped heat gains are encountered during day 4. Consistent with this observation is the fact that in Fig. 2-12, many more door opening occurrences were observed in the first 4 days of measurements.

Table 3-1: Calculated daily-averaged thermal inertia and heat gain in the freezer room. Reprinted with permission [65]**.**

Day	Daily-Averaged Thermal Inertia $[kJ/°C]$	Daily-Averaged Heat Gain $[W]$
1	519	1872
2	589	2113
3	606	2034
4	599	2041
5	566	1711

6	573	1751
7	588	1753
Average	577	1896

A detailed list of foodstuff stored in the freezer room with their corresponding weight and thermal inertia was prepared based on on-site measurements. Existing tabulated values in ASHRAE Handbook of Fundamentals [9] are used for calculation of thermal inertia. The collected data are used to validate the proposed inverse modeling approach. Table 3-2 shows the list of foodstuff stored in the freezer room during day 4. The summation of all measured thermal inertia values is considered as the total thermal inertia of the freezer room. Due to the demand-based addition and withdrawal of foods, the freezer contents have slightly changed during the week of study, but they are kept in roughly constant amounts to ensure steady fulfilment of kitchen orders. Thus, although these are the values of one sample day, they are also deemed to represent an average of the freezer contents for the whole week.

Both the mass and specific heat of the miscellaneous objects such as the evaporator, lights, shelves, and boxes are considerably smaller than those of the foodstuff. For instance, the specific heat of carbon steel, aluminum, and copper are $0.49 kJ/kg°C$, $0.91 kJ/kg°C$, and $0.39 kJ/kg°C$, respectively. These values are considerably smaller than the thermal inertia of white bread and corn which are $1.65 kJ/kg°C$ and $1.42 kJ/kg°C$, respectively. As a result, the miscellaneous thermal inertia can be neglected in many applications without significant loss of accuracy. Nonetheless, an estimation of the miscellaneous thermal inertia is calculated and added to the measured thermal inertia of the foodstuff in order to improve the validation. Assuming a combined mass of $100 kg$ for the miscellaneous objects including the evaporator coils and shelf structures, and using an average specific heat of $0.6 kJ/kg°C$ for the metallic components, the total miscellaneous thermal inertia is calculated as $60 kJ/°C$. This value is added to the total freezer thermal inertia in Table 3-2.

Table 3-2: Mass and thermal inertia values of the freezer contents on day 4 of the experiments. Reprinted with permission [65]**.**

Product	Mass $[kg]$	Thermal Inertia $[kJ/°C]$	Product	Mass $[kg]$	Thermal Inertia $[kJ/°C]$
Chicken cages	25.00	43.00	White bread	3.80	6.27
Dry ribs	25.00	38.50	Pesto	3.00	5.64
Sliced pepperoni	5.00	7.75	Corn	12.00	17.04
Sockeye	10.00	15.70	Peas	12.00	11.04
Shrimp	10.00	17.20	Raspberries	5.00	8.80
Halibut	25.00	41.75	Red tortilla	0.02	0.04
Lobster	6.00	10.32	Green tortilla	0.02	0.04
Calamari squid	25.00	42.00	Whole wheat tortilla	0.02	0.04
Crab meat chunky	25.00	43.00	Flour tortilla	25.00	41.25
Albacore loin	5.00	8.80	Gluten free pizza shells	25.00	40.00
Fries	15.00	21.15	Gluten free buns	25.00	40.00
Spicy chorizo	5.00	7.75	Brioche buns	25.00	42.50
Sweet potato fries	7.50	11.93	Chocolate shaving	2.50	3.18
Hash browns	15.00	21.15	Vanilla ice cream	11.00	18.37
Multi grain bread	2.10	3.47	Miscellaneous parts	100.00*	60.00*
* Estimated value			Total	455	628

The total measured value of the room bulk thermal inertia is $628 kJ/°C$, while the calculated average value of thermal inertia for the whole week of study is $577 kJ/°C$. Thus, there is an acceptable discrepancy of 8% between the calculated and measured thermal inertia.

There is generally no direct method for measuring the heat gain in an air conditioning or refrigeration application. Typically, a heat balance of the room alongside appropriate correlations is used to estimate the amount of heat gain prior to the system design. The results of these thermal analyses are often estimations of the heat gain and provide an approximate value with acceptable accuracy for the specific application at hand. Following the same approach, geometrical, material, and thermal properties of the freezer room are measured and summarized in Table 2-4. Convection heat transfer coefficients are estimated using correlations from ASHRAE [9] for turbulent natural

convection on vertical and horizontal flat plates. The walls are equipped with old polyurethane insulation which is degraded due to several years of operation, and therefore provides a poor thermal resistance. Degradation mechanisms can cause the polyurethane thermal resistance to decrease to half of its original value [92]. Based on the methodology of the heat balance method [9], the heat transfer across the closed walls of the room is estimated. The overall heat gain of the room air is thus equal to the summation of these wall heat fluxes:

$$\dot{Q}_h = \sum_{Walls} \frac{A(T_o - T_a)}{1/h_o + b/k + 1/h_i} \tag{3-6}$$

where A is the wall surface area, T_o is the ambient temperature, T_a is the room air temperature, b is the wall thickness, k is the average wall thermal conductivity, and h_o and h_i are the outside and inside convection heat transfer coefficients, respectively.

As observed in Fig. 3-3, the high and low set points are $-13.8\,°C$ and $-15.1\,°C$, respectively. In order to find an approximate temperature difference between the ambient and room temperature during the swings, the room temperature was assumed to be at the average of the set points, i.e., $T = -14.5\,°C$. The restaurant temperature was measured at several locations near the freezer room and the average value of $T_o = 22.0\,°C$ was obtained. Using the properties collected in Table 2-4, Eq. (3-6) yields a total ambient heat gain of $\dot{Q}_h = 1002\,W$. During the swinging regions of Fig. 3-8, the calculated heat gain varies approximately between $1050W$ and $1250W$, with an average value of $\dot{Q}_h = 1150W$. Thus, although the heat gain and room temperature vary with time, a comparison of the average calculated value with the heat gain acquired from the heat balance analysis of the freezer room shows a discrepancy of less than 15%.

The calculated results shown in Figs. 3-7 and 3-8 can be used in a dynamic control algorithm that modifies the supplied cooling load by the refrigeration unit based on the real-time thermal inertia and heat gain information. Since the algorithm provides a real-time estimation of the instantaneous heat gain, a refrigeration unit equipped with a variable-speed compressor can be intelligently controlled to provide the required

instantaneous cooling load to the freezer room. Such control algorithms might be able to reduce the annual energy consumption of air conditioning and refrigeration systems.

3.1.3. Conclusions

In this section, a new inverse method was proposed to estimate the real-time thermal inertia and heat gain in air conditioning and refrigeration systems based on on-site temperature measurements. The collected temperature data were smoothed and fed to a mathematical algorithm that detects periods of temperature swing between the set points. The pace and pattern of temperature variations during the swing regimes were used to calculate the thermal inertia and overall heat gain in the freezer room. Little information on the geometry, material, and usage pattern of the system was needed, which made the proposed algorithm ideal for inverse analysis and retrofit of existing refrigeration and air conditioning systems.

The algorithm was validated using experimental data collected from the walk-in freezer experimental setup of Section 2.2 during a week of its regular operation. The inverse approach enables the interpretation of detailed information on the usage pattern of the freezer room and the calculation of the system's thermal parameters. The method can be implemented in control systems of refrigeration units to reduce the overall energy consumption of stationary and mobile HVAC-R units.

3.2. In-House Experimental Testbed

In order to further test the developed models, an in-house experimental test bed was made. Fig. 3-9 shows the test bed built out of wood, plastic, and glass. It is designed as a generic chamber in which heating and air conditioning scenarios can be tested. Six pairs of T-type thermocouples (5SRTC-TT-T-30-36, Omega Engineering Inc., Laval, QC, Canada) are attached on its walls using duct tape. The thermocouples have a tolerance of $\pm 1.0°C$ and are connected to a data acquisition system (NI 9214DAQ, National Instruments Canada, Vaudreuil-Dorion, QC, Canada) that logs the temperatures once per second. There are four openings on the front and rear walls of

the chamber. They can be blocked for certain experiments. However, a small amount of infiltration may still exist due to imperfect air sealing.

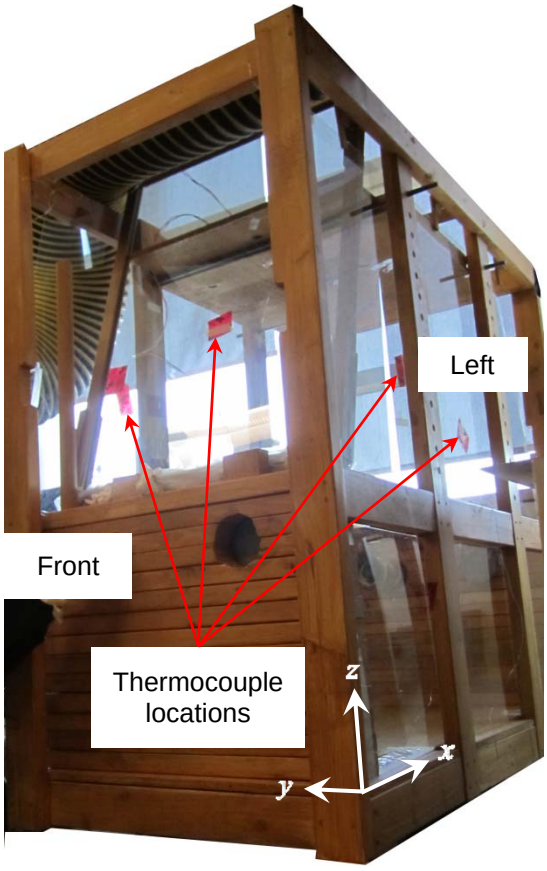

Figure 3-9: The in-house experimental testbed used for model validation and implementation. Six thermocouple pairs are attached to the walls with tape. Reprinted with permission [75], [93], [94]**.**

Table 3-3 shows the thermocouple locations with reference to the coordinate system shown in Fig. 3-9. Figure 3-10 shows a computer model of the chamber alongside its cross section in a cut view. Overall chamber dimensions are also shown in Fig. 3-10 and the names of different components are indicated.

An electrical heater with controlled power input was placed inside the chamber on the bottom plate. The heater was equipped with a fan to circulate air inside the chamber. The fan is kept at the same location for all tests. The fan power was measured to be $10\,W$ and was eventually converted to heat in the enclosed chamber due to damping of the air motion. Therefore, the fan power is also added to the total heating power in all calculations.

The heater consists of a resistor that provides Joule heating with controlled input power. The power provided to the heater is controlled and monitored by a programmable DC power supply (62000P, Chroma Systems Solutions Inc., Orange County, CA, US). According to uncertainty analysis based on the manufacture datasheets, the maximum error of the power measurements is 0.4%. Since no other heat source exists in the chamber, the known power input to the fan and heater can be assumed as the direct heat gain from internal sources.

Table 3-3: Location of thermocouples with reference to the coordinate system shown in Fig. 3-9. Reprinted with permission [75], [93], [94]**.**

Thermocouple Pair Name	$x\,(cm)$	$y\,(cm)$	$z\,(cm)$
Front	10	38	139
Rear	147	38	148
Left	80	0	85
Right	35	75	100
Top	55	55	131
Bottom	55	65	0

Various amounts of direct internal heat gain can be imposed on the chamber by varying the DC power provided to the heater. The heater power was kept constant at each level until steady-state conditions were reached. The measurements were recorded for analysis and calculation.

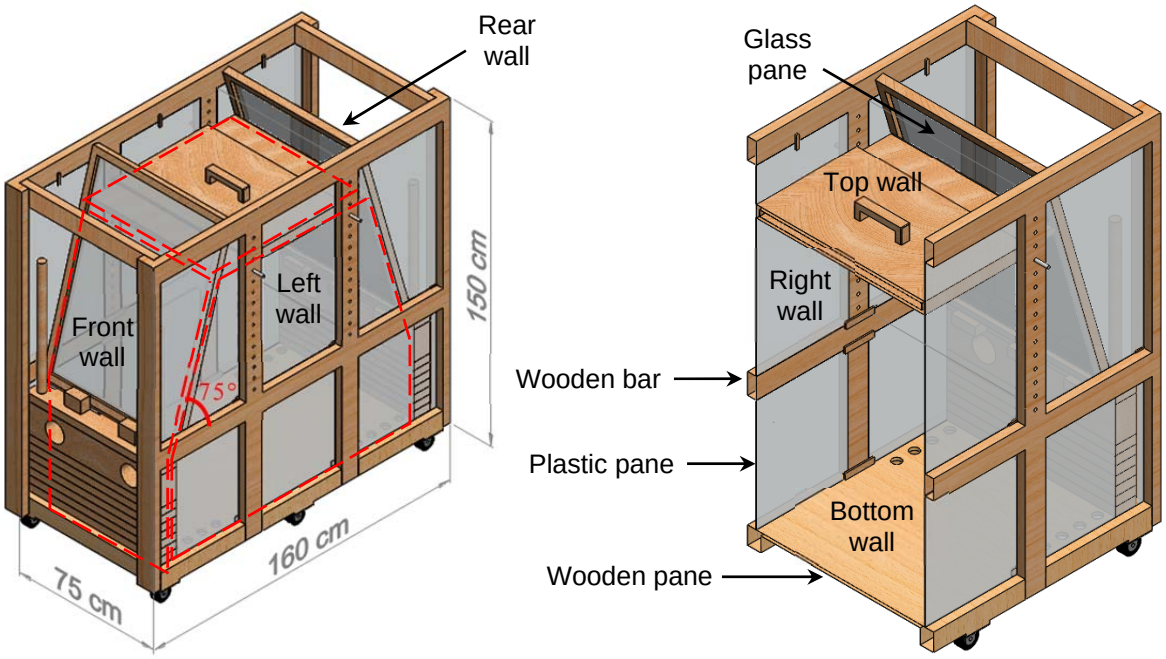

Figure 3-10: Computer model of the testbed showing its overall dimensions and components. (a) Full view. (b) Cross sectional view. Reprinted with permission [75], [93], [94]**.**

A fully-controlled refrigeration system was connected to the in-house experimental setup through the inlet and outlet connections on the front and rear walls. Figure 3-11 shows the refrigeration cycle and its components. The power provided to the compressor was controlled and measured by another programmable DC power supply (62000P, Chroma Systems Solutions Inc., Orange County, CA, US). The power level provided to the evaporator and condenser fans was also controlled and measured through a computer interface. The combination of the chamber and the refrigeration cycle was used to conduct experiments for validation and implementation of the developed methods.

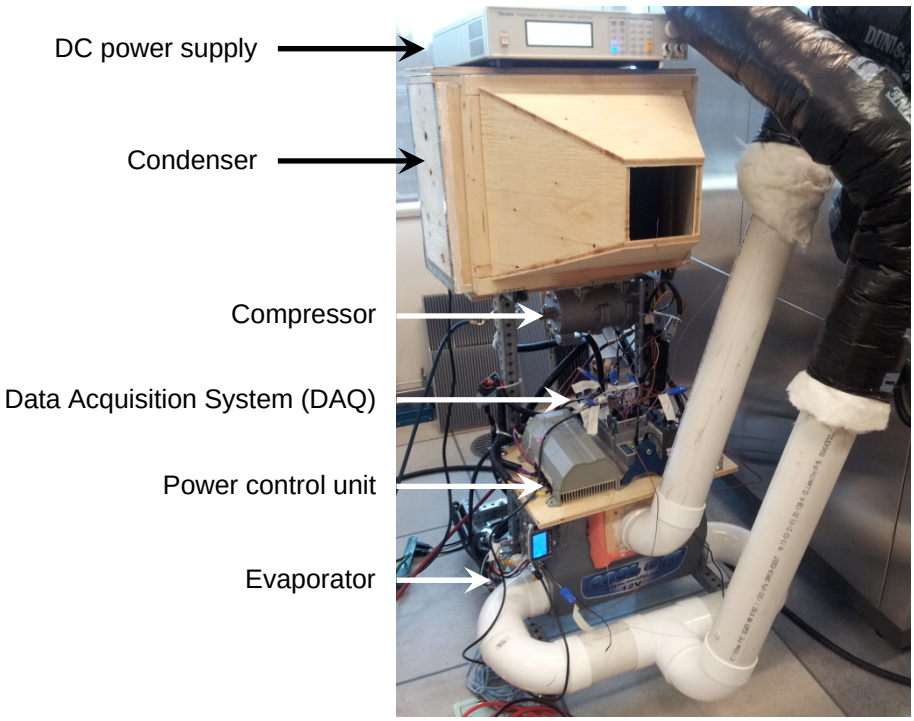

Figure 3-11: A picture of the fully-controlled refrigeration cycle and its components. Reprinted with permission [95]**.**

3.3. Automatic Estimation of Heat Transfer Coefficients

In this section, a self-adjusting method is proposed for real-time calculation of thermal loads by automatic calculation of wall heat transfer coefficients. In this data-driven method, the heat balance calculations are improved by real-time temperature data to achieve more accurate load estimations. An iterative mathematical algorithm is developed to adjust the heat transfer coefficients according to live measurements. Since the proposed method requires little engineering information about the room, it can be adopted as a simplified yet accurate method for the design and retrofit of new and existing HVAC-R systems.

3.3.1. Model Development: Convection Coefficients Estimation

The heat balance equation is considered as the basis for developing an algorithm for automatic estimation of convection coefficients. Figure 3-12 summarizes the heat balance method as described in the ASHRAE Handbook of Fundamentals [9]. As

indicated at the bottom of Fig. 3-12, for a heating application at the steady-state condition, i.e., when the heat transfer rates are constant, the heat balance equation is:

$$\dot{Q}_S = \dot{Q}_V + \dot{Q}_W \tag{3-7}$$

where $\dot{Q}_V$ is the rate of ventilation and infiltration heat loss, $\dot{Q}_W$ is the rate of total heat transfer across the walls, and $\dot{Q}_S$ is the heat gain from internal sources. Equation (3-7) is a balance of thermal energy for the room envelope surrounded by internal wall surfaces.

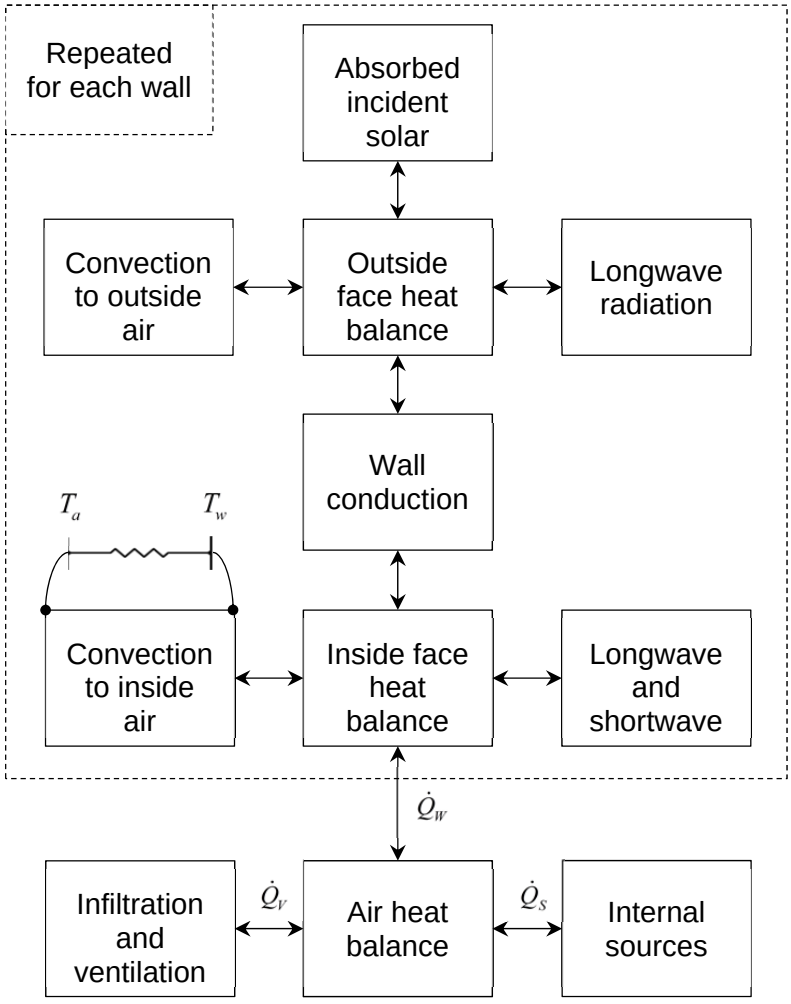

Figure 3-12: Schematic of the heat balance method [9] as incorporated in a data-driven approach for estimating convection coefficients. Reprinted with permission [94]**.**

Thermal energy is transferred to the wall surfaces by convection and radiation. Convection depends on various factors, such as wall orientation, air velocity, and air temperature. Finding the proper convection coefficients requires correlations that may not hold for all conditions experienced by the room, especially in vehicle applications. Therefore, it is useful to find an estimation of the convection coefficients without excessive experiments or computations.

Another mechanism for transferring heat to the wall surfaces is radiation. A portion of the incident radiation is absorbed by the surfaces and the rest is either reflected or transmitted through. Rather than directly increasing the air temperature, radiation transfers energy to the room surfaces, which is in turn transferred to the air through convection and conduction. The bulk of the radiation energy received at each surface contributes to the temperature increase on that surface. Therefore, by directly measuring the surface temperature, the radiation heat transfer is automatically considered in the model.

The calculation of $\dot{Q}_W$ consists of 3 steps: (1) outside face heat balance, (2) conduction through the wall, and (3) inside face heat balance. The total wall heat transfer rate $\dot{Q}_W$ is the summation of all individual wall heat transfer rates:

$$\dot{Q}_W = \sum_{j=1}^{n} h_j A_j \left(T_a - T_w\right)_j \tag{3-8}$$

where h is the convection coefficient over the internal surface, A is the wall surface area, T_a is the air temperature adjacent to the wall, T_w is the temperature on the wall interior surface, and n is the number of walls. In Eq. (3-8), it is assumed that the wall temperature and air temperature are uniform.

The heat transfer rate $\dot{Q}_V$ consists of both the ventilation and infiltration of air. Air may infiltrate into the room through windows and openings and there is often no means of direct measurement to find the volumetric rate of infiltrated air. As such, the accurate rate of heat transfer due to infiltration and ventilation is also unknown in typical applications. Thus, we assume a constant value for the unknown ventilation heat gain,

and define it as one of the parameters to be calculated by the algorithm. Replacing $w_0 = \dot{Q}_V$ and $w_j = h_j A_j$ in Eqs. (3-7) and (3-8), we arrive at:

$$\dot{Q}_V + \dot{Q}_W = w_0 + \sum_{j=1}^{n} w_j \left(T_a - T_w\right)_j \tag{3-9}$$

The right hand side of Eq. (3-9) is a linear function, w_0 is called the "bias weight", and w_j are called the "input weights" [24–27]. We apply a "transfer function" f to the calculation output, defining:

$$O = f\left(w_0 + \sum_{j=1}^{n} w_j \left(T_a - T_w\right)_j \right) \tag{3-10}$$

where O is the calculation output and f is the sigmoid function [98] with the following general form:

$$f\left(a\right) = \frac{1}{1 + \exp\left(-a\right)} \tag{3-11}$$

where a is a generic parameter.

Equation (3-9) is a reformulation of Eq. (3-7) which is the basic heat balance equation. The convection coefficients that are included in the weight factors "w" in Eq. (3-9) are unknown. However, the temperatures T_a and T_w can be measured in real-time. Therefore, an iterative process is proposed to guess and correct the weight factors using real-time temperature measurements. Since actual measurements are used to update the weight factors, the iterative calculations are called the "training" process.

The final step is to update the weight factors according to the current and desired calculation outputs. The original convergence procedure for adjusting the weights was developed by Rosenblatt [99]. Graupe [100] proved that the weights can be adjusted according to:

$$w_j^{k+1} = w_j^k + \eta \left(D - O \right)^k \left(T_a - T_w \right)_j^k \tag{3-12}$$

where k denotes the training step number. η is an arbitrary constant called the "learning rate", as it dictates the rate of correction for the weight factors [96]. Higher learning rates result in faster adjustment of w_j during the training process. However, large η may also cause the weights to diverge to infinity after a few steps. The value of η is often selected by experience. It is considered that $\eta = 0.05$ throughout this study.

The training procedure is repeated until the convergence criterion is met. Convergence is achieved when all the weights almost remain constant, i.e., their relative variation between two consecutive training steps is less than a certain threshold ε. In this study, a convergence threshold of $\varepsilon = 0.01$ is used.

Once the weights have converged, the training process stops and the weights can be used for the rest of the system's operation, i.e., for other situations when the actual heat gain $\dot{Q}_S$ is unknown. T_a and T_w are measured on all walls and the converged w_j are plugged in Eq. (3-9) to calculate the total thermal load $\dot{Q}_V + \dot{Q}_W$.

Figure 3-13 shows a flowchart summarizing the proposed algorithm for thermal load calculation. At the first step, the weight factors should be initiated. If prior estimations are available for h and A from measurements and correlations, the weight factors can be initiated from $w_j = h_j A_j$. However, they can also be initiated from $w_j = 0$, and the iterative process adjusts them until convergence is achieved.

After initializing the weights, the training iterations begin. At every training step, the air temperature T_a, the surface temperature T_w, and the internal heat gain $\dot{Q}_S$ are measured. In order to measure $\dot{Q}_S$, a known amount of thermal energy can be intentionally introduced into the room. An electrical heater with controllable power consumption can be used to implement the condition. According to Eq. (3-7), the total heat loss by ventilation, infiltration, and walls is equal to the produced internal heat gain at the steady state. The next step is to calculate the desired calculation output

$D = f\left(\dot{Q}_S\right)$ and the current calculation output O from Eq. (3-10). The procedure of updating the weights continues until convergence is achieved. The converged weight factors are further used for automatic estimation of thermal loads for the rest of the system's operation.

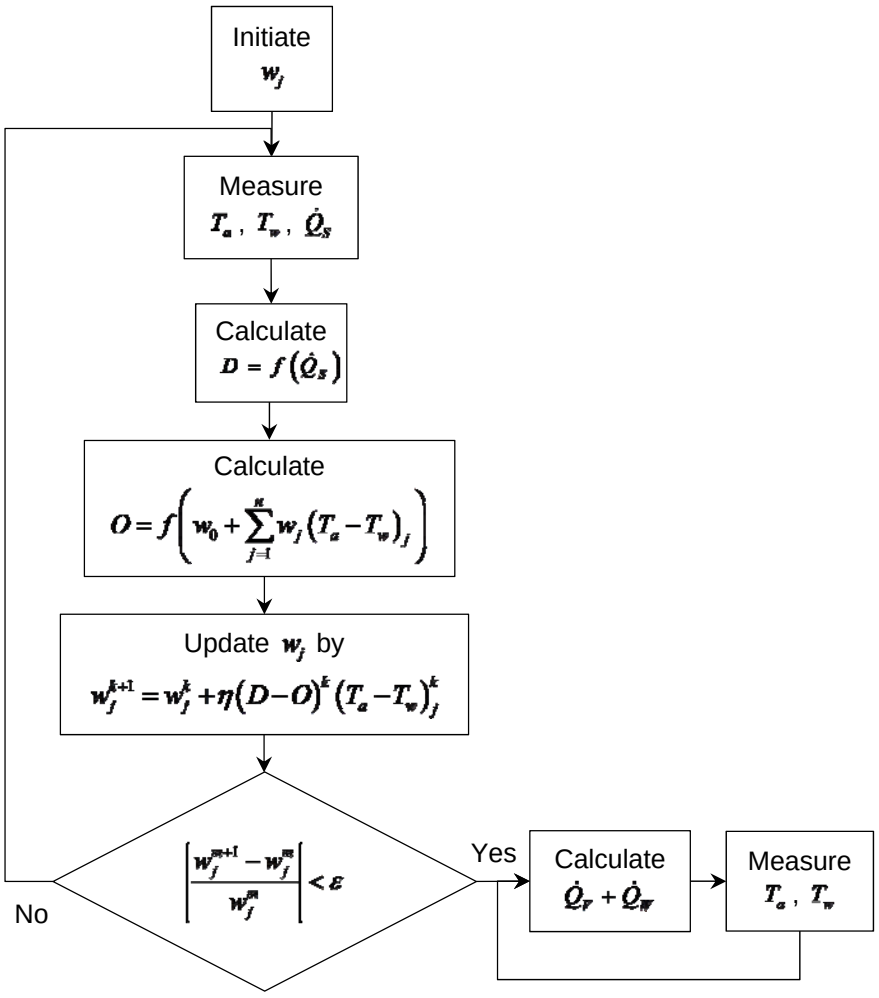

Figure 3-13: Flowchart of the algorithm for real-time thermal load calculation by automatic estimation of convection coefficients. Reprinted with permission [94]**.**

The model was validated for a heating scenario and the results are presented in the following section. Since the general heat balance equation is used for developing the model, it can be readily extended to cooling scenarios and different room dimensions.

3.3.2. Results and Discussion: Convection Coefficients Estimation

The model was validated by experiments conducted on the testbed of Section 3.2. Out of every thermocouple pair, one thermocouple is attached to the interior wall surface and the other is hung in the interior air adjacent to the same spot. The air-side thermocouple is located at an approximate distance of $1\,cm$ from the wall.

Heat convection heavily depends on both the surface geometry and the local flow characteristics. For instance, the measurements of a thermocouple pair located close to a wall edge is not identical to one installed on a wide open wall center. There is always conjugate (conduction and convection) heat transfer taking place at surface edges and the effect is more significant when non-conductive materials are involved. Thus, attributing a single convection coefficient to an entire wall is an approximate yet accepted approach. Although temperature readings are performed at individual spots, the proposed model also follows the same accepted approach and assumes a single convection coefficient (weight factor) for each wall.

More thermocouple pairs can definitely increase the accuracy of thermal load calculations. However, the locations of the limited number of thermocouple pairs used in this testbed are arbitrarily selected and, in turn, the self-adjusting algorithm attempts to iteratively adjust the coefficients using the local temperature readings. These locations are intentionally not symmetric, so that the generality of the self-adjusting technique for arbitrary configurations is showcased. Unless rigorous three-dimensional CFD simulations or extensive experiments are performed, the detailed heat convection from the surface is unknown. Thus, the weight factors w_j calculated for the thermocouple pairs are assumed as the average coefficient $h_j A_j$ at the corresponding wall.

To validate the present model, convection coefficient correlations were applied to the test bed and the resulting values were compared to the converged weight factors. Moreover, the total thermal load was calculated using both sets of coefficients to showcase the effectiveness of the proposed model. Equation (3-8) was used to calculate the heat gain by the convection coefficient correlations. Similarly, Eq. (3-9) was used to calculate the thermal load by the weight factors of the present model.

Table 3-4 shows the estimated convection coefficients based on Eqs. (2-27) and (2-28), in which the average values of the measured temperatures are used for T_a and T_w.

Table 3-4: Wall surface areas and convection coefficients calculated using ASHRAE correlations [9] shown in Eqs. (2-27) and (2-28). Refer to Fig. 3-10 for component names and locations. Reprinted with permission [94]**.**

Wall Name	Surface Area $A(m^2)$	Convection Coefficient $h\left[W/m^2{}^\circ C\right]$	Heat Transfer Coefficient $hA\left[W/{}^\circ C\right]$
Front	0.5	1.73	0.85
Rear	0.5	1.61	0.78
Left	2.0	1.76	3.42
Right	2.0	1.59	3.09
Top	2.0	1.61	3.23
Bottom	3.0	0.86	2.58

Equation (3-7), which is the basis of the present model, assumes steady-state conditions. Therefore, it is required to ensure that the steady-state condition is reached for every level of the heater power in the validation experiment. The steady-state values of the heat transfer rates $\dot{Q}$ are reached when all temperature differences ($T_a - T_w$) reach relatively constant levels. Thus, the exponential decay of the temperature differences is of the form:

$$T_a - T_w = c_1 + c_2 \exp(-c_3 t) \tag{3-13}$$

where c_2 is negative for temperature-increasing patterns. The correlation of Eq. (3-13) was applied to the measurements from all thermocouple pairs with the minimum coefficient of determination calculated to be $R^2 = 0.95$. Figure 3-14 shows the exponential decay of the temperature difference $T_a - T_w$ on the left wall from an initial steady-state. The exponential correlation fitted to the temperature difference has a time constant of 226 seconds, i.e., it takes less than 4 minutes for the temperature to reach 99% of its maximum steady-state value. The same procedure is applied to all walls and the maximum time constant was calculated to be 335 seconds on all walls. Thus, to

ensure that steady-state conditions were reached, the heater power was kept constant for 10 minutes at every level and the final measurements were used in the calculation of thermal loads.

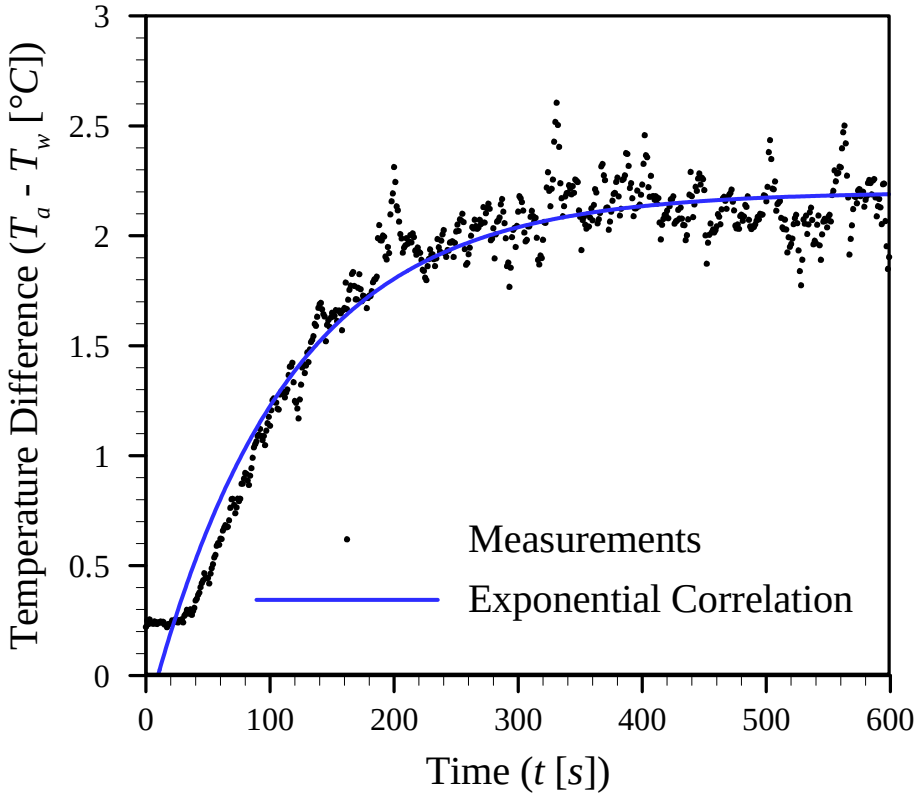

Figure 3-14: Exponential growth of the temperature difference ($T_a - T_w$) to the steady-state condition on the left wall. The exponential correlation of Eq. (3-13) is fitted to the measurements. Reprinted with permission [94]**.**

As shown in Fig. 3-13, the first part of the algorithm consists of training the weight factors through an experiment where the direct heat gain $\dot{Q}_S$ is known. In order to find the adjusted coefficients, the testbed was allowed to reach the steady state at an arbitrary level $\dot{Q}_S = 0.334\,kW$ of the heater power. Then, the training algorithm was run until the convergence criteria

$$\left| \frac{w_j^{m+1} - w_j^m}{w_j^m} \right| < \varepsilon \tag{3-14}$$

are met with $\varepsilon = 0.01$. At every step, the weight factors are corrected according to Eq. (3-12). Figure 3-15 shows the progressive adjustment of weight factors during the training process. All the weight factors were initialized to zero, and convergence was achieved within 10 steps.

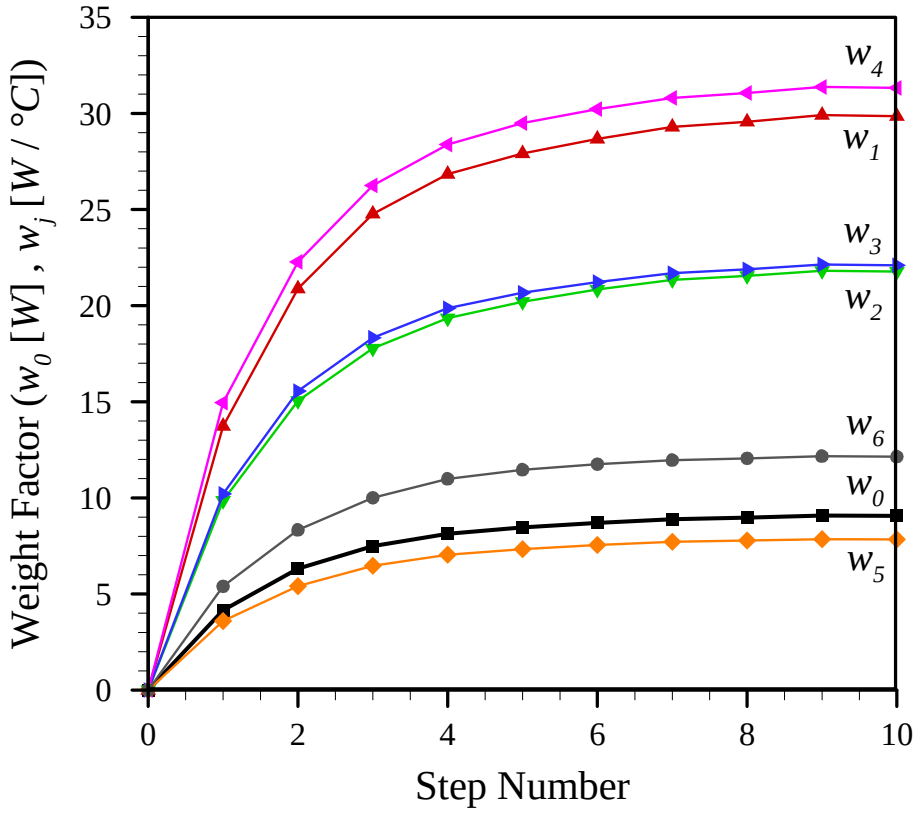

Figure 3-15: Progressive adjustment (training) of the weight factors at an arbitrary heater power of $\dot{Q}_s = 0.334kW$ for automatic estimation of convection coefficients. Reprinted with permission [94]**.**

Figure 3-16 shows the convergence of the calculated heat gain to the measured value during the training process. As the weight factors are updated, the calculation of the heat gain $\dot{Q}_s$ becomes more accurate step-by-step until convergence to the measured value is achieved.

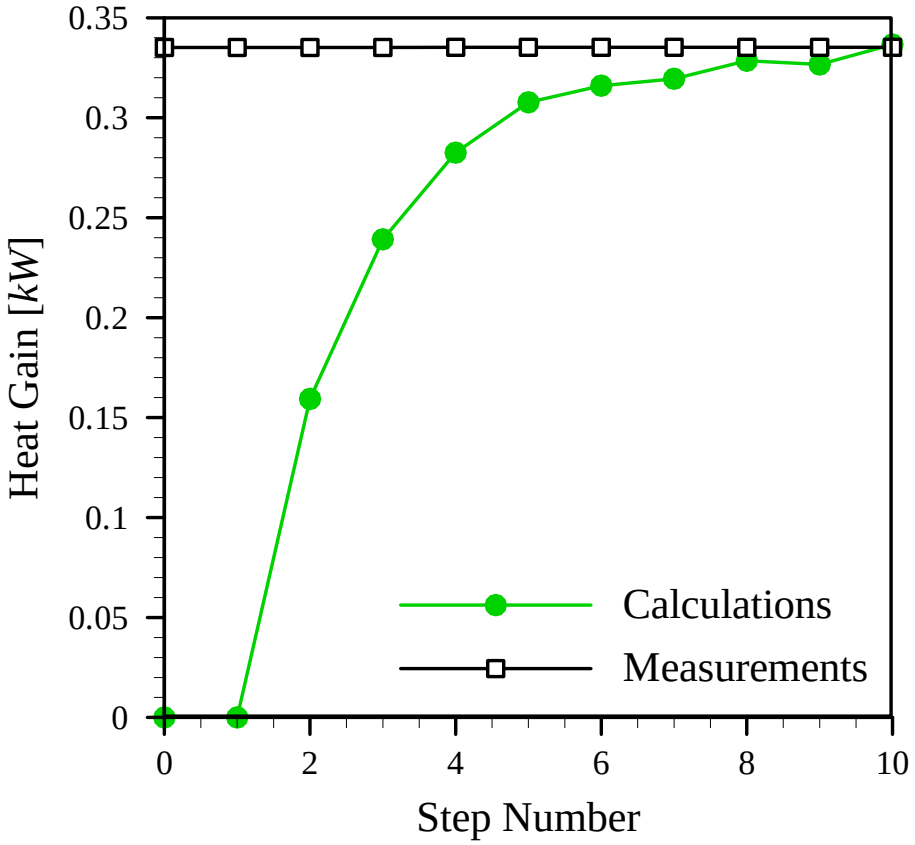

Figure 3-16: Progressive correction of the calculated heat gain during the training process at a measured heater power of $\dot{Q}_s = 0.334kW$. Reprinted with permission [94]**.**

Table 3-5 shows the converged values of the weight factors from Fig. 3-15. The coefficients hA from Table 3-4 for each wall are also repeated in Table 3-5 for comparison. Since $\dot{Q}_V$ is unknown, the converged value of its mathematical equivalent (w_0) is used for the ventilation term when calculating the total heat gain from analytical correlations. It is noted that the coefficients hA (calculated from ASHRAE correlations) and their mathematical equivalents w_j (adjusted by the training algorithm) can have remarkably different values. In this case, the available ASHRAE correlations largely underestimate the rate of heat transfer across the walls. Therefore, automatic adjustment of coefficients is beneficial for accurate estimation of thermal loads.

The analytical convection coefficients and the weights adjusted by the training algorithm of the present model are used to calculate the total heat gain. Figure 3-17

shows the results using both sets of coefficients at various levels of steady-state heater power. It is noted that analytical coefficients can result in large errors when used for calculating the total heat gain. In this specific case, there is a minimum of 67% error in the heat gain calculations using analytical coefficients. The adjusted weight factors, however, result in a maximum error of 9%.

Table 3-5: Comparison of adjusted weight factors with analytical convection coefficients. Reprinted with permission [94]**.**

Convection Coefficient	Correlation Value	Adjusted Value
Ventilation and Infiltration	$\dot{Q}_V = 9.11 W$ *	$w_0 = 9.11 W$
Front Wall	$h_1 A_1 = 0.85 W/°C$	$w_1 = 29.4 W/°C$
Rear Wall	$h_2 A_2 = 0.78 W/°C$	$w_2 = 21.1 W/°C$
Left Wall	$h_3 A_3 = 3.42 W/°C$	$w_3 = 21.8 W/°C$
Right Wall	$h_4 A_4 = 3.09 W/°C$	$w_4 = 26.7 W/°C$
Top Wall	$h_5 A_5 = 3.23 W/°C$	$w_5 = 7.82 W/°C$
Bottom Wall	$h_6 A_6 = 2.58 W/°C$	$w_6 = 12.0 W/°C$

* Estimated equal to w_0

The ASHRAE correlations are rigorously validated by analysis and experiment. But they contain certain assumptions that confine their usage. For instance, they assume natural convection over a flat wall and provide the average convection coefficient over the wall in its wide open area. They also assume uniform wall temperature. In practice, none of these assumptions completely hold. In the present experiment, the walls are surrounded by other enclosure walls, they are not completely flat, some forced convection may occur over them, and they have non-uniform temperatures. To find more accurate convection coefficients, detailed experiments or numerical simulations are necessary. The present algorithm is proposed as a tool for providing accurate thermal load calculations while avoiding extensive simulations and experiments.

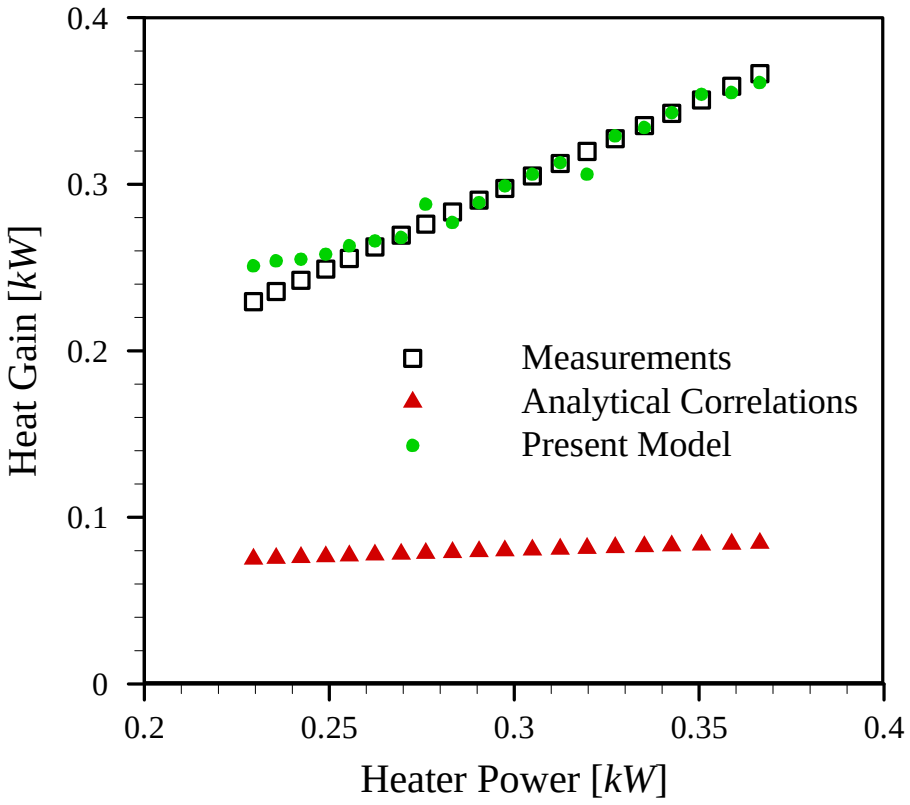

Figure 3-17: Comparison of heat gain calculation results by analytical correlations and the adjusted weight factors in automatic estimation of convection coefficients. Reprinted with permission [94]**.**

As a data-driven method, a disadvantage of the present model is that it requires training. Although the training can be performed within seconds, directly measuring the heat gain may be impossible in many cases. However, it is possible to artificially impose a known heat gain to an existing room using the same testing approach of this study, i.e., isolating the room from all possible thermal loads except a known source of internal heating or cooling. As such, this method can be used for retrofitting existing systems as well as designing new systems. Whenever it is impossible to directly test the room for the training process, conventional law-driven methods can be used to provide an estimation of the actual heat gain. The estimated heat gain can be fed to the algorithm as the training target for $\dot{Q}_S$. The algorithm can then use the adjusted coefficients to calculate the real-time thermal loads based on future temperature measurements.

3.3.3. Modeling and Results: Conduction Coefficients Estimation

A similar approach described in Section 3.3 is followed for real-time estimation of thermal loads based on automatic calculation of wall conduction coefficients. The heat balance methodology is followed as shown in Fig. 3-18. The room air is in thermal balance with internal sources load, ventilation load, and walls load, as shown by Eq. (3-7). In the absence of a cooling system and when the steady-state condition is reached, i.e., when the temperature is relatively constant throughout the room, the room is in thermal balance and Eq. (3-7) describes the thermal balance of the room and walls.

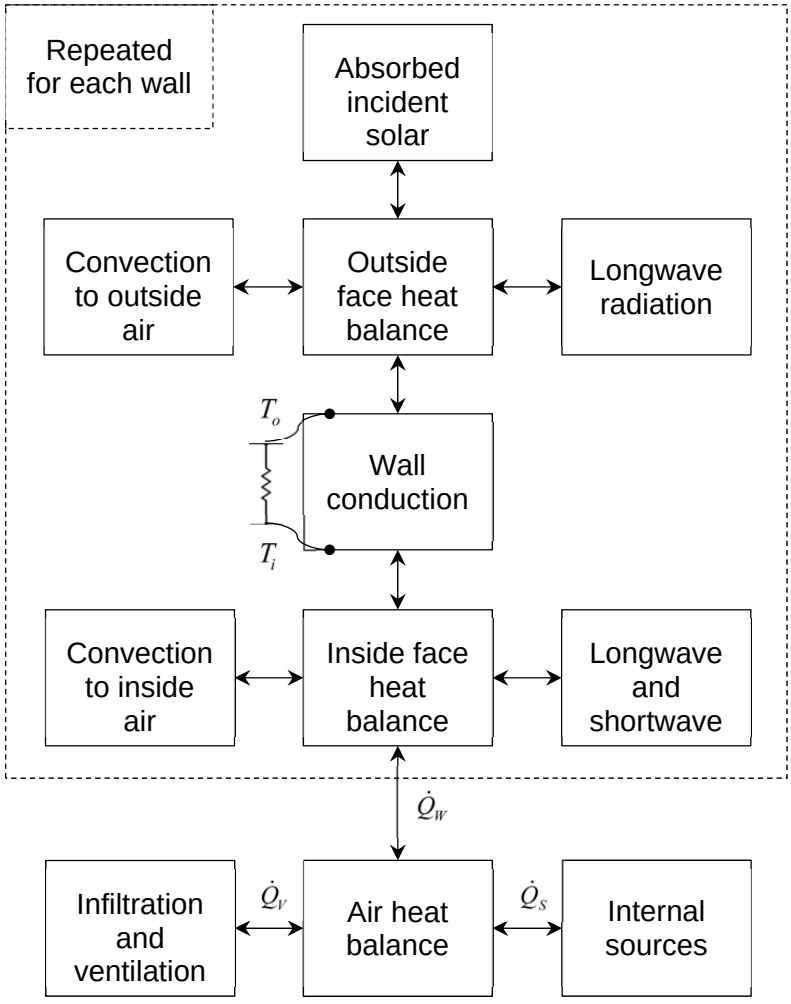

Figure 3-18: Schematic of the heat balance method [9] as incorporated in a data-driven approach for estimating convection coefficients. Reprinted with permission [93]**.**

The total wall heat transfer rate is the summation of all individual wall heat transfer values:

$$\dot{Q}_W = \sum_{j=1}^{n} \left(\frac{kA}{b} \right)_j \left(T_i - T_o \right)_j \tag{3-15}$$

where k is the conduction heat transfer coefficient, A is the wall surface area, b is the wall thickness, n is the number of walls, T_i is the wall temperature on the inside surface, and T_o is the wall temperature on the outside surface. The same analysis described in Section 3.3 is applied to arrive at

$$\dot{Q}_V + \dot{Q}_W = w_0 + \sum_{j=1}^{n} w_j \left(T_i - T_o \right)_j \tag{3-16}$$

which is similar to Eq. (3-9). Similarly, $w_0 = \dot{Q}_V$, with the wall weights replaced by the definition $w_j = \left(kA/b \right)_j$.

The same correction algorithm is proposed and the calculation output is calculated by

$$O = f\left(w_0 + \sum_{j=1}^{n} w_j \left(T_i - T_o \right)_j \right) \tag{3-17}$$

which is similar to Eq. (3-10). O is the actual calculation output and f is the Sigmoid function indicated in Eq. (3-11).

Finally, a similar training process is proposed in the form:

$$w_j^{k+1} = w_j^k + \eta \left(D - O \right)^k \left(T_i - T_o \right)_j^k \tag{3-18}$$

which is similar to Eq. (3-18). η is the learning rate, $D = f\left(\dot{Q}_S \right)$ is the desired calculation output, and k denotes the step number of the training algorithm. The found set of

weights is eventually inserted in Eq. (3-16) to arrive at the real-time thermal load for future cases where the direct heat gain from internal sources is unknown.

The thermal conductivity values of the chamber components were measured using a transient conductivity measurement machine. The thermal conductivity of the glass, wood, and plastic materials used for constructing the chamber are measured as $1.05 W/m°C$, $0.20 W/m°C$, and $0.26 W/m°C$, respectively. Table 3-6 shows the overall thicknesses and dimensions of the 6 walls surrounding the chamber. The walls of the chamber do not consist of uniform materials. Furthermore, the wall shapes are not necessarily flat and their thicknesses are also non-uniform. Thus, the numbers shown in Table 3-6 are approximate values only.

The model was applied to the test bed of Section 3.2 for various values of direct internal heat gain implemented by different heater power levels. At every level, the heater power was kept constant for 10 minutes in order to assure steady-state conditions are reached. Prior to the test, the training algorithm was applied on the weight factors for 20 seconds at an arbitrary heater power setting of $\dot{Q}_S = 0.334 kW$. A learning rate of $\eta = 0.05$ was used for the calculations as recommended by the literature.

Table 3-6: Dimensions and thicknesses of the 6 walls surrounding the chamber. Reprinted with permission [93]**.**

Wall Name	Surface Area $A(m^2)$	Thickness $b(mm)$	Heat Transfer Coefficient $kA/b(kW/°C)$
Front	0.5	5.5	0.095
Rear	0.5	5.5	0.095
Left	2.0	2.0	0.260
Right	2.0	2.0	0.260
Top	2.0	30.0	0.013
Bottom	3.0	30.0	0.020

Figure 3-19 shows the progressive correction of the weight factors according to Eq. (3-18). The temperature measurements were performed every second and the correction process was applied at the same rate. The training process was initialized with the weight factors set to zero.

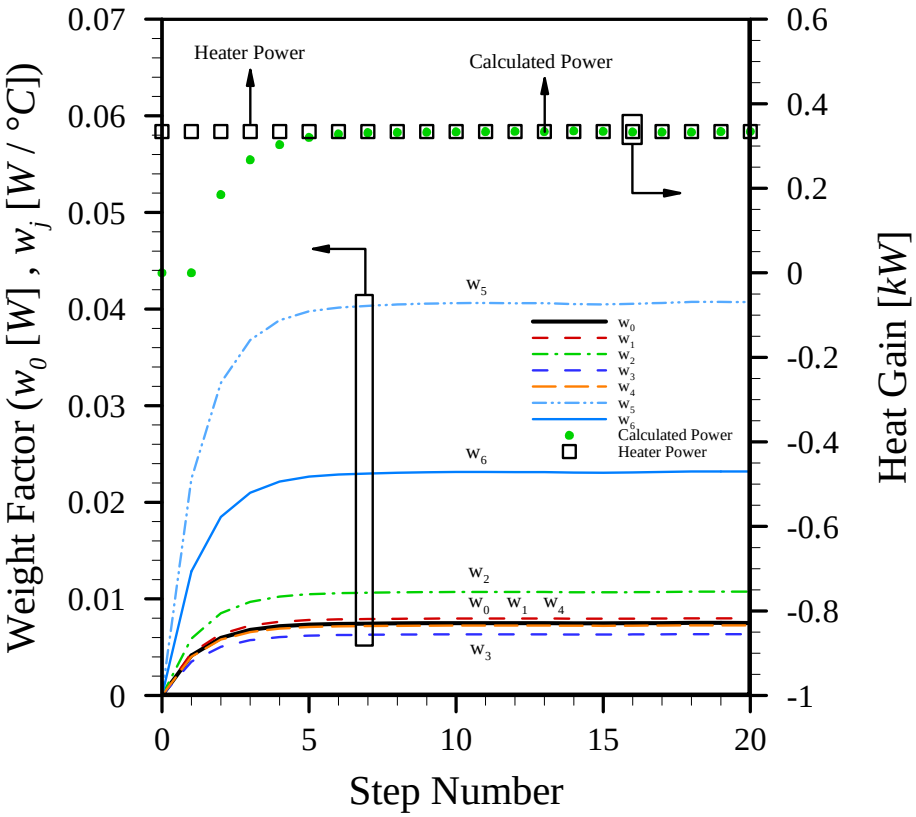

Figure 3-19: Progressive adjustment (training) of the weight factors at an arbitrary heater power of $\dot{Q}_s = 0.334kW$ for automatic estimation of conduction coefficients. Reprinted with permission [93]**.**

Figure 3-20 shows the calculated steady-state heat gain for different heater powers based on the corrected values of the weight factors. It is observed that the thermal load is calculated for various heater power levels with a maximum relative error of 25%.

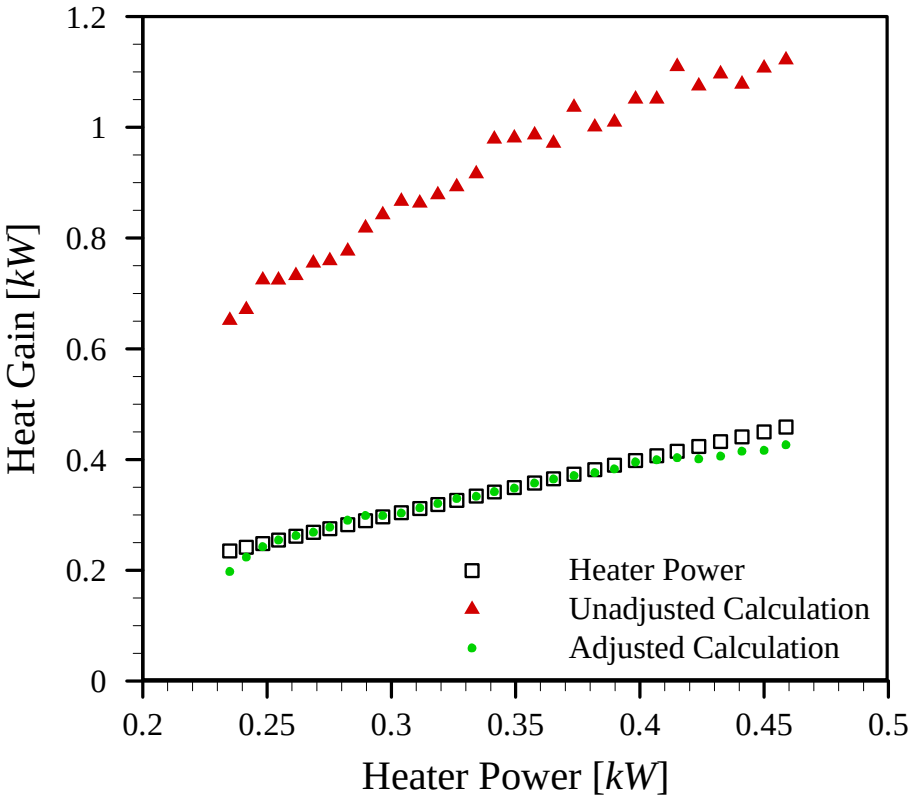

Figure 3-20: Comparison of heat gain calculation results by analytical correlations and the adjusted weight factors of the present model in automatic estimation of conduction coefficients. Reprinted with permission [93]**.**

3.3.4. Conclusions

In this section, a method was proposed for real-time calculation of thermal loads by automatic estimation of heat transfer coefficients. In two similar approaches, the convection and conduction coefficients were estimated and adjusted using a mathematical algorithm and temperature measurements. The proposed method was validated by experimental results. It was shown in a case study that the algorithm could calculate the heat gain with an acceptable accuracy, whereas the unadjusted heat transfer coefficients calculated from analytical correlations resulted in remarkable errors.

Since the proposed method is based on fundamental heat transfer equations, it can be used in a wide range of stationary and mobile applications. It provides a simple tool for designing new systems and retrofitting existing ones while avoiding extensive simulations and experiments. The self-adjusting technique proposed in this work lays the

foundation for the design of an intelligent controller which calculates the thermal loads in real-time and corrects its results as well. The calculated load can provide precious information to the HVAC-R system, resulting in advanced improvements in energy efficiency.

3.4. On/Off Set Point Selection

While novel controllers are being proposed in the literature, a huge number of commercially available HVAC-R controllers are still designed based on on/off logic. In this section, a new approach is proposed to optimize the selection of temperature set points with the intention of decreasing the overall energy consumption while maintaining the desired comfort level.

Several researchers have studied the optimization of on/off controllers. Chinnakani et al. [101] argued that a disadvantage of fixed gain PID control is that its performance can be poor under varying load conditions, so they developed an “intelligent on/off controller” that takes into account sensor delays and room inertia. However, they assumed linear functionality for determining the slope of the temperature-time curves. Although the linear assumption is acceptable, assuming exponential functionality can be more accurate considering the form of the governing heat transfer equations. Li and Alleyne [74] presented an optimal compressor on/off control algorithm with a relay feedback loop. They developed a generic cost function involving temperature variation from the set-point, power consumption, and compressor on/off cycling frequency for minimization. The optimal control scheme was tested on a refrigeration system to demonstrate the potential of the optimal on/off control for temperature regulation, component wear reduction, and fuel consumption savings. They discussed the importance of the temperature swing periods in the action of on/off controllers and proposed a method for optimizing the high and low set points to minimize the cost function. However, they assumed that the swing time periods have polynomial correlations with the set points, and calculated those parameters using simulation results rather than experiments. In the present study, it is proposed that exponential temperature correlations be used for the room thermal response. Moreover, the proposed set point optimization is based on experimental measurements without the

necessity of further simulations. The following section describes the model development and design strategy for optimizing HVAC-R on/off controllers.

3.4.1. Model Development

An on/off controller of an HVAC-R system keeps the temperature swinging within a narrow range of temperatures called the high set point T_H and the low set point T_L. Figure 3-21 shows an example of a temperature swing in an air-conditioned system. In the example shown in Fig. 3-21, in order to maintain the temperature at $26°C$, the high and low set points are selected as $T_H = 27.8°C$ and $T_L = 24.2°C$, respectively. Therefore, starting from a low temperature, the air conditioning system is off and the room gains heat. This phenomenon results in the room temperature increasing, creating a temperature trend called an “increasing process”. When the temperature reaches T_H, i.e., the maximum allowable temperature, the AC system is turned on and the temperature begins to decrease. There is some lag in the process and a temperature overshoot is expected due to the thermal inertia of the room. This temperature overshoot is visible in Fig. 3-21 at the end of the increasing process denoted by time t_I. Afterwards, the refrigeration cycle works to pull down the room temperature during a period called the “decreasing process” that lasts for time t_D. These processes occur consecutively in air conditioned and refrigerated spaces. We call every two consecutive processes a “temperature swing”. Useful information can be extracted from the study of temperature swings in any HVAC-R application [65].

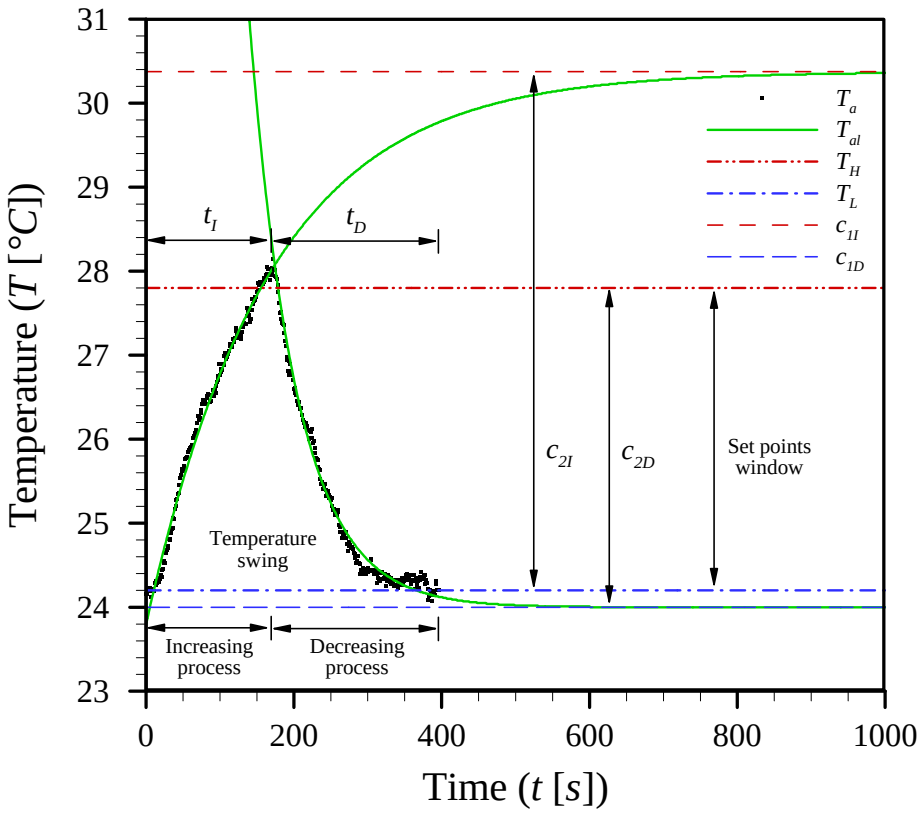

Figure 3-21: Demonstration of a typical temperature swing resulting from an air conditioning on/off control action. Reprinted with permission [75]**.**

The aim of the present model is to adopt a gray-box approach that will provide formulas for calculating energy-efficient set point values in HVAC-R on/off controllers. To combine the heat transfer equations with real-time data, the heat balance equation of a room envelop surrounded by n walls numbered by j can be written as [28–33]

$$m_a c_a \frac{dT_a}{dt} = \sum_{j=1}^{n} h_j A_j \left(T_i - T_a\right)_j + \dot{m}_V c_a \left(T_o - T_a\right) + \dot{Q}_S + \dot{Q}_{AC} \tag{3-19}$$

where

T_a is the homogeneous room air temperature and t is time;

$m_a c_a \frac{dT_a}{dt}$ is the rate of increase in the energy of room air of mass m_a and specific heat c_a;

$\sum_{j=1}^{n} h_j A_j \left(T_i - T_a\right)_j$ is the convective heat transfer rate from surfaces A_j, with inside convection coefficients h_j, and inside surface temperatures T_i;

$\dot{m}_V c_a \left(T_o - T_a\right)$ is the heat transfer rate due to air mass flow rate $\dot{m}_V$ from outside air temperature T_o by ventilation and infiltration;

$\dot{Q}_S$ is the heat gain from internal sources; and

$\dot{Q}_{AC}$ is the heat flow to or from the HVAC-R system. $\dot{Q}_{AC}$ also includes any latent heat transfer due to condensation or evaporation.

Equation (3-19) can be viewed as a differential equation with respect to the variable T_a. Rearranging Eq. (3-19), we arrive at

$$K_1 \frac{dT_a}{dt} = -K_2 T_a + K_3 \tag{3-20}$$

where K_1, K_2, and K_3 are positive values containing all the parameters included in Eq. (3-19). In general, these coefficients are also functions of T_a. K_1 is a function of the air mass, the air specific heat, and the deep thermal mass of the objects inside the room. K_2 is a function of the wall convective coefficients and the ventilation flow rate. K_3 can also have a complicated dependency on the heat gain, HVAC-R load, outside temperature, and ventilation temperature.

The physical parameters included in K_1, K_2, and K_3 are generally time-dependent. It is often necessary to gather information about the ambient conditions, the material properties, and the room's geometrical shape to estimate such parameters. However, when the room temperature is swinging between the set points, it has a relatively constant value. Therefore, most parameters such as the ambient temperature and ventilation rate have negligible variation and can be assumed constant. Although variations in the radiation load can occur in the room, these changes occur gradually compared to the small time span of a temperature swing. Therefore, it is reasonable to

assume that all the parameters in Eq. (3-20) are constant during an instance of a temperature swing. Any variation in the room conditions may still occur from one swing to the next, but as long as the swinging pattern is maintained, every parameter in Eq. (3-20) is assumed constant during a swing instance. Thus, the solution to the differential equation of Eq. (3-20) has the following exponential form:

$$T_{al} = c_1 + c_2 \exp\left[-\frac{t - t_0}{c_3}\right] \tag{3-21}$$

where c_1, c_2, and c_3 are:

$$c_1 = \frac{K_3}{K_2} \tag{3-22}$$

$$c_2 = T_{a0} - \frac{K_3}{K_2} \tag{3-23}$$

$$c_3 = \frac{K_1}{K_2} \tag{3-24}$$

and t_0 and T_{a0} are the initial time and temperature of the specific process under consideration and T_{al} is the correlated room air temperature. Equation (3-21) is an exponential curve that is fit to the temperature variation during an increasing or decreasing process. The correlation of an increasing process has the following form:

$$T_{al} = c_{1I} + c_{2I} \exp\left[-\frac{t - t_0}{c_{3I}}\right] \tag{3-25}$$

whereas the temperature correlation of a decreasing process has the following form:

$$T_{al} = c_{1D} + c_{2D} \exp\left[-\frac{t - t_0}{c_{3D}}\right] \tag{3-26}$$

The subscript "I" denotes the parameters pertaining to an increasing process and "D" denotes the parameters of a decreasing process. Table 3-7 shows the physical interpretation of the correlations parameters.

Table 3-7: Physical interpretation of the c -parameters in the temperature correlation formula of Eqs. (3-25) and (3-26). Reprinted with permission [75]**.**

Parameter	Unit	Physical Interpretation
c_{1I}	$[°C]$	Maximum steady-state room temperature reached in the current conditions if the cooling system is always off.
c_{1D}	$[°C]$	Minimum steady-state room temperature reached in the current conditions if the cooling system is always on.
c_{2I}	$[°C]$	Difference between c_{1I} and the low temperature set point ($T_L - c_{1I}$). c_{2I} is negative.
c_{2D}	$[°C]$	Difference between c_{1D} and the high temperature set point ($T_H - c_{1D}$). c_{2D} is positive.
c_{3I}	$[s]$	Time constant of the exponential temperature correlation for an increasing process i.e., the time required for the room temperature to cover 63% of its total increase and reach $T_a = c_{1I} + 0.37c_{2I}$ where c_{2I} is negative.
c_{3D}	$[s]$	Time constant of the exponential temperature correlation for a decreasing process, i.e., the time required for the room temperature to cover 63% of its total decrease and reach $T_a = c_{1D} + 0.37c_{2D}$ where c_{2D} is positive.

The values of the c -parameters in Table 3-7 are unknown; they can be acquired through measurements. If the temperature in a room is recorded, Eqs. (3-25) and (3-26) can be used to fit exponential curves to the temperature values. After fitting exponential curves to the temperature data, the values of the c -parameters are found and they can be further used to assist the design and improvement of the controller set points. For every increasing or decreasing process, an exponential correlation can be found and a new set of c -parameters can be calculated.

An important aspect of the temperature swing patterns is the time span of each process. Rearranging Eq. (3-21) and using Eqs. (3-25) and (3-26), the time required for the room to reach temperature T_a through a process starting from $t = t_0$ and $T_a = T_{a0}$ is:

$$t - t_0 = c_3 \ln\left(\frac{T_{a0} - c_1}{T_a - c_1}\right) \tag{3-27}$$

In ideal conditions, every increasing process starts from $T_a = T_L$ and ends at $T_a = T_H$, while every decreasing process starts from $T_a = T_H$ and ends at $T_a = T_L$. Therefore, for an increasing process, the total time is

$$t_I = c_{3I} \ln\left(\frac{T_L - c_{1I}}{T_H - c_{1I}}\right) \tag{3-28}$$

and for a decreasing process, we have

$$t_D = c_{3D} \ln\left(\frac{T_H - c_{1D}}{T_L - c_{1D}}\right) \tag{3-29}$$

where T_L and T_H are the low and high set points.

The temperature pattern during the entire operation of the system is merely a repetition of the swinging pattern. Therefore, the average swing temperature is equal to the overall average temperature, as long as the swinging pattern is maintained. As such, the average swing temperature is an important design objective. The average swing temperature is calculated by:

$$T_{ml} = \frac{\int_{t_I} T_a dt + \int_{t_D} T_a dt}{t_I + t_D} \tag{3-30}$$

where T_{ml} is the mean temperature calculated based on the temperature correlations. A temperature swing consists of an increasing process followed by a consecutive decreasing process. As such, for an entire temperature swing, using the correlations of

Eqs. (3-25) and (3-26) for T_{al}, and the definitions of Eqs. (3-28) and (3-29) for t_I and t_D, we arrive at:

$$T_{ml} = \frac{1}{t_I + t_D}\left[c_{1I}t_I + c_{1D}t_D + c_{2I}c_{3I} + c_{2D}c_{3D} - c_{2I}c_{3I}\exp\left(-\frac{t_I}{c_{3I}}\right) - c_{2D}c_{3D}\exp\left(-\frac{t_D}{c_{3D}}\right)\right] \quad (3\text{-}31)$$

It is required to keep the average temperature at the desired level by proper selection of the set points. Therefore, given either T_L or T_H, the other quantity can be found by implicitly solving Eq. (3-31) with t_I and t_D from Eqs. (3-28) and (3-29) so that the requirement for T_{ml} is met.

Another important parameter for the design of set point hysteresis is the overall power consumption. The compressor of the refrigeration cycle is off during increasing processes, and it is on during decreasing processes. When the compressor is on, the amount of power consumed depends on several factors such as air temperature, ambient temperature, and refrigerant pressure. However, within the narrow range of the set points, the compressor power can be assumed constant [65]. Therefore, the average compressor energy consumption per unit time is directly proportional to the amount of time that it is on. Assuming that the compressor consumes the power E_{comp} when it is on, the average power consumption over a swing period is calculated as:

$$E_{ml} = \frac{t_D}{t_I + t_D}E_{comp} \quad (3\text{-}32)$$

where E_{ml} is the average power consumption calculated based on the temperature correlations. Thus, proper selection of the set point levels directly affects the overall energy consumption through changing t_I and t_D in Eq. (3-32).

The number of compressor starts per hour is another important parameter in the design of refrigeration systems. Having found the process times t_I and t_D, we have:

$$\omega_l = \frac{3600}{t_I + t_D} \quad (3\text{-}33)$$

where ω_l is the estimated number of compressor starts per hour. Excessive number of compressor starts can reduce the lifetime of the compressor due to fatigue. It can also damage other components of the system including the valves and contactors. The increased current draw that happens at every new start also increases the total power consumption. A limit is often set by the manufacturers on the maximum allowable number of compressor starts per hour. As such, Eq. (3-33) can be used to design the set points subject to the constraint on the maximum allowable ω_i.

Equations (3-31) to (3-33) are crucial to the proposed method for selection of on/off set points. In the following section, a design strategy is described for using the present model as a tool for selecting the set points.

Design Strategy

The optimization problem for selecting the on/off set points is formulated as minimizing the overall energy consumption subject to the following constraints:

- Minimum error between the average temperature and the desired temperature
- Minimum temperature deviation from the desired temperature
- Minimum number of compressor starts per hour

The above constraints create competing trends for the selection of set points. Of course, there are specific obligations and preferences in every design case. For instance, minimizing the temperature deviation from the desired level may be critical in certain applications such as in refrigerated transportation of food products. In such a case, a higher number of compressor starts per hour may be acceptable as a sacrifice for selecting a narrow set point range. The present approach offers a design tool that can be flexibly used according to the needs of every specific engineering case.

The procedure for solving the optimization problem in a cooling scenario is as follows:

1. Find the c-parameters by fitting the correlations of Eqs. (3-25) and (3-26) on temperature measurements.
2. Decide upon the maximum allowable temperature deviation from the desired temperature.

3. Decide upon the maximum allowable number of compressor starts per hour.
4. Solve Eqs. (3-31) and (3-33) simultaneously for t_I and t_D subject to:
   - T_{ml} = Desired temperature
   - ω_l = Maximum allowable number of compressor starts per hour
5. Solve Eqs. (3-28) and (3-29) simultaneously for the minimum allowable T_H.
6. Find the maximum allowable T_H based on the maximum allowable temperature deviation.
7. Select the maximum suitable T_H within the range specified by steps 5 and 6.
8. Find T_L for the selected T_H by solving Eq. (3-31) using Eqs. (3-28) and (3-29) for t_I and t_D, subject to:
   - T_{ml} = Desired temperature
9. Estimate the optimized average power consumption using Eq. (3-32).
10. Estimate the number of compressor starts per hour using Eq. (3-33).

In the following section, the model is validated by an experiment and the potentials for improving the overall energy efficiency are investigated.

3.4.2. Results and Discussion

The developed design strategy is validated by an experiment in the testbed of Section 3.2. In the experiment, the heater and its fan generate a total internal heat gain of $\dot{Q}_S = 641\,W$. The instantaneous compressor power consumption varies between $490\,W$ and $520\,W$ when it is on. The on/off controller switches the compressor on or off at the set points. However, the evaporator and condenser fans are always on during the tests. Every temperature swing consists of an increasing process, during which the compressor is off, followed by a decreasing process, during which the compressor is on. As discussed in the model development section, the compressor power can be assumed constant when it is operating within the narrow range of the set points. Therefore, according to the measurements, an average value of $E_{comp} = 497.7\,W$ is considered as the compressor power consumption.

Model Validation

In a test designed for model validation, the high and low set points are varied every half an hour during the regular action of the refrigeration cycle connected to the chamber. An arbitrary value of $26°C$ is selected as the desired temperature. A symmetric on/off set point hysteresis is selected, and its value is varied from $\pm 1°C$ to $\pm 1.8°C$ with increments of $0.2°C$ at every 30 minutes. As such, the high set point varies from $T_H = 27°C$ up to $T_H = 27.8°C$ while the low set point varies from $T_L = 25°C$ down to $T_L = 24.2°C$ during an overall period of 150 minutes.

Figure 3-22 shows the temperature results throughout the 150 minutes (9000 seconds) of the cooling system's operation. T_a shows the air temperature as measured in the chamber. T_H and T_L are the high and low set points, respectively. At the bottom of Fig. 3-22, a zoomed-in view shows a single temperature swing with curve fits for T_{al} using Eqs. (3-25) and (3-26). After identifying all the temperature swings, curve fits are applied to the increasing and decreasing processes of every swing instance separately. The minimum coefficient of determination for all the correlations is $R^2 = 0.98$.

In Fig. 3-22 it can be seen that the air temperature surpasses the high set point by up to $1°C$ before it is pulled back down by the initiation of the cooling cycle's operation. There is also an overshoot at the low set point, but it is not as dramatic because the heat gains quickly increase the temperature once the cooling cycle is turned off. The surpassing of the air temperature beyond the set points is due to the chamber's thermal inertia as well as the residual cooling effect available in the evaporator after the compressor is turned off. As such, the set points create an approximate window of action for temperature control. The overshoot is less noticeable for larger hysteresis values, i.e., to the right of Fig. 3-22. The temperature overshoot is often unavoidable in typical HVAC-R systems equipped with on/off controllers.

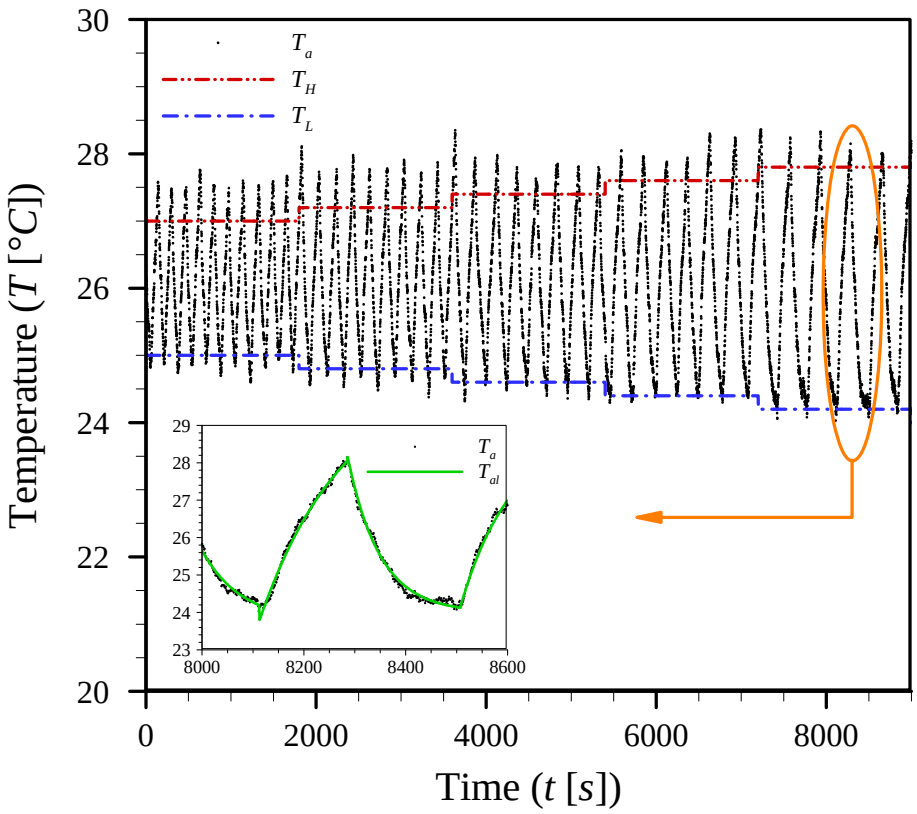

Figure 3-22: Air temperature measurement results. Exponential correlations are applied with a minimum coefficient of determination of $R^2 = 0.98$. Reprinted with permission [75]**.**

In the next step, the c-parameters for each temperature swing are found by applying the curve fits of Eqs. (3-25) and (3-26). The increasing time t_I and the decreasing time t_D are then calculated using Eqs. (3-28) and (3-29). The mean temperature and power consumption are calculated based on Eqs. (3-31) and (3-32). Since the average temperature and power calculated in this method are found based on the correlations, the subscript "l" is added to distinguish between the measured data and the calculated values.

Figure 3-23 shows a comparison between the calculated average temperature T_{ml} and the measured average temperature T_m. The calculated average power E_{ml} is also compared with the measured average power E_m in Fig. 3-23. The measured mean temperature T_m is found by taking the average of the air temperature T_a over every swing period. The average power E_m is also calculated by taking the average of the

measured compressor power over every temperature swing. Since the c-parameters correspond to the entire period of every temperature swing separately, the calculations are also performed for every swing. Therefore, T_m, T_{ml}, E_m, and E_{ml} are shown as discreet points at every swing occurrence. The maximum relative error for the calculation of mean temperature is 1%. The mean power consumption is calculated with a maximum relative error of 16%.

It is observed in Fig. 3-23 that, although the set points are symmetrically selected around the desired temperature of $26°C$, the measured average power can vary from $E_m = 217\,W$ up to $E_m = 323\,W$. Therefore, it is shown in this experiment that only by changing the symmetric hysteresis of the set points, the energy consumption can be affected by up to 49%. Moreover, the measured mean temperature is below the desired temperature of $26°C$ in large hysteresis cases. This results in increased overall energy consumption and is an indication of the necessity for proper selection of set points.

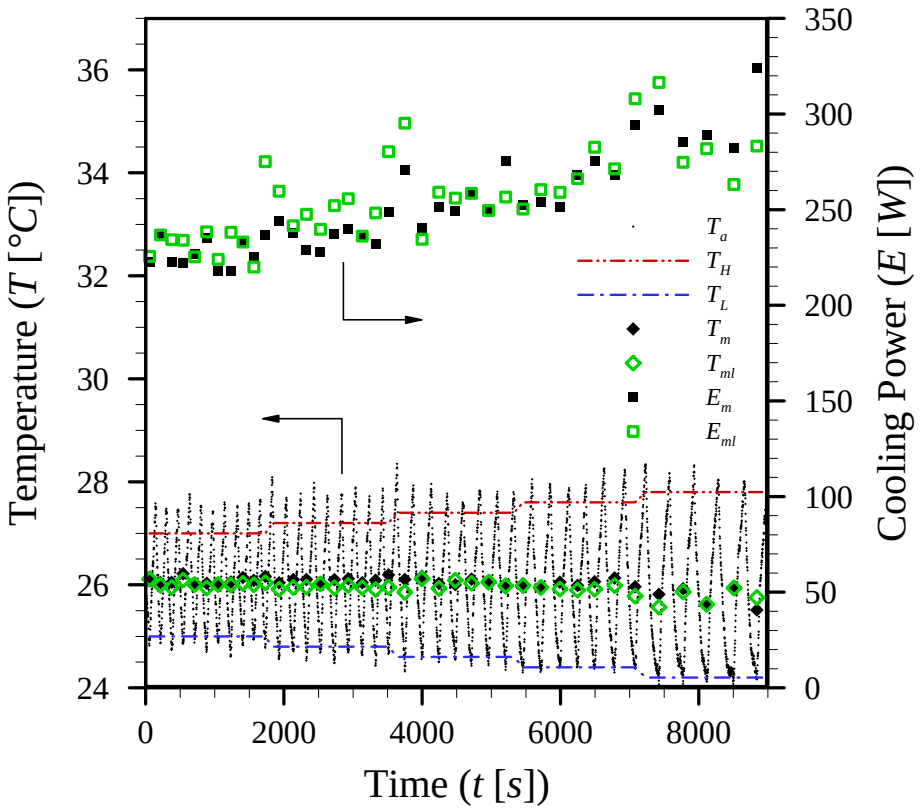

Figure 3-23: Average temperature and power as measured and calculated using the exponential correlations. The maximum relative errors of average temperature and power are 1% and 16%, respectively. Reprinted with permission [75]**.**

As observed in Fig. 3-23, for higher values of symmetric hysteresis, the compressor needs to stay on during a larger portion of the temperature swings, *i.e.*, t_D increases more dramatically than t_I for higher hysteresis values. As a consequence, the average temperature decreases. In this test, although the desired temperature is set at $26°C$, mean temperatures as low as $25.5°C$ are achieved for a hysteresis of $\pm 1.8°C$. This proves that with selecting an improper pair of set points, the actual value of average temperature can be different from the desired temperature. In such cases, excessive cooling or heating is provided to the system which may not be necessary. Furthermore, high hysteresis values result in excessive temperature deviations from the desired value which may not be acceptable in certain applications.

Figure 3-23 also shows the mean compressor power. As described above, the overall energy consumption increases with increasing symmetric hysteresis. Thus, when

symmetric set points are to be selected around the desired temperature, it is preferable to choose narrower ones to avoid excessive temperature deviation and energy consumption. On the other hand, low hysteresis values result in high numbers of compressor starts per hour. Therefore, to avoid excessive compressor starts, the set points should not be too narrow.

Figure 3-24 shows the estimated number of compressor starts per hour calculated by Eq. (3-33). As expected, increasing the gap between T_L and T_H results in decreasing ω_l which is calculated based on the exponential temperature correlations. During every half-hour period when T_L and T_H are constant, the ω_l values of different swing instances are almost equal to each other. But at the times when T_L and T_H change, the value of ω_l also changes accordingly. Figure 3-24 shows the average ω_l calculated over the entire half-hour period of every set point pair.

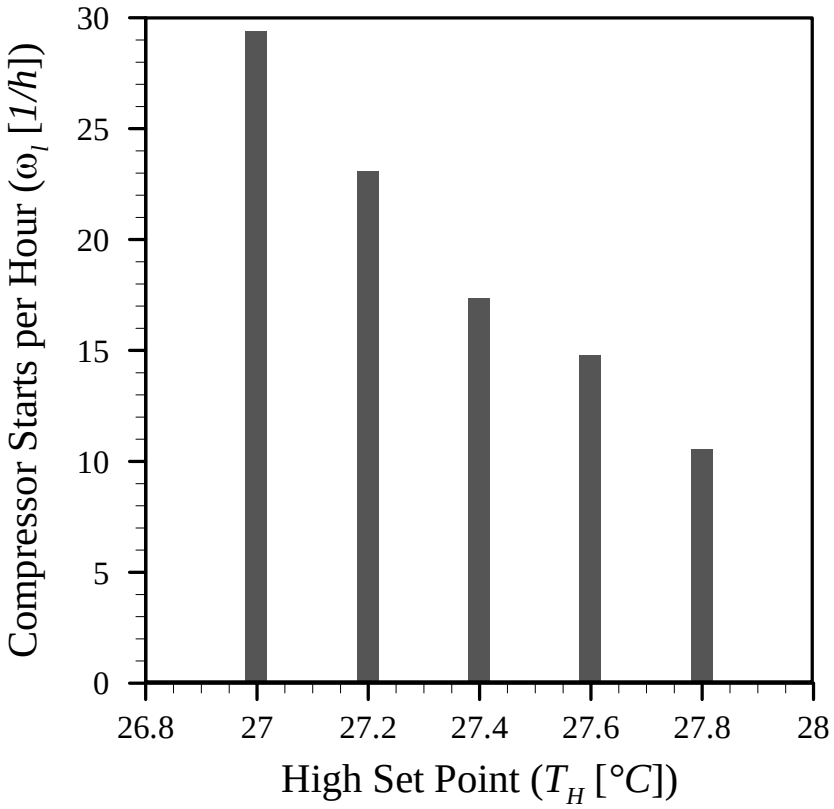

Figure 3-24: Estimated number of compressor starts per hour for various set points. Reprinted with permission [75]**.**

The validated model can be used as a tool for set point design in any type of HVAC-R system equipped with an on/off controller. The proposed design strategy is used in the following section as a basis for energy-efficient design of set points in the present experiment.

Set Point Design

In this section, the design strategy outlined in the model development section is followed to select the set points for the experimental setup described above. It is necessary to find the c-parameters of the exponential correlations (step 1). Adopting a gray-box approach for an existing system, the c-parameters can be found by performing an experiment in which the room experiences a few swings. Then, the c-parameters can be used for analysis. In this example, we arbitrarily select the parameters listed in Table 3-8 as they are found by piecewise correlations at $t = 4479\ s$ of the experiment shown in Fig. 3-22. Nevertheless, in an automatic system, the c-parameters can be updated at every swing, therefore providing more accurate parameters for the upcoming conditions.

Table 3-8: c-parameters calculated at $t = 4479\ s$ of the experiment presented in Fig. 3-22. Reprinted with permission [75]**.**

Parameter	Value	Parameter	Value
c_{1I}	$29.9°C$	c_{1D}	$22.3°C$
c_{2I}	$-5.5°C$	c_{2D}	$5.6°C$
c_{3I}	$126s$	c_{3D}	$128s$

The maximum allowable temperature deviation from the desired level is assumed to be $1.6°C$ (step 2). The maximum number of compressor starts per hour is assumed to be 16 (step 3). The next step is to find the proper t_I and t_D for keeping the mean temperature at the desired level and ω_l equal to the maximum allowable number of compressor starts per hour (step 4). Figure 3-25 shows ω_l versus T_H. For every value of T_H in Fig. 3-25, the corresponding T_L is calculated by solving Eq. (3-31) subject to

T_{ml} equal to the desired temperature. Therefore, for every T_H, if T_L is correctly selected, T_{ml} is equal to the desired temperature and ω_l can be found from Fig. 3-25. The minimum allowable T_H corresponding to $\omega_l = 16$ is thus estimated as $27.4°C$ (step 5). On the other hand, the maximum allowable T_H is $27.6°C$, due to the decided maximum temperature deviation (step 6).

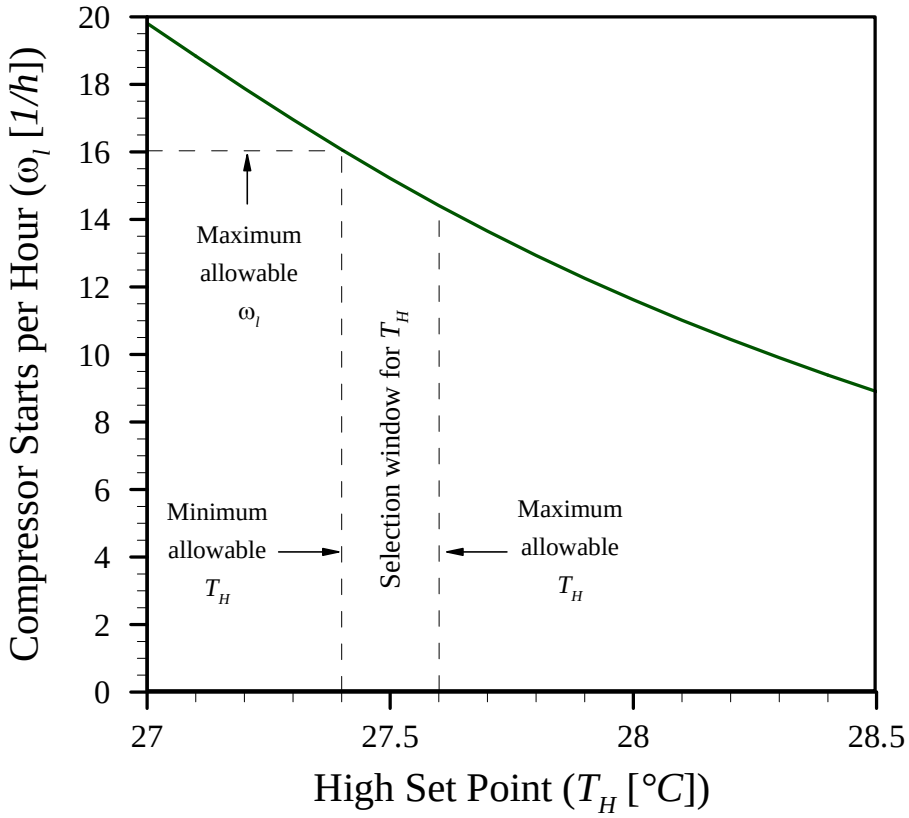

Figure 3-25: Calculated number of compressor starts per hour (ω_l) as a function of T_H. It is assumed that T_L is properly selected to achieve $T_{ml} = 26°C$ at every T_H level. Reprinted with permission [75]**.**

At this stage, the window of selection for T_H is found, i.e., $27.4°C < T_H < 27.6°C$. Within this range, the number of compressor starts per hour and the temperature deviation are both less than their respective maximum allowable values. By proper selection of T_L for every T_H, the resulting mean temperature will also be equal to its desired value. Hence, all the constraints of the optimization problem are satisfied. The last stage of the design is to select a T_H value that minimizes E_{ml}. Figure 3-26 shows

the plot of the average power E_{ml} versus T_H, given that T_L is properly selected for every T_H so that T_{ml} is equal to the desired temperature of $26°C$. As observed in Fig. 3-26, the power consumption decreases with increasing T_H for this experiment. Therefore, the most energy-efficient value of T_H within its allowable range is $T_H = 27.6°C$ (step 7). By solving Eq. (3-31), the low set point is further found to be $T_L = 24.1°C$, as also determined from Fig. 3-26 (step 8). The average power consumption can thus be calculated using Eq. (3-32) or Fig. 3-26 as $E_{ml} = 265.3W$ (step 9). The number of compressor starts per hour is also calculated using Eq. (3-33) or Fig. 3-25 as $\omega_l = 14$ starts per hour (step 10).

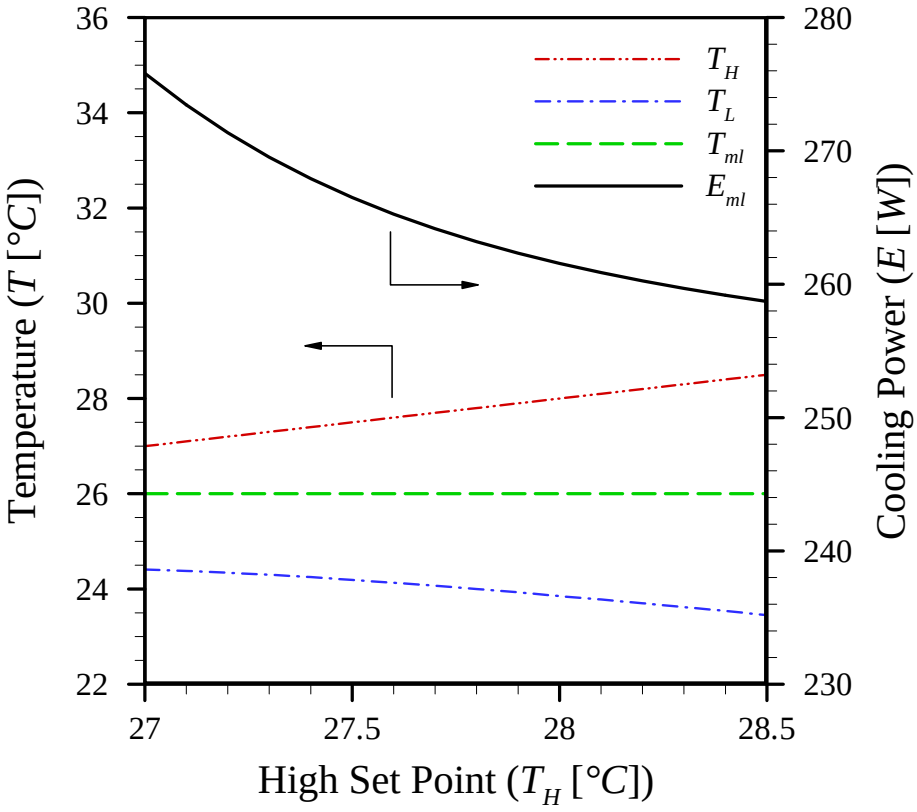

Figure 3-26: Calculated average power consumption (E_{ml}) as a function of T_H. It is assumed that T_L is properly selected to achieve $T_{ml} = 26°C$ at every T_H level. Reprinted with permission [75]**.**

Figure 3-26 shows that by selecting different set point pairs, the average power consumption for providing the same average temperature can vary from $E_{ml} = 275W$

down to $E_{ml} = 258W$. Thus, a proper selection of asymmetric set points can save 6.6% of the overall energy. The slight decrease in the effective power consumption for higher hysteresis is because when the cycle is commanded to start at a higher T_H value, the cooling load provided to the chamber slightly increases. Hence, the higher temperature gradient between the chamber air and the cold air leads to a higher cooling effect for the same compressor power. Therefore, less overall energy is consumed by the cycle for the same mean temperature.

It should be noted that symmetric selection of hysteresis, as is done in Fig. 3-23, yields to different results compared with the asymmetric selection of set points according to the present model. Figure 3-23 shows that if the set points are symmetrically selected around the desired temperature, larger hysteresis results in higher energy consumption. However, the mean temperature may not be equal to the desired value. As a result, more energy may be consumed to maintain an undesired average temperature. However, by selecting the set points using the present model, the average temperature is more accurately maintained at the desired level, and higher hysteresis yields to slightly less energy consumption.

The proposed design strategy forms an analytical tool for proper selection of the set points in any HVAC-R system equipped with an on/off controller. The prerequisite to using this method is to know the correlation parameters, an example of which is reported in Table 3-8. In order to find those parameters, it is necessary to have the temperature data for at least one temperature swing. Thus, the proposed method is readily applicable to existing systems. On the other hand, for new systems where the temperature data may not be available, the proposed method can still be used by knowing the physical parameters of Eq. (3-19). Similar to white-box approaches, the designer can collect the physical and geometrical parameters of the governing equation. The proposed design strategy can then be used to reformulate the heat balance equation and utilize the resulting c -parameters for energy-efficient selection of on/off set points.

3.4.3. Conclusions

In this section, a design strategy was proposed for energy-efficient selection of high and low temperature set points. The objective was to select the set points for minimizing the overall energy consumption subject to the following constraints:

- Minimum error between the average temperature and the desired temperature
- Minimum temperature deviation from the desired temperature
- Minimum number of compressor starts per hour

Following a gray-box approach, exponential correlations were fitted to raw temperature measurements. Based on the heat balance equation, the design strategy was formulated to provide analytical estimations of all the corresponding quantities. The model was validated by estimating the mean temperature and the average power consumption with acceptable accuracies. It was experimentally shown that the set points could affect the overall energy consumption by as much as 49%, if they were symmetrically selected around the desired temperature. It was further shown that while maintaining the exact desired temperature, there was an opportunity to further increase the energy efficiency by 6.6% using different high and low hysteresis values.

Chapter 4. Summary and Future Work

4.1. Summary

In this thesis, several novel methods are proposed for improving thermal load calculations in HVAC-R systems. Improved thermal load estimations provide the possibility of reducing the overall energy consumption of the system.

Both stationary and mobile applications are investigated to make a rigorous contribution to the field. It is noted that while the literature's focus has mostly been on building air conditioning systems, the literature lacks a comprehensive approach for load calculation in mobile systems. Therefore, a model is developed in this thesis for mobile load calculations. New methods for estimation of thermal loads and thermal inertia of a room are also developed and applied to stationary applications. Such methods are established based on general heat transfer equations and are theoretically applicable to both stationary and mobile applications.

In this thesis, refrigeration is studied alongside heating and air conditioning problems. An actual freezer room of a restaurant is used for refrigeration experiments, while an in-house testbed is developed in the lab for heating and air-conditioning experiments. Remarkable opportunities for reduction of energy consumption and emissions were identified and reported through the study of each proposed method.

The proposed methods of this thesis are categorized into law-driven and data-driven approaches. Conventional methods that are mostly based on the governing laws of heat transfer are studied. Nevertheless, data-driven approaches are used for the larger part of this thesis to develop novel methods relying on sensor measurements.

The palette of methods developed in this thesis is ready to be implemented in HVAC-R controllers for intelligent control of refrigeration and air conditioning systems. The load-

based control of the HVAC-R systems can lead to considerable reductions in energy consumption.

4.2. Future Work

The following future work is suggested to further improve the model presented in this thesis:

- Combining the proposed load estimation models with an optimization algorithm for real-time selection of compressor and fans speeds in the air conditioning cycle.
- Improving the models by incorporation of higher numbers of sensors.
- Coupling the developed lumped-body approaches with 3D CFD simulations for improving the accuracy of the results.
- Developing algorithms for optimized control of the refrigeration cycle components based on the acquired load estimations.

References

[1] L. Pérez-Lombard, J. Ortiz, and C. Pout, “A review on buildings energy consumption information,” *Energy and Buildings*, vol. 40, no. 3, pp. 394–398, Jan. 2008.

[2] K. J. Chua, S. K. Chou, W. M. Yang, and J. Yan, “Achieving better energy-efficient air conditioning – A review of technologies and strategies,” *Applied Energy*, vol. 104, pp. 87–104, Apr. 2013.

[3] T. Hovgaard, L. Larsen, M. Skovrup, and J. Jørgensen, “Power consumption in refrigeration systems-modeling for optimization,” in *Proceedings of the 2011 4th International International Symposium on Advanced Control of Industrial Processes*, 2011, pp. 234–239.

[4] R. Farrington, M. Cuddy, M. Keyser, and J. Rugh, “Opportunities to Reduce Air-Conditioning Loads Through Lower Cabin Soak Temperatures,” in *Proceedings of the 16th Electric Vehicle Symposium*, 1999.

[5] R. Farrington and J. Rugh, “Impact of vehicle air-conditioning on fuel economy, tailpipe emissions, and electric vehicle range,” in *Earth Technologies Forum*, 2000, no. September.

[6] J. Welstand, H. Haskew, R. Gunst, and O. Bevilacqua, “Evaluation of the effects of air conditioning operation and associated environmental conditions on vehicle emissions and fuel economy,” *SAE Transactions*, 2003.

[7] V. H. Johnson, “Fuel Used for Vehicle Air Conditioning: A State-by-State Thermal Comfort-Based Approach,” *SAE Transactions*, 2002.

[8] M. A. Lambert and B. J. Jones, “Automotive Adsorption Air Conditioner Powered by Exhaust Heat. Part 1: Conceptual and Embodiment Design,” *Proceedings of the Institution of Mechanical Engineers, Part D: Journal of Automobile Engineering*, vol. 220, no. 7, pp. 959–972, Dec. 2006.

[9] ASHRAE, “Handbook of Fundamentals, SI Edition,” American Society of Heating, Refrigerating and Air-Conditioning, Atlanta, 1988.

[10] C. O. Pedersen, D. E. Fisher, and R. J. Liesen, “Development of a heat balance procedure for calculating cooling loads,” *ASHRAE Transactions*, vol. 103, pp. 459–468, 1997.

[11] C. S. Barnaby, J. D. Spitler, and D. Xiao, “The Residential Heat Balance Method for Heating and Cooling Load Calculations,” *ASHRAE Transactions*, vol. 111, no. 1, pp. 308–319, 2005.

[12] M. A. Fayazbakhsh and M. Bahrami, “Comprehensive Modeling of Vehicle Air Conditioning Loads Using Heat Balance Method,” in *SAE Transactions*, 2013.

[13] ASHRAE, “Standard 90.1-2013, Energy standard for buildings except low rise residential buildings,” *American Society of Heating, Refrigerating and Air Conditioning Engineers*, 2013.

[14] D. L. Loveday and A. H. Taki, “Convective heat transfer coefficients at a plane surface on a full-scale building facade,” *International Journal of Heat and Mass Transfer*, vol. 39, no. 8, pp. 1729–1742, May 1996.

[15] Y. Kurazumi, L. Rezgals, and A. Melikov, “Convective Heat Transfer Coefficients of the Human Body under Forced Convection from Ceiling,” *Journal of Ergonomics*, vol. 4, no. 1, pp. 1–6, 2014.

[16] L. Lei, S. Wang, and T. (Tim) Zhang, “Inverse determination of wall boundary convective heat fluxes in indoor environments based on CFD,” *Energy and Buildings*, vol. 73, pp. 130–136, Apr. 2014.

[17] Z. Zhai, Q. Chen, P. Haves, and J. H. Klems, “On approaches to couple energy simulation and computational fluid dynamics programs,” *Building and Environment*, vol. 37, pp. 857–864, 2002.

[18] Z. Zhai and Q. Chen, “Impact of determination of convective heat transfer on the coupled energy and CFD simulation for buildings,” *Proceedings of Building Simulation Conference*, pp. 1467–1474, 2003.

[19] Z. Zhai, Q. Chen, J. H. Klems, and P. Haves, “Strategies for coupling energy simulation and computational fluid dynamics programs,” 2001.

[20] Z. Zhai and Q. Chen, “Solution characters of iterative coupling between energy simulation and CFD programs,” *Energy and Buildings*, vol. 35, pp. 493–505, 2003.

[21] Z. Zhai and Q. (Yan) Chen, “Numerical determination and treatment of convective heat transfer coefficient in the coupled building energy and CFD simulation,” *Building and Environment*, vol. 39, no. 8, pp. 1001–1009, Aug. 2004.

[22] Z. J. Zhai and Q. Y. Chen, “Performance of coupled building energy and CFD simulations,” *Energy and Buildings*, vol. 37, no. 4, pp. 333–344, Apr. 2005.

[23] A. Khalifa, “Natural convective heat transfer coefficient–a review: I. Isolated vertical and horizontal surfaces,” *Energy Conversion and Management*, vol. 42, 2001.

[24] A. Khalifa, “Natural convective heat transfer coefficient–a review: II. Surfaces in two-and three-dimensional enclosures,” *Energy Conversion and Management*, vol. 42, 2001.

[25] E. Sartori, “Convection coefficient equations for forced air flow over flat surfaces,” *Solar Energy*, vol. 80, no. 9, pp. 1063–1071, Sep. 2006.

[26] J. a. Palyvos, “A survey of wind convection coefficient correlations for building envelope energy systems’ modeling,” *Applied Thermal Engineering*, vol. 28, no. 8–9, pp. 801–808, Jun. 2008.

[27] T. Defraeye, B. Blocken, and J. Carmeliet, “Convective heat transfer coefficients for exterior building surfaces: Existing correlations and CFD modelling,” *Energy Conversion and Management*, vol. 32, no. 0, pp. 1–20, 2011.

[28] P. O. Fanger, *Thermal Comfort: Analysis and Applications in Environmental Engineering*. New York: McGraw-Hill, 1972.

[29] J. Ingersoll, T. Kalman, L. Maxwell, and R. Niemiec, “Automobile passenger compartment thermal comfort model-Part II: Human thermal comfort calculation,” in *SAE transactions*, 1992.

[30] Y. Zheng, B. Mark, and H. Youmans, “A Simple Method to Calculate Vehicle Heat Load,” SAE International, Apr. 2011.

[31] O. Arici, S. Yang, D. Huang, and E. Oker, “Computer model for automobile climate control system simulation and application,” *International Journal of Applied Thermodynamics*, vol. 2, no. 2, pp. 59–68, 1999.

[32] Y. Ding and R. Zito, “Cabin heat transfer and air conditioning capacity,” *SAE Technical Paper*, 2001.

[33] J. Selow, M. Wallis, S. Zoz, and M. Wiseman, “Towards a Virtual Vehicle for Thermal Analysis,” in *SAE Technical Paper*, 1997.

[34] H. Khayyam, A. Z. Kouzani, and E. J. Hu, “Reducing energy consumption of vehicle air conditioning system by an energy management system,” in *2009 IEEE Intelligent Vehicles Symposium*, 2009, vol. i, no. 1, pp. 752–757.

[35] H. Khayyam, A. Z. Kouzani, E. J. Hu, and S. Nahavandi, “Coordinated energy management of vehicle air conditioning system,” *Applied Thermal Engineering*, vol. 31, no. 5, pp. 750–764, Apr. 2011.

[36] K. C. Wei and G. a. Dage, “An intelligent automotive climate control system,” *1995 IEEE International Conference on Systems, Man and Cybernetics. Intelligent Systems for the 21st Century*, vol. 4, pp. 2977–2982, 1995.

[37] A. Alexandrov, V. Kudriavtsev, and M. Reggio, “Analysis of Flow Patterns and Heat Transfer in Generic Passenger Car Mini-Environment,” in *9th Annual Conference of the CFD Society of Canada*, 2001.

[38] B. Bueno, L. Norford, G. Pigeon, and R. Britter, “A resistance-capacitance network model for the analysis of the interactions between the energy performance of buildings and the urban climate,” *Building and Environment*, vol. 54, pp. 116–125, Aug. 2012.

[39] Y. Yener and S. Kakaç, *Heat conduction*. Taylor & Francis Group, 2008.

[40] R. Zhao, L. Gosselin, M. Fafard, and D. P. Ziegler, “Heat transfer in upper part of electrolytic cells: Thermal circuit and sensitivity analysis,” *Applied Thermal Engineering*, vol. 54, no. 1, pp. 212–225, May 2013.

[41] A. Abo El-Nasr and S. M. El-Haggar, “Effective thermal conductivity of heat pipes,” *Heat and Mass Transfer*, vol. 32, no. 1–2, pp. 97–101, Nov. 1996.

[42] S. Moghaddam, M. Rada, a. Shooshtari, M. Ohadi, and Y. Joshi, “Evaluation of analytical models for thermal analysis and design of electronic packages,” *Microelectronics Journal*, vol. 34, no. 3, pp. 223–230, Mar. 2003.

[43] A. Gholami, M. Ahmadi, and M. Bahrami, “A New Analytical Approach for Dynamic Modeling of Passive Multicomponent Cooling Systems,” *Journal of Electronic Packaging*, vol. 136, no. 3, p. 031010, May 2014.

[44] W. Shi, B. Wang, and X. Li, “A measurement method of ice layer thickness based on resistance-capacitance circuit for closed loop external melt ice storage tank,” *Applied Thermal Engineering*, vol. 25, no. 11–12, pp. 1697–1707, Aug. 2005.

[45] a. Mezrhab and M. Bouzidi, “Computation of thermal comfort inside a passenger car compartment,” *Applied Thermal Engineering*, vol. 26, no. 14–15, pp. 1697–1704, Oct. 2006.

[46] N. Zhu, S. Wang, Z. Ma, and Y. Sun, “Energy performance and optimal control of air-conditioned buildings with envelopes enhanced by phase change materials,” *Energy Conversion and Management*, vol. 52, no. 10, pp. 3197–3205, Sep. 2011.

[47] O. T. Ogunsola, L. Song, and G. Wang, “Development and validation of a time-series model for real-time thermal load estimation,” *Energy and Buildings*, vol. 76, pp. 440–449, Jun. 2014.

[48] K. Deng, P. Barooah, P. G. Mehta, and M. S. P., “Building thermal model reduction via aggregation of states,” in *2010 American Control Conference*, 2010, pp. 5118–5123.

[49] F. Haldi and D. Robinson, “The Impact of Occupants’ Behaviour on Urban Energy

Demand," in *BauSim 2010*, 2010, pp. 343–348.

[50] S. Wang and X. Xu, "Parameter estimation of internal thermal mass of building dynamic models using genetic algorithm," *Energy Conversion and Management*, vol. 47, no. 13–14, pp. 1927–1941, Aug. 2006.

[51] F. Oldewurtel, A. Parisio, C. N. Jones, D. Gyalistras, M. Gwerder, V. Stauch, B. Lehmann, and M. Morari, "Use of model predictive control and weather forecasts for energy efficient building climate control," *Energy and Buildings*, vol. 45, pp. 15–27, Feb. 2012.

[52] M. Maasoumy, M. Razmara, M. Shahbakhti, and a. S. Vincentelli, "Handling model uncertainty in model predictive control for energy efficient buildings," *Energy and Buildings*, vol. 77, pp. 377–392, Jul. 2014.

[53] G. Platt, J. Li, R. Li, G. Poulton, G. James, and J. Wall, "Adaptive HVAC zone modeling for sustainable buildings," *Energy and Buildings*, vol. 42, no. 4, pp. 412–421, Apr. 2010.

[54] M. A. Fayazbakhsh, F. Bagheri, and M. Bahrami, "A Resistance–Capacitance Model for Real-Time Calculation of Cooling Load in HVAC-R Systems," *Journal of Thermal Science and Engineering Applications*, vol. 7, no. 4, p. 041008, 2015.

[55] F. Ansari and A. Mokhtar, "A simple approach for building cooling load estimation," *American Journal of Environmental Sciences*, vol. 1, no. 3, pp. 209–212, 2005.

[56] N. Kashiwagi and T. Tobi, "Heating and Cooling Load Prediction Using a Neural Network System," in *Proceedings of 1993 International Conference on Neural Networks (IJCNN-93-Nagoya, Japan)*, 1993, vol. 1, pp. 939–942.

[57] A. E. Ben-Nakhi and M. A. Mahmoud, "Cooling load prediction for buildings using general regression neural networks," *Energy Conversion and Management*, vol. 45, no. 13–14, pp. 2127–2141, Aug. 2004.

[58] Q. Li, Q. Meng, J. Cai, H. Yoshino, and A. Mochida, "Predicting hourly cooling load in the building: A comparison of support vector machine and different artificial neural networks," *Energy Conversion and Management*, vol. 50, no. 1, pp. 90–96, Jan. 2009.

[59] Y. Yao, Z. Lian, S. Liu, and Z. Hou, "Hourly cooling load prediction by a combined forecasting model based on Analytic Hierarchy Process," *International Journal of Thermal Sciences*, vol. 43, no. 11, pp. 1107–1118, Nov. 2004.

[60] O. Solmaz, M. Ozgoren, and M. H. Aksoy, "Hourly cooling load prediction of a vehicle in the southern region of Turkey by Artificial Neural Network," *Energy Conversion and Management*, vol. 82, pp. 177–187, Jun. 2014.

[61] J. M. Sousa, R. Babuška, and H. B. Verbruggen, “Fuzzy predictive control applied to an air-conditioning system,” *Control Engineering Practice*, vol. 5, no. 10, pp. 1395–1406, Oct. 1997.

[62] H. Khayyam, S. Nahavandi, E. Hu, A. Kouzani, A. Chonka, J. Abawajy, V. Marano, and S. Davis, “Intelligent energy management control of vehicle air conditioning via look-ahead system,” *Applied Thermal Engineering*, vol. 31, no. 16, pp. 3147–3160, Nov. 2011.

[63] S. Wang and X. Xu, “Simplified building model for transient thermal performance estimation using GA-based parameter identification,” *International Journal of Thermal Sciences*, vol. 45, no. 4, pp. 419–432, Apr. 2006.

[64] H. Khayyam, “Adaptive intelligent control of vehicle air conditioning system,” *Applied Thermal Engineering*, vol. 51, no. 1–2, pp. 1154–1161, Mar. 2013.

[65] M. A. Fayazbakhsh, F. Bagheri, and M. Bahrami, “An inverse method for calculation of thermal inertia and heat gain in air conditioning and refrigeration systems,” *Applied Energy*, vol. 138, pp. 496–504, Jan. 2015.

[66] X. Li and J. Wen, “Review of building energy modeling for control and operation,” *Renewable and Sustainable Energy Reviews*, vol. 37, pp. 517–537, Sep. 2014.

[67] H. Mirinejad, K. Welch, and L. Spicer, “A review of intelligent control techniques in HVAC systems,” *Energytech, 2012 IEEE*, pp. 1–5, 2012.

[68] R. Haines and D. Hittle, *Control systems for heating, ventilating, and air conditioning*, 6th ed. Springer, 2006.

[69] B. Arguello-Serrano and M. Velez-Reyes, “Nonlinear control of a heating, ventilating, and air conditioning system with thermal load estimation,” *IEEE Transactions on Control Systems Technology*, vol. 7, no. 1, pp. 56–63, 1999.

[70] A. Afram and F. Janabi-Sharifi, “Gray-box modeling and validation of residential HVAC system for control system design,” *Applied Energy*, vol. 137, pp. 134–150, Jan. 2015.

[71] Y. Zhu, X. Jin, X. Fang, and Z. Du, “Optimal control of combined air conditioning system with variable refrigerant flow and variable air volume for energy saving,” *International Journal of Refrigeration*, vol. 42, pp. 14–25, Jun. 2014.

[72] T. Qureshi and S. Tassou, “Variable-speed capacity control in refrigeration systems,” *Applied Thermal Engineering*, vol. 16, no. 2, pp. 103–113, 1996.

[73] A. P. Wemhoff, “Calibration of HVAC equipment PID coefficients for energy conservation,” *Energy and Buildings*, vol. 45, pp. 60–66, Feb. 2012.

[74] B. L. Bin Li and A. G. Alleyne, “Optimal on-off control of an air conditioning and refrigeration system,” *American Control Conference (ACC), 2010*, pp. 5892–5897, 2010.

[75] M. A. Fayazbakhsh, F. Bagheri, and M. Bahrami, “Gray-box model for energy-efficient selection of set point hysteresis in heating, ventilation, air conditioning, and refrigeration controllers,” *Energy Conversion and Management*, vol. 103, pp. 459–467, 2015.

[76] S. Wang and Z. Ma, “Supervisory and Optimal Control of Building HVAC Systems: A Review,” *HVAC&R Research*, vol. 14, no. March 2015, pp. 3–32, 2008.

[77] I. 8996, “Ergonomics of the thermal environment - Determination of metabolic heat production,” 2004.

[78] M. Talbi and B. Agnew, “Energy recovery from diesel engine exhaust gases for performance enhancement and air conditioning,” *Applied thermal engineering*, vol. 1, no. 5, pp. 5–10, 2002.

[79] A. K. Singh, H. Singh, S. P. Singh, and R. L. Sawhney, “Numerical calculation of psychrometric properties on a calculator,” *Building and Environment*, vol. 37, no. 4, pp. 415–419, Apr. 2002.

[80] “ASHRAE 55, Thermal environmental conditions for human occupancy,” *American Society of Heating, Refrigerating and Air Conditioning*, 1992.

[81] “Future Vehicle Technologies.” [Online]. Available: http://www.futurevehicletechnologies.com.

[82] “United States Environmental Protection Agency.” [Online]. Available: http://www.epa.gov.

[83] M. Arndt and M. Sauer, “Spectroscopic carbon dioxide sensor for automotive applications,” *Sensors, 2004. Proceedings of IEEE*, pp. 252–255, 2004.

[84] B. Fletcher and C. Saunders, “Air change rates in stationary and moving motor vehicles,” *Journal of Hazardous Materials*, vol. 38, pp. 243–256, 1994.

[85] A. Stegou-Sagia, K. Antonopoulos, C. Angelopoulou, and G. Kotsiovelos, “The impact of glazing on energy consumption and comfort,” *Energy Conversion and Management*, vol. 48, no. 11, pp. 2844–2852, Nov. 2007.

[86] J. Allard and R. Heinzen, “Adaptive defrost,” *IEEE Transactions on Industry Applications*, vol. 24, no. 1, pp. 39–42, 1988.

[87] Massachusetts: The MathWorks Inc., “MATLAB Version R2011b.” 2011.

[88] J. J. Monaghan, “Smoothed particle hydrodynamics,” *Reports on Progress in Physics*, vol. 68, no. 8, pp. 1703–1759, Aug. 2005.

[89] J. Jabardo, W. Mamani, and M. Ianella, “Modeling and experimental evaluation of an automotive air conditioning system with a variable capacity compressor,” *International Journal of Refrigeration*, vol. 25, pp. 1157–1172, 2002.

[90] S. Wang, J. Gu, T. Dickson, J. Dexter, and I. McGregor, “Vapor quality and performance of an automotive air conditioning system,” *Experimental Thermal and Fluid Science*, vol. 30, no. 1, pp. 59–66, Oct. 2005.

[91] P. Bansal, D. Fothergill, and R. Fernandes, “Thermal analysis of the defrost cycle in a domestic freezer,” *International Journal of Refrigeration*, vol. 33, no. 3, pp. 589–599, May 2010.

[92] M. Bomberg and M. Kumaran, *Use of Field-Applied Polyurethane Foams in Buildings*. Institute for Research in Construction, National Research Council of Canada, 1999.

[93] M. A. Fayazbakhsh, F. Bagheri, and M. Bahrami, “A Self-Adjusting Method for Real-Time Calculation of Thermal Loads in HVAC-R Applications,” *Journal of Thermal Science and Engineering Applications*, no. c, 2015.

[94] M. A. Fayazbakhsh, F. Bagheri, and M. Bahrami, “Real-time thermal load calculation by automatic estimation of convection coefficients,” *International Journal of Refrigeration*, vol. 57, pp. 229–238, 2015.

[95] F. Bagheri, M. A. Fayazbakhsh, P. Cheppudira Thimmaiah, and M. Bahrami, “Theoretical and experimental investigation into anti-idling A/C system for trucks,” *Energy Conversion and Management*, vol. 98, pp. 173–183, 2015.

[96] R. P. Lippmann, “An introduction to computing with neural nets,” *ACM SIGARCH Computer Architecture News*, vol. 16, no. 1, pp. 7–25, Mar. 1988.

[97] J. Liang and R. Du, “Thermal comfort control based on neural network for HVAC application,” *Proceedings of 2005 IEEE Conference on Control Applications, 2005. CCA 2005.*, pp. 819–824, 2005.

[98] K. Mehrotra, C. Mohan, and S. Ranka, *Elements of artificial neural networks*. MIT press, 1997.

[99] F. Rosenblatt, *Principles of neurodynamics*. 1962.

[100] D. Graupe, *Principles of artificial neural networks*. 1997.

[101] K. Chinnakani, A. Krishnamurthy, J. Moyne, and F. Gu, “Comparison of energy consumption in HVAC systems using simple ON-OFF, intelligent ON-OFF and

optimal controllers," *IEEE Power and Energy Society General Meeting*, pp. 1–6, 2011.

[102] C. Ghiaus, "Causality issue in the heat balance method for calculating the design heating and cooling load," *Energy*, vol. 50, pp. 292–301, Feb. 2013.

Appendix A. Duty Cycle Identification for Refrigerated Trucks

Refrigerated trucks are major consumers of energy that is spent on keeping their products refrigerated. Since the materials transported by such trucks are mostly food products, failure to provide the required cooling load may result in corruption of the stored products. Certain food types may also need specific temperature or humidity levels. Therefore, product safety is an important factor in the design of control systems for refrigerated trucks.

While the thermal safety of the food products is maintained, it is desirable to fulfill this objective with less energy consumption. The task of the refrigeration system's controller is to react to the thermal load variations and control the device accordingly. In conventional applications, no knowledge of the upcoming patterns is provided to the controller. However, if the duty cycle of the system is known, the load variations will be predictable. Energy-smart applications can therefore be designed to use this knowledge for efficient control of the refrigeration system.

As a part of this project, the temperatures inside the refrigerated cabin of a truck are measured at several locations. Wireless data loggers are utilized to store the temperature value every 10 seconds during a time span of one week. The truck has provided the regular service of transporting dairy products during the week of study. The aim of this study is to identify the duty cycle of the refrigerated truck for establishing proper guidelines on the control and operation of the refrigerated system. Incorporating the knowledge of the duty cycle pattern can improve the automatic functionality of the controller.

Figure A-1 shows the measurement instruments used for recording temperature variations in the refrigerated truck. Rotronic temperature and humidity data loggers are used for high-accuracy measurement of temperature and relative humidity at the evaporator inlet and outlet. The Track-It temperature data loggers record the air temperature at several locations of the refrigerated cabin. The 4-channel data logger thermometer is used for collecting the temperature values from thermocouples attached to the piping system of the refrigeration system. The portable anemometer is used to

measure the air velocity at the outlet of the evaporator and condenser. The lux meter is also attached on the roof of the truck for acquiring accurate measurements of the solar radiation. Refer to Section 2.2 for detailed information on the sensors and their accuracies.

Rotronic Temperature and Humidity Data Logger

4-Channel Data Logging Thermometer

Portable Anemometer

Lux Meter

Track-It Temperature Data Logger

Figure A-1: Measurement instruments used for recording temperature variations in the refrigerated truck.

Figure A-2 shows a plot of the recorded cabin temperature during one week of the truck's regular operation. The data shows the average cabin temperature starting and ending at Thursday noon. As discussed in the previous chapters, distinct regimes of temperature variation are also observed in this data set.

Since the refrigerated trucks are also on/off controlled, swinging regimes occur when the refrigeration system is on. Such swinging patterns are visible in Fig. A-2. As

observed in Fig. A-2, whenever the temperature swings between $2°C$ and $5°C$, it is a sign of the refrigeration system being on and the cabin door being closed. Nevertheless, there are periods of time when the temperature increases to the ambient temperature level, i.e., above $20°C$. During such periods of time, the refrigeration system is turned off and the temperature needs to be pulled down whenever the cooling system is turned back on. The third visible temperature pattern consists of time periods when the temperature shows irregularities that resemble neither a regular swinging nor a sharp increase in temperature. Such periods are candidates for identification of loading and unloading of products while the refrigerator is on. In such patterns, door openings occur while the refrigerator succeeds in keeping the average temperature low. However, the temperature does not swing as regularly as the case with no door opening.

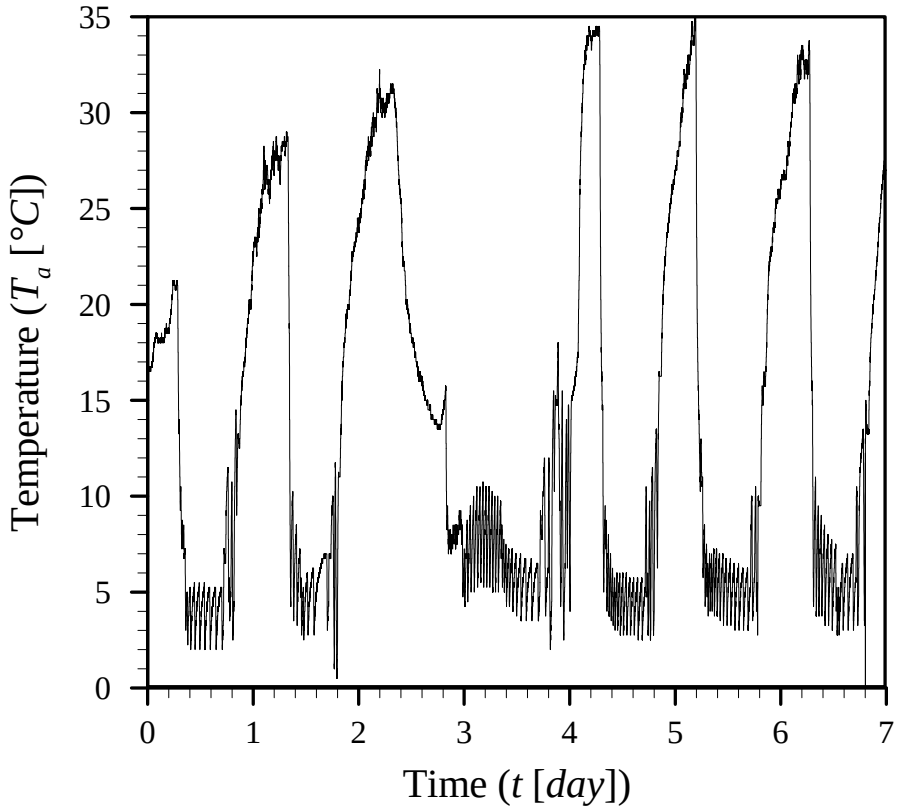

Figure A-2: Temperature variation pattern of the refrigerated truck during one week of its regular operation starting from Thursday noon.

The duty cycle of the truck's refrigeration system can be deduced from the observations made on Fig. A-2. The discussed identification process is verified with the data acquired from the user company's schedule. Figures A-3 to A-5 show the results of

the identification procedure as observed in Fig. A-2 and verified by the company's schedule.

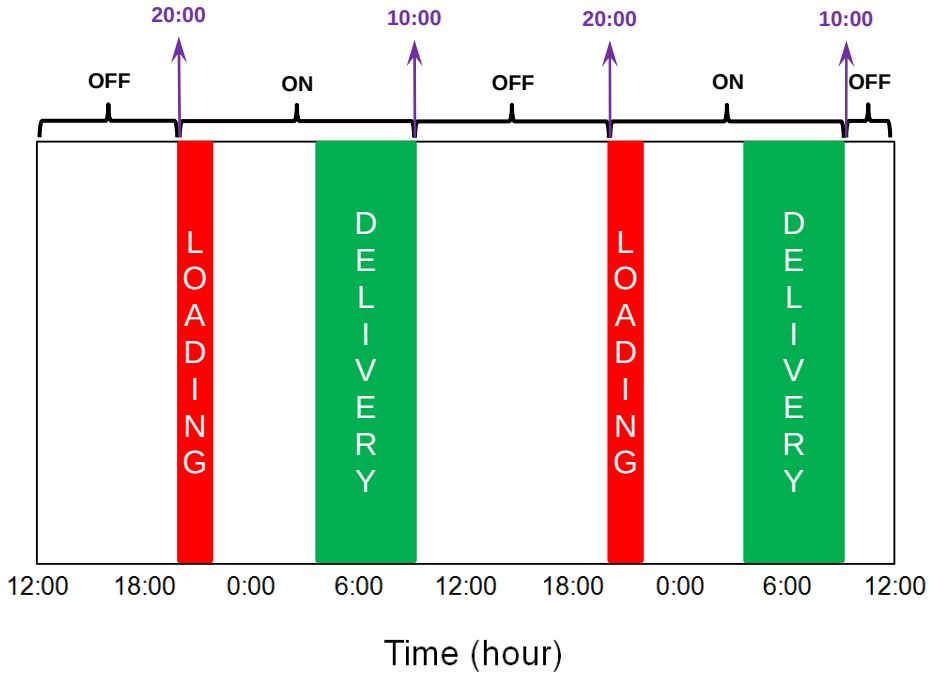

Figure A-3: Duty cycle of the refrigerated truck from Thursday to Saturday.

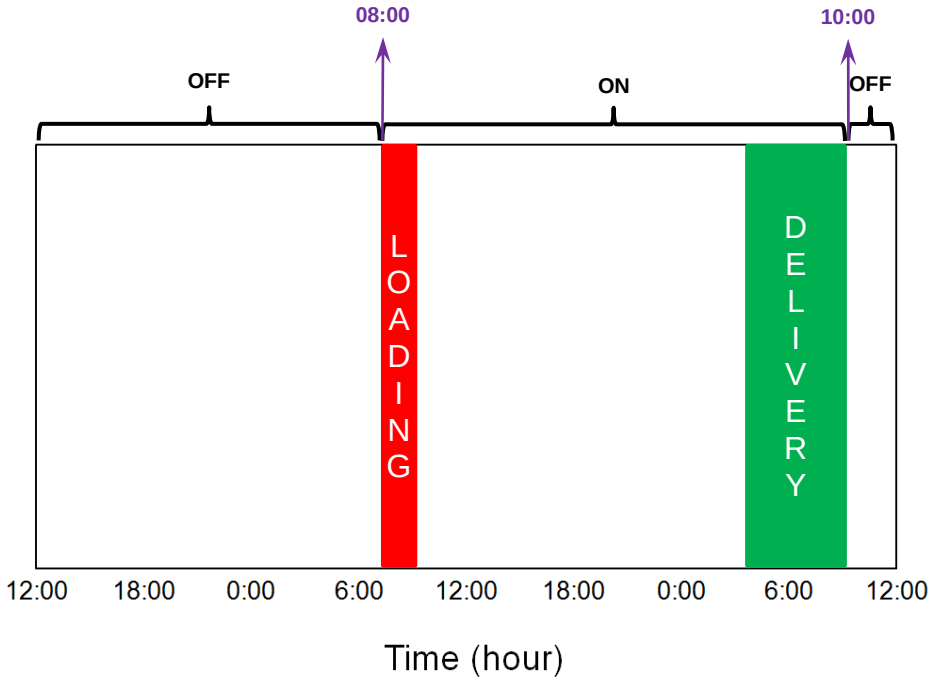

Figure A-4: Duty cycle of the refrigerated truck from Saturday to Monday.

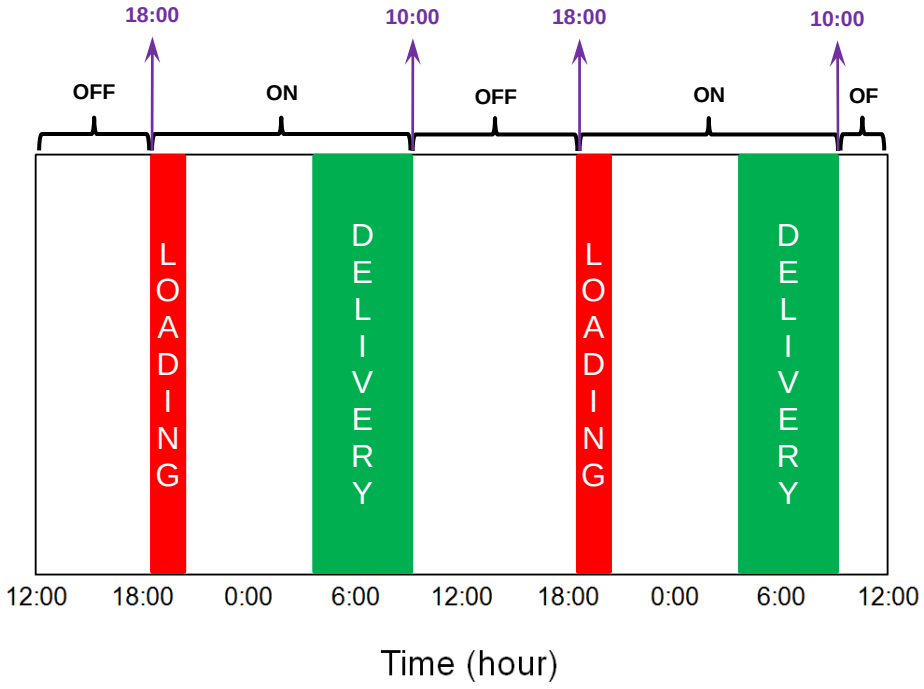

Figure A-5: Duty cycle of the refrigerated truck from Monday to Thursday.

As shown in the above figures, the loading and delivery times of the dairy products vary during different days of the week. The schedule of the weekends is also significantly different than the other days. These trends are obviously visible in the temperature pattern of Fig. A-2. For instance, the data of the third day clearly shows that the refrigeration system is turned off during the entire period of the day.

The identification of the duty cycle based on the measured temperature is beneficial for energy-efficient control of the refrigeration system. The method used in this section can be implemented in feedback controllers for improved operation of such systems both in automotive and stationary applications.